

**Deciphering proteome dynamics using cell-type
selective metabolic protein labeling in the fruit fly**

Drosophila melanogaster

Dissertation

zur Erlangung des akademischen Grades

doctor rerum naturalium

(Dr. rer. nat.)

genehmigt durch die Fakultät für Naturwissenschaften

der Otto-von-Guericke Universität Magdeburg

von

M. Sc. Ines Erdmann

geb. am 30. März 1988 in Leipzig

Gutachter:

Prof. Dr. Daniela C. Dieterich

Prof. Dr. Christian Wegener

eingereicht am 03. März 2016

verteidigt am 12. Oktober 2016

For my beloved ones

Acknowledgements

Die hier vorliegende Arbeit entstand im Zeitraum von Dezember 2011 bis Februar 2016 am Leibniz Institut für Neurobiologie (LiN) Magdeburg, sowie am Institut für Pharmakologie und Toxikologie der Otto-von-Guericke (OvG) Universität Magdeburg, in der Forschergruppe Neuralomics/Neurale Plastizität und Kommunikation (NPK). Diese Arbeit wurden zum einen von der "Leibniz Graduate School for Synptogenetics" und zum anderen durch ein Promotionsstipendium im Rahmen der leistungsorientierten Mittelvergabe (LOM) zur Förderung von Doktoranden der OvG-Universität Magdeburg finanziert.

Ein besonderer Dank geht an Prof. Dr. Daniela C. Dieterich, die mir die Möglichkeit gegeben hat dieses wundervolle Projekt zu bearbeiten. Durch viele anregende Diskussionen und Hilfestellungen wurde ich während des Bearbeitens dieser Arbeit stetig unterstützt. Außerdem möchte ich ihr danken, dass sie mir die Möglichkeit gegeben hat auf vielen internationalen Meetings meine Arbeit vorzustellen und diese mit anderen Wissenschaftlern zu diskutieren. Des Weiteren, möchte ich ihr für das Vertrauen danken, welches sie mir entgegen brachte, als es darum ging, eigenständig ein Fliegenlabor aufzubauen.

Dr. Ulrich Thomas möchte ich für die immerwährende Unterstützung bei meinen vielen Fliegen-Fragen danken, sei es von der Zucht der Fliegen bis hin zur Fliegengenetik. Außerdem möchte ich ihm für die vielen hilfreichen Diskussionen und Anregungen zum Projekt und den ein oder anderen Keks oder Gummibärchen zwischendurch danken.

Ein weiterer Dank geht an das LiN und die Universität Magdeburg für die Bereitstellung aller notwendigen Einrichtungen, Gerätschaften, die Administration, sowie das Anbieten von vielen Seminaren und Workshops.

Dr. Kathrin Marter möchte ich ins Besondere für die Hilfe bei der Bearbeitung des FlyNCAT Projekts danken. Außerdem geht ein herzlicher Dank an Dr. Anke Müller für einen sehr entscheidenden Tipp während der Bearbeitung des FlyNCAT-Projekts – D A N K E. Oliver Kobler möchte ich ebenfalls meinen Dank für die Unterstützung im FlyNCAT Projekts danken. Ein weiter Dank geht an Julia Abele für die Unterstützung im Rhinoceros-Projekt. Dr. Peter Landgraf möchte ich für die stetige ANL und Biotin-Sonden Synthese danken, sowie für das geduldige Beantworten vieler vieler Fragen.

Ein weiterer Dank geht an unsere Kooperationspartner in Münster, Dr. Erik Storkebaum, Dr. Sven Niehues und Julia Bussmann, für die Möglichkeit am CMT-Projekt mitzuarbeiten. Dr. Sven Niehues möchte ich außerdem für die Unterstützung beim FlyNCAT Projekt danken.

Dr. Karl-Heinz Smalla und Kathrin Pohlmann danke ich für die 2D Gelelektrophorese und für die Hilfe beim Analysieren und Auswerten der Daten. Des Weiteren geht ein Dank an Dr. Thilo Kähne, Yvonne Ducho und Dr. Tamar Ziv, die die MS-Analysen dieser Arbeit durchgeführt haben.

Kathrin Gruß möchte ich für die liebevolle Fliegenpflege danken als die Fliegen noch im LiN Unterschlupf fanden und für die vielen hilfreichen Tipps bei der Fliegenpflege.

Außerdem möchte ich der Arbeitsgruppe Neuralomics/NPK für die Unterstützung, die vielen Ratschläge, für das Aufbauen nach fehlgeschlagenen Experimenten danken, sowie für die tollen Kaffee- und Kuchenpausen, die durch viele wissenschaftliche Diskussionen bereichert wurden und zu vielen Ahaaa-Effekten führten.

Paula, Karina, Anke, Evi und Julia möchte ich für die tolle Freundschaft und die Aufmunterung und Versüßung bei nicht gelungen Experimenten danken. Danke, dass ich immer auf euch zählen konnte.

Ein besonderer Dank geht auch an alle meine Freunde, die mich während dieser Zeit in vielerlei Hinsicht unterstützt und aufgebaut haben. Ohne euch wäre es nicht möglich gewesen. Danke, dass ihr so unglaublich (!) toll seid und immer an mich geglaubt habt.

Zum Schluss möchte ich noch meiner Familie, meinen Eltern Martina und Lutz, sowie meiner Schwester Sandra für ihre immerwährende Unterstützung, Aufmunterung und das stete Vorantreiben danken. Danke, dass ihr immer mein Anker seid!!!

Table of Content

List of Figures.....	III
List of Tables.....	IV
List of Abbreviations.....	V
Zusammenfassung.....	VIII
Abstract.....	X
1 Introduction.....	1
1.1 <i>Drosophila melanogaster</i> – an invaluable model organism.....	1
1.2 Labeling strategies to track protein dynamics.....	4
1.3 Cell-type selective analysis of proteomes <i>in vivo</i>	6
1.4 Possible applications for cell-type selective protein labeling <i>in vivo</i>	9
1.4.1 A <i>Drosophila</i> model for Charcot-Marie-Tooth neuropathy.....	9
1.4.2 FMRP and its role in protein synthesis.....	10
1.4.3 The Rsh learning mutant.....	11
1.5 Objectives.....	14
2 Material and Methods.....	16
2.1 Material.....	16
2.1.1 Chemicals.....	16
2.1.2 Laboratory animals.....	17
2.2 Methods.....	17
2.2.1 Molecular biological methods.....	17
2.2.1.1 Extraction of genomic DNA of <i>Drosophila melanogaster</i>	17
2.2.1.2 Polymerase chain reaction (PCR)	17
2.2.1.3 Restriction digest of DNA.....	18
2.2.1.4 Agarose gel electrophoresis.....	18
2.2.1.5 DNA extraction from agarose gels.....	18
2.2.1.6 Cloning of expression vectors.....	18
2.2.1.7 Plasmid-DNA preparation from <i>E. coli</i>	19
2.2.2 Cytological Methods.....	20
2.2.2.1 Culturing of Hek293T cells.....	20
2.2.2.2 Transient transfection of Hek293T cells.....	20
2.2.3 <i>Drosophila melanogaster</i> handling.....	20
2.2.3.1 <i>Drosophila melanogaster</i> farming.....	20
2.2.3.2 <i>Drosophila melanogaster</i> fly strains.....	21
2.2.3.3 Metabolic labeling of proteins.....	22
2.2.3.4 Toxicity of ANL towards <i>Drosophila</i> larvae and flies.....	23
2.2.4 Biochemical methods.....	24
2.2.4.1 Protein extractions.....	24
2.2.4.1.1 Protein extraction from Hek293T cells.....	24
2.2.4.1.2 Protein extraction from larval body walls, larval brains and adult fly heads of <i>Drosophila melanogaster</i>	24
2.2.4.2 Bio-orthogonal non-canonical amino acid tagging (BONCAT).....	25
2.2.4.3 Determination of protein concentrations with amido black assay.....	25
2.2.4.4 NeutrAvidin purification of ANL- or AHA-labeled biotin-tagged proteins.....	26
2.2.4.5 Purification of GFP-tagged proteins and mass spectrometry analysis.....	26
2.2.4.6 Sodium dodecyl sulfate polyacrylamide gel electrophoreses (SDS- PAGE).....	27
2.2.4.7 Silver gel staining.....	28
2.2.4.8 Western blot analysis	29
2.2.4.9 Dot blot analysis, immuno-detection and statistical analysis.....	30
2.2.4.10 2D Gel electrophoresis and mass spectrometry analysis.....	30
2.2.4.11 Generation of fusion proteins.....	31
2.2.5 Fluorescent staining methods.....	32

2.2.5.1 Immunocytochemistry of transfected Hek293T cells.....	32
2.2.5.2 Fluorescent non-canonical amino acid tagging (FUNCAT) and immunocytochemistry of larval body walls.....	32
2.2.5.3 Microscopy.....	33
2.2.6 Data Bank analysis.....	33
2.2.7 Antibody generation.....	34
3 Results.....	35
3.1 Endogenous wild-type Methionyl-tRNA synthetase (MetRS) incorporates ANL, but not ANL into proteins of <i>Drosophila melanogaster</i>	35
3.2 Generation of transgenic MetRS ^{LtoG} flies.....	36
3.3 Visualization of cell-type specific protein labeling with ANL using FUNCAT.....	37
3.4 Identification of cell-type specific protein labeling with ANL using BONCAT.....	40
3.5 ANL-labeling correlates with the duration of ANL exposure.....	45
3.6 Methionine is replaced by ANL at internal amino acid positions within a protein...	47
3.7 Limited side effect upon chronic ANL incorporation.....	48
3.8 Investigation of protein synthesis rates in different mutant backgrounds applying cell-type selective amino acid tagging.....	53
3.8.1 Reduced protein synthesis in a <i>Drosophila</i> model for GARS-associated Charcot-Marie-Tooth (CMT) neuropathy.....	53
3.8.2 Reduced protein synthesis rate in dFMR1 knockdown larvae.....	55
3.8.3 Reduced protein synthesis in <i>rsh</i> ¹ mutant flies.....	56
3.9 Analysis of global protein expression pattern in <i>rsh</i> ¹ mutant flies.....	58
3.10 Sequence analysis of Radish (Rsh) and Rhinoceros (Rno)	69
3.11 Radish antibody generation	72
4 Discussion.....	77
4.1 MetRS ^{LtoG} -mediated ANL incorporation enables cell-type specific identification of newly synthesized protein <i>in vivo</i>	77
4.2 First applications of FlyNCAT in the nervous system of <i>Drosophila melanogaster</i> to unravel proteome dynamics under pathological conditions.....	81
4.2.1 Reduced protein synthesis rate in motor and sensory neurons of a <i>Drosophila</i> model for Charcot-Marie-Tooth neuropathy.....	81
4.2.2 Reduced protein synthesis rate in neurons of dFmr1 knockdown larvae.....	82
4.2.3 Reduced protein synthesis rate in neurons of the <i>rsh</i> ¹ learning mutant.....	84
4.3 FlyNCAT and sequence analysis suggest a putative role for Rsh for protein synthesis	86
4.4 RNAi-based knockdown of Rsh in neurons and glia cells.....	90
5 Outlook.....	92
6 References.....	93
7 Appendix.....	106
7.1 Used primers for cloning.....	106
7.2 Used vectors for cloning.....	106
7.3 Expression vectors.....	106
7.4 Supplementary Figures.....	107
Curriculum vitae.....	114
List of Publications.....	116
Statutory declaration.....	117

List of Figures

Figure 1: Life cycle of <i>Drosophila melanogaster</i> .	1
Figure 2: The principle of the Gal4/UAS-system.	2
Figure 3: Gross comparison of the brain structures between <i>Drosophila</i> and humans.	3
Figure 4: Metabolic labeling strategy using non-canonical amino acids.	8
Figure 5: Comparison of total protein expression pattern between <i>wt</i> (CS) and <i>rsh</i> ¹ mutant flies.	13
Figure 6: <i>Drosophila</i> larvae are able to use AHA as a substrate to label proteins for their detection using click chemistry (BONCAT).	36
Figure 7: Sequence alignment of orthologous MetRS.	37
Figure 8: ANL incorporation upon target expression of MetRS ^{LtoG} -EGFP in neurons and glia cells of <i>Drosophila</i> larvae.	39
Figure 9: Detection of affinity purified biotin-tagged proteins in <i>Drosophila</i> larvae and flies using BONCAT.	42
Figure 10: Chronic ANL incorporation into muscle, neuronal and glial proteins using differing ANL concentrations.	43
Figure 11: Cell-type specificity of ANL-labeling.	44
Figure 12: Short-term labeling of proteins with ANL.	46
Figure 13: Fate of larval ANL-labeled neuronal proteins after metamorphosis in adult <i>Drosophila</i> flies.	47
Figure 14: ANL is incorporated at internal amino acid positions within a protein.	48
Figure 15: Limited toxic side effects on MetRS ^{LtoG} -expressing larvae and flies after chronic ANL exposure.	50
Figure 16: Normal survival rate of dMetRS ^{L262G} -EGFP-expressing flies after chronic ANL exposure.	51
Figure 17: Reduced protein translation rate in GARS-associated CMT larvae.	54
Figure 18: Reduced protein translation rate in GARS-associated CMT flies.	55
Figure 19: Reduced protein synthesis rate in dFMR1 knockdown larvae.	56
Figure 20: Reduced protein synthesis rate in neurons of heterozygous <i>rsh</i> ¹ mutant flies.	57
Figure 21: Silver stained 2D-gels of <i>rsh</i> ¹ mutant and <i>wt</i> head lysates.	59
Figure 22: Example for 2D gel analysis.	60
Figure 23: <i>rsh</i> ^Δ splice variants and Rsh isoforms.	70
Figure 24: <i>rno</i> splice variants and Rno isoforms.	72
Figure 25: Antibody characterization of anti-Rsh antisera using IF staining.	74
Figure 26: Antibody characterization of anti-Rsh antisera using western blot.	76
Supplementary Figure 1: MetRS ^{LtoG} results in incorporation of ANL into internal methionine residues.	107
Supplementary Figure 2: Multiple sequence alignment of Rsh isoforms.	108

List of Tables

Table 1: Primary antibodies	16
Table 2: Secondary antibodies	17
Table 3: Fly strains	21
Table 4: Immunization of guinea pigs and rabbits with MPB-Rsh ²³⁵⁻⁵¹⁵ fusion protein	34
Table 5: Number of spots identified by PDQuest software and their respective protein fraction in <i>rsh</i> ¹ mutant and <i>wt</i> flies	60
Table 6: Number of spots per genotype after verification using student's T-Test.	62
Table 7: 2D gel analysis of protein fraction from <i>rsh</i> ¹ mutant and <i>wt</i> (CS) flies	63
Table 8: Sequence analysis of <i>rsh</i> ¹ gene and Rsh protein	71
Table 9: Sequence analysis of <i>rno</i> gene and Rno protein	72
Supplementary Table 1: Primers used for vector cloning	106
Supplementary Table 2: Cloning vectors	106
Supplementary Table 3: Expression vectors	106

List of Abbreviations

w/v	weight per volume percentage
5HT	5-hydroxytryptamine, Serotonin
aa	amino acid
AARS	alanyl-tRNA synthetase
ADHD	attention-deficit hyperactivity disorder
AHA	azidohomoalanine
ANL	azidonorleucine
APS	ammonium persulfate
ARM	anesthesia-resistant memory
ASM	anesthesia-sensitive memory
Azf	<i>p</i> -azido-L-phenylalanine
BONCAT	bio-orthogonal non-canonical amino acid tagging
bp	base pair
Brp	Bruchpilot
BSA	bovine serum albumin
BTB/POZ	Broad Complex, Tramtrack & bric a brac/Poxvirus and Zinc-finger
C	cytosine
cDNA	complementary deoxyribonucleic acid
ChIP	chromatin immune precipitation
CMT	Charcot-Marie-Tooth
CNS	central nervous system
CS	<i>Canton-S</i>
ctrl	control
CuAAC	copper-catalyzed [3+2] azide-alkyne-cycloaddition
DB	dot blot
dMetRS ^{L262G}	<i>Drosophila</i> methionyl-tRNA synthetase with leucine- to glycine-mutation at position 262
DMSO	dimethyl sulfoxide
DNA	deoxyribonucleic acid
dNTPS	nucleoside triphosphate
dsRNA	double stranded ribonucleic acid
DTT	dithiothreitol
E	eluate
<i>E. coli</i>	<i>Escherichia coli</i>
EAAT1	excitatory amino acid transporter 1
ECL	electrochemiluminescence
EcMetRS ^{L13G}	<i>Escherichia coli</i> methionyl-tRNA synthetase with leucine- to glycine-mutation at position 13
EcMetRS ^{NLL}	<i>Escherichia coli</i> methionyl-tRNA synthetase with leucine- to glycine substitution at position 13, tyrosine to leucine substitution at position 260, histidine to leucine substitution at position 301
EDTA	ethylenediaminetetraacetic acid
EGFP	enhanced green fluorescent protein
EGFR	epidermal growth factor receptor
exp	experimental
FCS	fetal calf serum
FlyNCAT	fly non-canonical amino acid tagging
<i>Fmr1</i>	<i>fragile X mental retardation 1</i> gene
FMRP	fragile X mental retardation protein
FUNCAT	fluorescent non-canonical amino acid tagging
FXS	fragile X syndrome
FYVE	Fab1, YOTB, Vac 1, EEA1
Gaps	GTPase activating proteins
GARS	glycyl-tRNA synthetase

Gefs	guanine nucleotide exchange factors
GFP	green fluorescent protein
GINCAT	genetically introduced non-canonical amino acid tagging
GLAST	glutamate-aspartate transporter
GLT-1	glutamate transporter-1
gp	guinea pig
Gs2	glutamine synthetase 2
GTP	guanosine triphosphate
HARS	histidyl-tRNA synthetase
HAT	histone acetyltransferase
HBSS	Hank's buffered salt solution
Hek293T	human embryonic kidney 293T cell line
HEPES	2-(4-(2-Hydroxyethyl)-1-piperanzinyl)-ethansulfon acid
hGARS	human glycyl-tRNA synthetase
HPG	homopropargylglycine
HRP	horse-radish peroxidase
I	input
IF	immunofluorescence
IP	immune precipitation
IPTG	Isopropyl- β -D-thiogalactopyranoside
kd	knockdown
KPSI	kilo-pound per square inch
LB-medium	lysogeny broth-medium
LIM	Lin11, Isl-1 & Mec-3.
LTD	long-term depression
LTM	long-term memory
LTP	long-term potentiation
MaPKM ζ	mouse atypical protein kinase M ζ
MARS	methionyl-tRNA synthetase
MBP	maltose binding protein
Met	methionine
MetRS	methionyl-tRNA synthetase
MetRS ^{mut}	mutant methionyl-tRNA synthetase
MiMIC	minos-mediated integration cassette
mM	millimol
mMetRS ^{L274G}	murine methionyl-tRNA synthetase with leucine- to glycine-mutation at position 274
MPH	methylphenidate
mRNA	messenger ribonucleic acid
MTM	middle-term memory
mut	mutant
MW/Mr	molecular weight
n.s.	not significant
n/s	not specified
neg	negative
NMJ	neuromuscular junction
NMS	neuromuscular synapse
no.	number
OD	optic density
ONM	Otto-Normal-Medium
ORF	open reading frame
overe	overexpression
OvGU	Otto-von-Guericke University
PB	phosphate buffer
PBS	phosphate buffered saline
PCR	polymerase chain reaction

PFA	paraformaldehyde
PHD	plant homeo domain
PheRS	phenylalanyl-tRNA synthetase
PI	protease inhibitor
PLA2	phospholipase-2
PMCA	plasma membrane calcium ATPase
Pnt	pointed
POZ	pox virus and Zinc finger
RapGap	Rap GTPase activating protein domain
rb	rabbit
Rel.	relative
RING	Really interesting New Gene
RMCE	recombinase mediated cassette exchange
RNA	ribonucleic acid
RNAi	ribonucleic acid interference
Rno	Rhinoceros
Rpl10a	ribosomal protein L10a
Rsh	Radish
RT	room temperature
SD	standard deviation
SDS-PAGE	sodium dodecyl sulfate polyacrylamide gel
SEM	standard error of the mean
shRNA	short hairpin ribonucleic acid
SILAC	stable isotope labeling with amino acids in cell culture
siRNA	small interfering ribonucleic acid
SOC medium	super optimal broth with Catabolite repression
STM	short-term memory
Su(H)	Suppressor of Hairless
T	thymine
TAE	Tris-acetate-EDTA-buffer
TAMRA	tetramethylrhodamine
TBS	tris buffered saline
TCEP	Tris[(1-benzyl-1H-1,2,3-triazo-4-yl)methyl]amine)
TEMED	tetramethylethylenediamine
theor	theoretical
Thr412Gly-CePheRS	mutant phenylalanyl-tRNA synthetase
tRNA	transfer ribonucleic acid
ts	temperature sensitive
tub	tubulin
U	unbound
UTR	untranslated region
v/v	volume percentage
VDRC	Vienna <i>Drosophila</i> RNAi Center
w/	with
w/o	without
WB	western blot
wt	wild type
YARS	tyrosyl-tRNA synthase

Zusammenfassung

Das Überleben eines Organismus ist abhängig von seiner Fähigkeit auf positive und negative Stimuli der Umwelt zu reagieren, wie z.B. während der Nahrungs- und Partnersuche oder beim Erkennen von Gefahrensituationen. Diese Reaktionsfähigkeit auf diverse Stimuli wird auf zellulärer Ebene durch Änderungen des Proteoms realisiert und kontrolliert. Dies beinhaltet Änderungen in der Gesamtheit aller zellulären Proteine einschließlich posttranslationaler Modifikationen, Proteindegradation, subzellulären Lokalisationen und Protein-Neusynthese. Das Überleben eines Organismus hängt von seiner Reaktionsfähigkeit gegenüber positiven und negativen Stimuli seiner Umwelt ab, so z.B. während der Nahrungs- und Partnersuche oder beim Erkennen von Gefahrensituationen. Auf zellulärer Ebene wird diese Reaktionsfähigkeit gegenüber diesen Stimuli durch die Änderung des Proteoms – der Gesamtheit aller Proteine einschließlich posttranslationaler Modifikationen, Proteindegradation, subzellulären Lokalisation und Proteinneusynthese – kontrolliert. Mit herkömmlichen Proteinmarkierungsmethoden war es bisher nicht möglich, diese Geschehnisse zell-spezifisch zu untersuchen, da sowohl neue als auch bereits existierende Proteine aus dem gleichen Pool an Aminosäuren bestehen.

Im Rahmen dieser Doktorarbeit wurde ein Verfahren zur zell-spezifischen Proteinmarkierung in der Taufliede realisiert (GINCAT – *genetically introduced non-canonical amino acid tagging*), welches auf der Expression einer mutierten Methionyl-tRNA Synthetase (MetRS) und dem Einbau der Azid-modifizierten Aminosäure Azidonorleucin beruht. Azidonorleucin-tragende Proteine können dann mit Hilfe der bereits bekannten FUNCAT (*fluorescent non-canonical amino acid tagging*) and BONCAT (*bioorthogonal non-canonical amino acid tagging*) Techniken detektiert werden. Eine Leucin- zu Glycin-Substitution vergrößert die MetRS-Bindungstasche im mutierten MetRS^{LtoG}-Enzym in dem Maße, dass die nicht-kanonische Aminosäure Azidonorleucin (ANL) aktiviert und somit an Stelle von Methionin in neu-synthetisierte Proteine eingebaut werden kann. Neu-synthetisierte Proteine können mit Hilfe der Kupfer (I)-katalysierten [3+2] Azid-Alkin Cycloaddition – kurz „Klick Chemie“ – nachgewiesen werden. Bei dieser Reaktion wird die Azid-Gruppe des ANLs kovalent an die Alkin-Gruppe einer Sonde gebunden. Diese Sonden dienen zur Detektion der ANL-markierten Proteine mittels fluoreszenter oder biochemischer Verfahren. Hier wurde eine zell-spezifische Proteinmarkierung durch die zell-spezifische Expression der mutierten MetRS^{LtoG} in *Drosophila*-Larven und -Fliegen mit Hilfe des Gal4/UAS-Systems erreicht. Sowohl FUNCAT als auch BONCAT zeigten, dass mit Hilfe der MetRS^{LtoG} Proteine zell-spezifisch mit ANL markiert und nachgewiesen werden können. FlyNCAT (*fly non-canonical amino acid tagging*, GIN-/FUN-/BONCAT) kann demzufolge als eine Methode verwendet werden, um zell-spezifisch die Dynamik eines Proteoms unter physiologischen und pathologischen Prozessen in einem komplexen und sich verhaltenden Organismus wie der

Taufliege darzustellen. Diese Methode wurde im Weiteren angewandt um die Proteintranslationsrate bei verschiedenen pathologischen Prozessen zu ermitteln. Zum einen wurde eine Reduzierung der relativen Proteintranslationsrate in motorischen und sensorischen Neuronen eines *Drosophila* Charcot-Marie-Tooth Modells festgestellt. Des Weiteren wurde mit Hilfe von FlyNCAT gezeigt, dass die relative Proteintranslationsrate in Neuronen von *Fragile X mental retardation-1* knockout Larven reduziert ist. Außerdem konnte gezeigt werden, dass die *Drosophila* Lernmutante *radish*¹ Defizite in der Proteinsynthese aufweist. 1D und 2D Gelelektrophorese-Experimenten gaben den Hinweis darauf, dass eine Reihe von Proteine, z.B. Rhinoceros, der eukaryontische Elongationsfaktor EEF1B2, der eukaryontische Initiationsfaktor EIF3J, Complexin and das Nucleoplasmin-ähnliches Protein, unterschiedlich zwischen wildtypischen Fliegen und *radish*¹ Lernmutanten exprimiert zu sein scheinen. Zusammen mit der reduzierten Proteintranslationsrate weist dies darauf hin, dass das Radish Protein, möglicherweise zusammen mit Rhinoceros, vermutlich eine Rolle während der Transkription und/oder Proteintranslation spielt. Diese Erkenntnisse können perspektivisch zu einem besseren Verständnis von Lern- und Gedächtnismechanismen beitragen.

Abstract

The survival of every single organism depends on its responsiveness to positive and negative stimuli within its environment, e.g. food, courtship partners, enemies and danger. This responsiveness is tightly controlled and largely depends on dynamic proteome alterations in the respective cells and circuits including post-translational modifications, protein degradation, their correct subcellular localization and appropriate *de novo* protein synthesis. However, monitoring protein alterations with cell-type specific resolution remained challenging so far as all proteins, “old” and “new” ones, share the same pool of amino acids. In the scope of this thesis, we introduce a cell-type specific protein labeling strategy by combining the target expression of a mutant methionyl-tRNA synthetase (MetRS^{LtoG}) with the previously reported bio-orthogonal and fluorescent non-canonical amino acid tagging techniques (BONCAT and FUNCAT). A leucine to glycine substitution leads to an enlargement of the MetRS binding pocket, resulting in the ability of the mutated synthetase to activate the non-canonical amino acid azidonorleucine (ANL), and hence, in subsequent incorporation of ANL into proteins during protein translation instead of methionine. Newly synthesized, ANL-bearing proteins can be tagged via copper (I)-catalyzed [3+2] azide-alkyne-cycloaddition or “click chemistry”, coupling the azide group of ANL to alkyne-bearing fluorescent- or affinity-tags. We tested the cell-type specific protein labeling *in vivo* by expressing the mutant MetRS^{LtoG} variant cell-type specifically in *Drosophila melanogaster* larvae and flies using the Gal4/UAS-system (GINCAT – genetically introduced non-canonical amino acid tagging). Both, FUNCAT and BONCAT revealed that ANL is incorporated into proteins exclusively in cells expressing the MetRS^{LtoG} variant. Thus, the FlyNCAT (fly non-canonical amino acid tagging, including GIN-/BON- and FUNCAT) technique can be used to study protein synthesis dependent processes in complex and behaving organisms during physiological and pathological events. Indeed, we are able to demonstrate a reduced protein synthesis rate in motor and sensory neurons of a *Drosophila* Charcot-Marie-Tooth model, in neurons of *Fragile X mental retardation-1* knockdown larvae and in neurons of *radish*¹ learning mutant flies using the FlyNCAT technique. 1D and 2D gel electrophoresis indicate that a variety of proteins were found to be differently expressed in heads of *radish*¹ mutant and wild type flies, including the putative transcription factor Rhinoceros, the eukaryotic elongation factor EEF1B2, the eukaryotic initiation factor EIF3J, Complexin and the nucleoplasmin-like protein. The reduced protein translation rate and the altered expression of certain proteins in *radish*¹ mutant compared to wild type flies suggest that Radish might play a role during transcription and/or protein translation, possibly together with Rhinoceros. Unraveling the function of Radish and Rhinoceros in the *Drosophila* brain would provide a new basis in understanding the underlying mechanisms during learning and memory formation.

1 Introduction

1.1 *Drosophila melanogaster* – an invaluable model organism

The fruit fly *Drosophila melanogaster* is a popular model organism used in many laboratories to study genetic and developmental processes, behavior, and disease models. Many relevant biological discoveries, including the theory of inheritance by Thomas Hunt Morgan (Nobel Prize in Physiology or Medicine, 1933 “for his discoveries concerning the role played by the chromosome in heredity”, http://nobelprize.org/nobel_prizes/medicine/laureates/1933/ (1933)) or the influence of genes on developmental processes by Christiane Nüsslein-Volhard, Eric Wieschaus, and Ed Lewis (Nobel Prize in Physiology or Medicine “for their discoveries concerning the genetic control of early embryonic development”, http://nobelprize.org/nobel_prizes/medicine/laureates/1995/ (1995)), were discovered using *Drosophila melanogaster*.

The fruit fly shows complex behavior such as aggression, learning and formation of memory, but is yet relatively easy to handle and to manipulate, has a simple diet, a short life span (Figure 1) and last but not least is an inexpensive model organism [1].

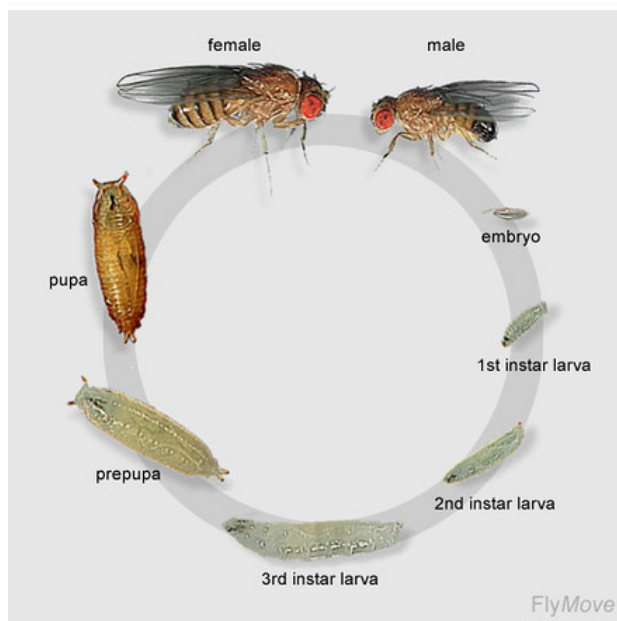


Figure 1: Life cycle of *Drosophila melanogaster*. At a temperature of 25°C a complete life cycle of a *Drosophila* fly from the egg through larval and pupal phase until the adult stage takes approximately 10-11 days. 24 h after egg laying the *Drosophila* larvae hatches from the egg. After 24 h the larvae molts for the first time and reaches the second larval stage. Another 24 h the larvae molts for the second time at reaches the third larval phase. The larvae stays within the third instar phase for two to three days before it pupates. The pupal stage lasts for five days before a fully developed fly hatches from its pupae. When the flies are kept at a temperature of 18°C the generation time last for 20 days. Whereas a temperature of 28°C accelerates the life cycle and it lasts around seven days [2, 3]. Modified from flyMove.uni-muenster.de.

Drosophila embryos, larvae and flies can be used to investigate different biological questions. For instance, *Drosophila* embryos and larvae are extensively used to investigate the developing nervous system, to resolve neuroepithelia patterning, neuronal cell-fate specifications, asymmetric cell division, specification of neuronal temporal identity, axon guidance and neuromuscular junction (NMJ) morphogenesis [4-6]. Adult *Drosophila* flies are used in many labs as well to investigate different processes and their underlying molecular mechanisms within the brain leading to different behaviors, like the circadian rhythm as well

as learning and memory formation [7]. *Drosophila* larvae and flies are genetically easy to manipulate either by removing or adding certain genes to investigate their impact on the larvae or flies' behavior. Various tools for the genetic manipulation of *Drosophila melanogaster* larvae and flies have been generated in the last decades. Among them the Gal4/UAS-system [8, 9], which is an invaluable tool to control gene expression in a defined spatial and temporal manner (Figure 2). Here, the cell-type specific expression of the yeast transcriptional factor Gal4 results in a cell-type specific expression of the gene of interest by Gal4-binding to the upstream activating sequence (UAS) [8, 9]. Using the temperature-sensitive yeast Gal80 repressor a temporal control of gene expression is obtained [10]. It was shown, that Gal80 blocks Gal4 activity when the flies are kept at a permissive temperature of 25°C. By shifting the flies to a restrictive temperature of 30°C Gal80 does not repress Gal4 activity and thus the gene of interest will be expressed [10]. As *Drosophila melanogaster* has 'only' four chromosomes the genetic manipulation of *Drosophila melanogaster* is rather simple compared to the mammals.

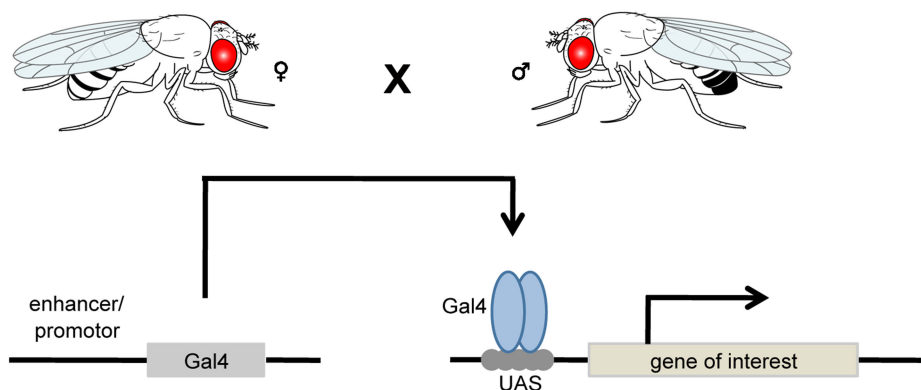


Figure 2: The principle of the Gal4/UAS-system. The yeast transcriptional activator Gal4 binds to an upstream activating sequence (UAS), thereby initiating the gene expression of the gene of interest. Modified after Erdmann *et al.*, 2015 [11] and Shimosako *et al.*, 2014 [12].

However, the approximately 14,000 *Drosophila* genes encoded by the four chromosomes [13] show crucial molecular similarities to their mammalian counterparts. For instance, sequencing of the *Drosophila* genome revealed that around 77% of human disease-causing genes are found homologous in *Drosophila melanogaster* [14]. Several genes that were initially discovered in *Drosophila melanogaster* have been isolated and studied in the mammalian system as well, such as *Notch* (4 Notch genes in mammals: Notch1-4 [15, 16]), *hedgehog* (mammalian “*sonic hedgehog*” [17]) and *Wnt* (mammalian *wingless* and *INT-related* [18]).

Despite the apparent differences in the complexity of mammalia and *Drosophila*, both share many common features, for instance similar neurotransmitter systems and several behavioral traits, including learning, memory forms, synaptic plasticity, circadian behaviors and to some

extend also social behavior [19]. The general architecture of the *Drosophila* and mammalian brain is likewise; they consist of (i) two hemispheres (Figure 3a-c) and (ii) a ventral nerve cord (Figure 3a) or a spinal cord (Figure 3c). Even at the cellular level, both *Drosophila* and mammals possess cell types with similarities in morphology and function, e.g. subtypes of glia cells [20]. The brain of *Drosophila melanogaster* is composed, like the mammalian brain, of the previously named glia cells and of neurons. They are tightly organized in the bilateral symmetrical brain, which is connected to the ventral nerve cord, innervating the thorax and abdomen (Figure 3a, b). *Drosophila* neurons and glia cells share a lot of functional and molecular characteristics with their mammalian counterparts, like axons with their transport machinery, pumps and voltage-gated channels controlled by action potential transmission, presynaptic terminals with active zones and the machinery for synaptic vesicle release/recycling, and dendrites as post-synaptic compartments with localized receptor fields [19]. Glia cells are found, like in the mammalian brain, in close association with neurons [20] and are divided into four main classes: cortex, neuropil, peripheral and surface glia. The cortex glia cell is coequal with astrocytes in vertebrates, whereas neuropil glia cells share functional equality with oligodendrocytes. Peripheral glia cells ensheat nerves in the peripheral nervous system, thus are coequal with Schwann cells in the vertebrate system. Last but not least, cortex, neuropil and surface glia cells in the *Drosophila* brain show microglial features of the mammalian microglial cells [21].

Both *Drosophila melanogaster* larvae and flies constitute an extraordinarily well suited model organism to investigate fundamental principles of neural circuits and their behavioral impact [1] as well as many other areas of biological research. In other words, the cellular and, thus, the impacts of gene products on *Drosophila* behavior such as learning, circadian behavior and responses to addictive substances or disease models like attention-deficit hyperactivity disorder (ADHD) [22] or Charcot-Marie Tooth (CMT) neuropathy [23] can be investigated in *Drosophila* as (i) its experimental manipulation is rather simple and (ii) the complexity of the brain is high enough to investigate behavior adaptable to the mammalian behavior

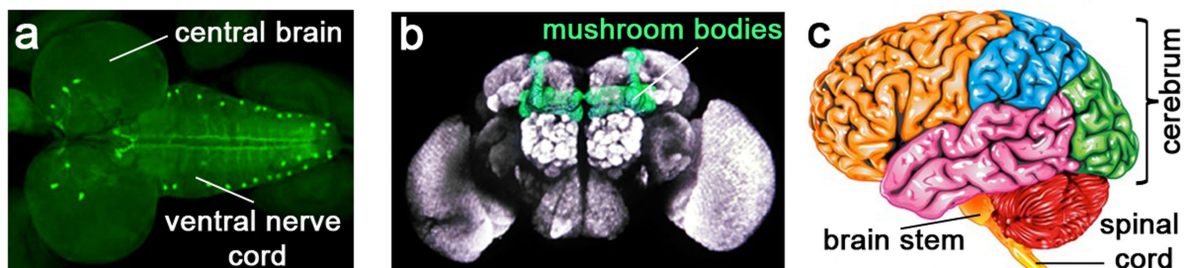


Figure 3: Gross comparison of the brain structures between *Drosophila* and humans. Both *Drosophila* (larval and adult) and human brain are constructed of two hemispheres (a-c), a ventral nerve cord (a, b) or a spinal cord (c). (a) The *Drosophila* brain of a 3rd instar larvae depicted here shows neuroendocrine cells in the central brain and in the ventral nerve cord by using the Gal4/UAS-system (green). (b) The bilateral adult *Drosophila* brain with optical lobes (most exterior structure right and left from the brain) and the mushroom bodies (MBs), known to be the center of olfactory learning

in *Drosophila melanogaster*. (c) The human brain with its much more complex architecture compared to the *Drosophila* brain. Its cerebrum is divided into the frontal (orange), the parietal (blue), the temporal (pink), the occipital lobe (green) and the cerebellum (red). Images taken and modified from (a) James Walker, Massachusetts General Hospital, (b) Martin Heisenberg, Würzburg, (c) <http://www.brainmadesimple.com>

1.2 Labeling strategies to track protein dynamics

Neurons and glia cells, despite their functional diversity, share a wealth of identical proteins, including neurotransmitter receptors, cell adhesion molecules and signal transduction proteins. Thus, considering this cellular heterogeneity of the nervous system rigorous identification of a cell's proteome, the comparison with proteomes of other cells or the identification of certain subproteomes within one structure, e.g. synaptic structures, is extremely challenging as both neurons and glia cells are almost physically inseparable. However, identifying the alterations of the protein entity of a certain cell type in response to extrinsic and/or intrinsic stimuli is crucial to figure out cell-type specific mechanisms under physiological and pathological conditions in single cells, organs and whole organisms. Various methods have been reported to assess the proteome of eukaryotic cell lines, distinct tissues and isolated cell types such as blood cells or sperm [24-27]. Protein fractionation and enrichment according to various criteria have led to the identification of cellular subproteomes. For instance posttranslational modifications like phosphorylation allows for the purification and enrichment of the "phosphoproteome" [28] and even proteins designated for degradation can be identified via ubiquitination or sumoylation [29, 30] using different biochemical tools. Pielot *et al.* (2012) summarized 12 proteomic studies of detergent-resistant synaptic junction fractions of mammalia brains and revealed more than 2,700 proteins as components of excitatory synapses on the pre- and post-synaptic side [31]. However, reducing the sample complexity by selectively enriching for newly synthesized proteins has been troublesome so far, as all proteins, "old" and "new" ones, share the same pool of 20 amino acids.

In the last 15 years metabolic labeling strategies have been developed to globally label newly synthesized proteins using, to name two examples, the incorporation of either (i) stable isotopic labeled amino acids (SILAC) [32] or (ii) small bio-orthogonal reporter molecules using the endogenous biosynthetic machinery [33] employing azide-or alkyne bearing non-canonical amino acids [34] and functionalized derivatives of the protein synthesis inhibitor puromycin [35].

The SILAC (stable isotope labeling by amino acids in cell culture) method is a quantitative approach for proteome investigations, which allows for a simultaneous and automated investigation. This method uses the *in vivo* incorporation of specific isotopically labeled 'heavy' amino acids, e.g. deuterated leucine (Leu-d), $^{13}\text{C}_6$ L-Lysine and $^{13}\text{C}_6$ L-Arginine, into all proteins. Such isotopically labeled „heavy“ samples and control, i.e. „light“, samples, are

pooled and analyzed via mass spectrometry enabling the in-depth investigation of relative quantitative changes in protein expression patterns between „heavy“ and „light“ labeled peptide levels [32]. However, cellular resolution, meaning the distinct cellular origin of certain proteins, cannot be achieved in a multicellular organism using SILAC.

Functionalized bio-orthogonal reporter molecules, like non-canonical amino acids [34] or derivatives of the protein synthesis inhibitor puromycin [35], are incorporated into biomolecules using the cell's own biosynthetic machinery and can be detected using chemo-selective reactions with exogenously delivered tags. Depending on the nature of these tags the biomolecule is targeted for visualization, detection, isolation or purification [36, 37]. The incorporation of bio-orthogonal molecules bearing functionalized groups, such as ketones, alkynes or azides, into proteins [34, 38-41], glycans [41-45] and lipids [46] facilitates their selective modification via copper (I)-catalyzed [3+2] azide-alkyne-cycloaddition (CuAAC), also known as 'click chemistry' (Figure 4c) [47] or via strain-promoted cycloaddition, which is a copper-free (Cu-free) 'click chemistry' reaction [48]. Both methods use the advantage of the high reactivity of alkyne groups towards azide-bearing tags (and *vice versa*). In more detail, an azide group reacts with a terminal alkyne group resulting in a stable triazol formation. Both reactions are characterized by a high specificity, efficiency and are unaffected by outside influences [48].

The usage of an alkyne analog of the protein synthesis inhibitor puromycin (O-propargyl-puromycin, OP-puro) is one example to monitor changes of the protein entity in terms of 'click chemistry' [35]. Puromycin mimics an aminoacyl-tRNA molecule. Consequently, OP-puro binds to the acceptor side of a translating ribosome, resulting in an efficient incorporation of OP-puro at the C-terminus of nascent polypeptides chains. CuAAC-mediated coupling of azide-bearing fluorescent or affinity tags lead to the visualization and the identification of nascent proteins *in vivo* under physiological and pathological conditions [35]. However, one major disadvantage of this method is, that OP-puro blocks protein synthesis, thus monitoring protein dynamics only as a snapshot, and ultimately leads to truncated proteins. Hence, uncovering activity-dependent protein changes over longer time periods, e.g. during long-term memory (LTM) formation, is difficult using OP-puro protein labeling. Furthermore, this method might not be sensitive enough for investigations of low abundant proteins as only one OP-puro molecule is incorporated per nascent protein chain.

The incorporation of the non-canonical amino acids azidohomoalanine (AHA) or homopropargylglycine (HPG) into proteins enables to metabolically label proteins during protein synthesis using the cell's own translation machinery leading to mature properly functioning proteins. AHA and HPG are methionine (Met) surrogates (Figure 4a) and thus are incorporated into proteins after loading them onto their cognate tRNA (Met-tRNA) via the methionyl-tRNA synthetase (MetRS, Figure 4b). Incorporated azide-bearing AHA or alkyne-

bearing HPG provide a new chemical functionality to proteins enabling for their visualization (FUNCAT – fluorescent non-canonical amino acid tagging [49-51]) and identification (BONCAT - bio-orthogonal non-canonical amino acid tagging [52, 53]) via CuAAC (Figure 4c). Until now, AHA and HPG were used in a variety of model systems to monitor global and local protein synthesis including bacteria [54], mammalian cell cultures [49, 50, 55-57] and larval zebrafish [58]. For instance, it was shown that protein synthesis can be monitored in the soma and dendrites of rat hippocampal neurons and even the mobility of newly synthesized proteins was shown using FUNCAT [50]. Other publications uncovered different functions of proteins within the nervous system using these methods. Tcherkezian *et al.* (2010) showed that the transmembrane receptor DCC co-localizes with newly synthesized proteins [56] or Yoon *et al.* (2012) revealed that lamin B2 is localized in the axon and not as previously assumed only in the soma of retinal ganglion cells and that lamin B2 is critical for axon survival [57].

Several studies combined the SILAC and BONCAT technique to quantitatively investigate the stimulus-induced protein dynamics in T-cells [59], rat cortical neurons [60], multiple cell lines [61] and in brain slices [62]. SILAC-based mass spectrometry analysis allows for quantification of steady-state proteomic changes [32], but the identification of immediate, early or minor changes of the proteome during a complex biological process is troublesome as short SILAC pulses label only a small fraction of the protein pool [63]. In contrast, labeling of newly synthesized proteins using BONCAT allows for a non-quantitative mass spectrometric analysis of newly synthesized proteins, as shown in mammalian cells [52]. However, CuAAC-mediated tagging of non-canonical amino acid labeled proteins is site- and protein-dependent and might not be homogenous for all proteins [64, 65]. But the advantage of CuAAC-mediated coupling of affinity tags to the proteins is, that those proteins can be enriched using affinity purification, thus dilutional effects are minimized.

Despite the significant methodological progress in the last years to monitor protein dynamics, unraveling cell-type specific protein dynamics *in vivo* in terms of spatial resolution (e.g. in distinct cell types of the brain or different parts of a cell, like at synapses) with the previously reported methods was impossible so far.

1.3 Cell-type selective analysis of proteomes *in vivo*

The usage of stable isotopic labeled amino acids or non-canonical amino acids, like AHA or HPG, has its limitations to uncover protein dynamics in multi-cellular organisms relating to spatial resolution, as these non-canonical amino acids are incorporated by the endogenous MetRS into any protein of any cell type. Thus, investigating cell-type specific protein dynamics in multicellular organisms is troublesome as the different cell types are tightly

embedded in their respective tissue and different cell types share a common pool of the same proteins, hence, the origin of the AHA- or HPG-labeled proteins is not clear.

The non-canonical amino acid azidonorleucine (ANL, Figure 4a) is a methionine surrogate like AHA or HPG, but is excluded from the binding pocket of the endogenous MetRS due to its enlarged side chain. Thus, ANL cannot be loaded onto the Met-tRNA and consequently is not incorporated into proteins. Recently, mutagenesis libraries of *E. coli* MetRSs (EcMetRS) were screened for mutant MetRS variants that are able to use ANL as a substrate. The mutant EcMetRS^{L13G} [66, 67] and EcMetRS^{NLL} [68, 69] mutant variants were found to activate ANL, leading to its efficient incorporation into proteins of bacteria and transfected mammalian cells. ANL-labeling of proteins can be achieved under physiological conditions, i.e. in the presence of Met, as the mutant MetRS variants are more likely to bind ANL rather than Met [66]. This is a major advantage compared to AHA- or HPG-labeling of proteins, as both have a similar binding affinity to the MetRS^{wt} binding pocket and thus in the presence of Met, AHA or HPG compete with Met for the binding at the MetRS^{wt} binding pocket [70, 71]. To achieve sufficient labeling efficiencies, AHA or HPG has to only be applied in Met-depleted culture medium or food.

As many other small chemical reporter molecules ANL harbors an azide group. Hence, ANL-harboring proteins can be tagged in terms of FUNCAT [49-51] and BONCAT [52, 53], using either fluorescent-alkyne or alkyne-affinity-tags respectively (Figure 4c). Tagging of ANL using FUNCAT and BONCAT showed that cell-type specific expression of either mutant MetRS variant leads to a cell-type selective incorporation of ANL into proteins [66-69]. However, the EcMetRS^{NLL} loads ANL only to the initiator tRNA leading only to ANL incorporation solely at a protein's N-terminal [69]. This represents a severe limitation for the investigation of cell-type selective proteome dynamics as many proteins, undergo either (i) N-terminal proteolytic cleavage of the signal sequence, like most transmembrane proteins or (ii) activity-dependent proteolytic cleavage, or even both, like it is the case for Notch [72].

So far expression of the mutant MetRS variants *in vivo* was not successful. Yuet *et al.* (2015) tried to generate transgenic *Caenorhabditis elegans* (*C. elegans*) using different mutant MetRS variants. However, these were not able to use ANL as a substrate [73]. Thus, establishing cell-type selective labeling of proteins *in vivo*, like in *Drosophila melanogaster*, rat or mice using ANL would expand the toolbox to investigate protein dynamics under physiological and pathological conditions. Deciphering such proteomic processes in turn could be used as a starting point to develop cell-type specific therapeutic treatment for various diseases, possibly reducing side effects of available medications.

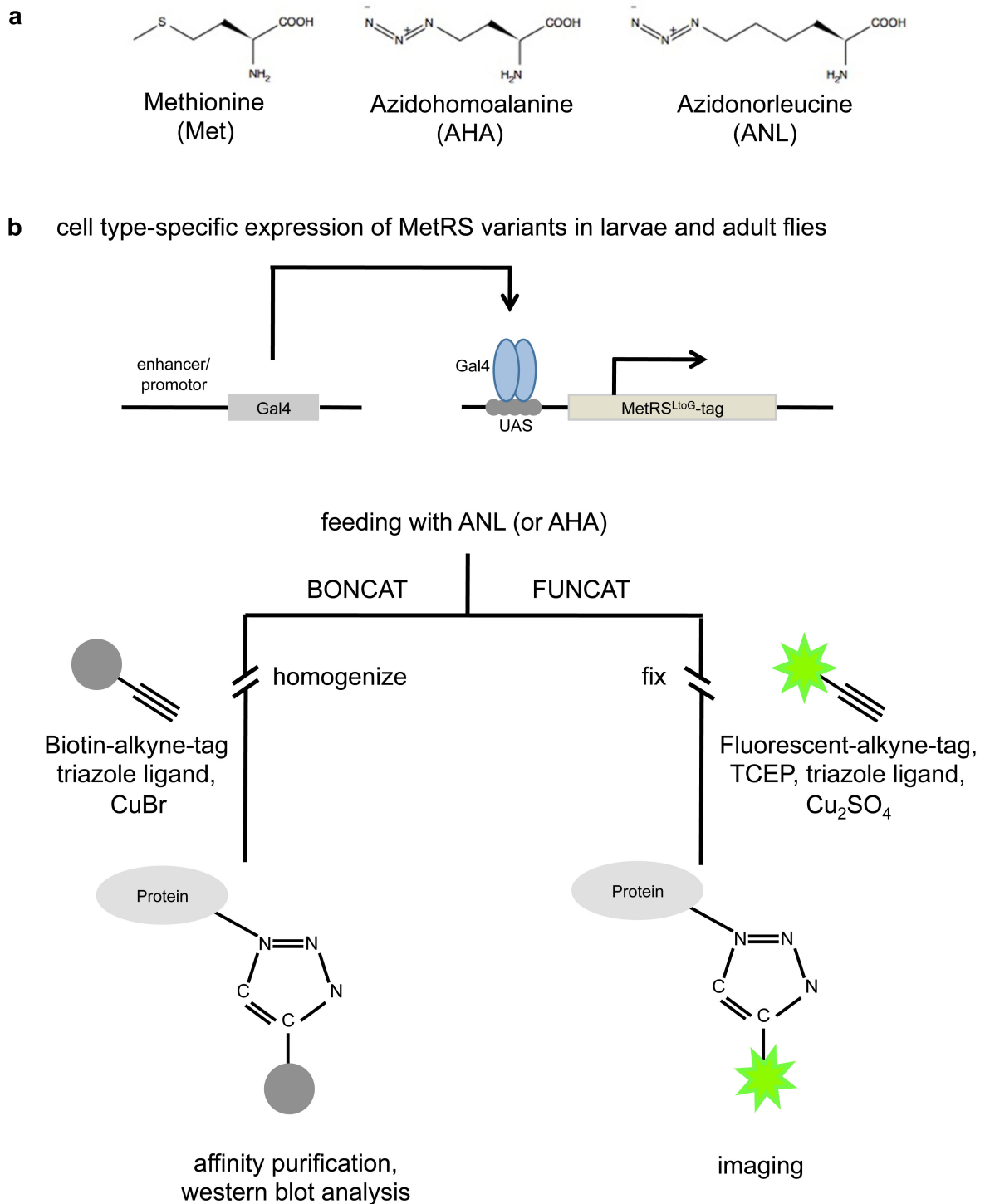


Figure 4: Metabolic labeling strategy using non-canonical amino acids. (a) The non-canonical amino acids Azidohomoalanine (AHA) and Azidonorleucine (ANL) are Methionine (Met) surrogates and can be incorporated into proteins instead of Met. (b) While AHA is activated by the endogenous methionyl-tRNA synthetase (MetRS^{wt}), ANL is excluded from the binding pocket of the MetRS^{wt} due to its larger side chain. Only mutant MetRS variants with an enlarged binding pocket are able to activate ANL. Cell-type specific expression of the mutant MetRS enables cell-type specific labeling of proteins with ANL. This method is, therefore, called GINCAT, i.e. genetically introduced non-canonical amino acid tagging. (c) Both AHA and ANL harbor an azide group, which is highly reactive towards alkyne groups (and *vice versa*). Thus, alkyne-bearing tags can be covalently coupled to azide-bearing chemical reporter molecules (and *vice versa*) mediated by copper (I)-catalyzed [3+2] azide-alkyne-cycloaddition (CuAAC). Fluorescent tags can be used to visualize protein synthesis using fluorescent non-canonical amino acids tagging (FUNCAT), whereas bio-orthogonal non-canonical amino acid tagging (BONCAT)-mediated coupling of biotin-affinity tags to AHA or ANL enables for affinity

purification and subsequent analysis on western blot or via mass spectrometry. Modified after Erdmann *et al.* (2015).

1.4 Possible applications for cell-type selective protein labeling *in vivo*

Cell-type selective protein labeling can be used to uncover molecular mechanisms of various processes that take place in the brain, like the activity-dependent alterations of protein dynamics in neurons and glia cells that occur upon stimulation. Additionally, in many cases, the molecular cause of a mutant phenotype or a particular disease is not known. Thus, unraveling protein dynamics of certain pathological events cell-type specifically could possibly help to uncover the accompanied phenotypic consequences of several diseases. Additionally, these findings can then be utilized for the development of new strategies for pharmacological treatments that act specifically in the affected cell type. Here, three cases are introduced exemplarily, in which cell-type selective protein labeling approaches might prove to be useful to uncover protein dynamics.

1.4.1 A *Drosophila* model for Charcot-Marie-Tooth neuropathy

Charcot-Marie-Tooth (CMT) neuropathy is with the prevalence of 1 in 2,500 the most common inherited neuromuscular disease [74]. Progressive distal muscle weakness and wasting, decreased reflexes, sensory loss and foot deformities are characteristics of CMT [75]. The classical symptoms are evoked by “dying-back” degeneration of peripheral motor and sensory axons [75]. CMT is known to be heterogeneous on the clinical and on the genetic level including more than 30 causative genes [75-77]. Among them mutations in five distinct aminoacyl-tRNA synthetases give rise to CMT: glycyl-tRNA synthetase (GARS), tyrosyl-tRNA synthase (YARS), alanyl-tRNA synthetase (AARS), histidyl-tRNA synthetase (HARS) and methionyl-tRNA synthetase (MARS/MetRS) [78-83]. Niehues *et al.* (2015) reported a *Drosophila* model for GARS-associated CMT. They generated transgenic flies carrying mutations in the human glycyl-tRNA synthetase (hGARS) protein and investigated the phenotypic impact of different mutations in the hGARS proteins [23]. They found that hGARS-mutant *Drosophila* display a phenotype similar to CMT, including deficits in motor performances, morphology of motor and sensory neurons as well as a shortened life span. Correct subcellular localization of aminoacyl-tRNA synthetases is important to ensure normal local protein synthesis. Several studies showed that mutant YARS and GARS proteins were mislocalized in mouse neuroblastoma (N2A), human neuroblastoma (SH-Sy5Y) and mouse motor neuron (MN-1) cell-lines [80, 84, 85]. However, in the recently reported CMT-associated *Drosophila* model the subcellular localization of mutant hGARS proteins was not altered [23]. This lies in line with a reported CMT mouse model. Here, the subcellular localization of mutant GARS proteins was not altered too [86]. Thus, defective local protein synthesis through altered subcellular localization of the mutant hGARS proteins seemed not

to be the cause of CMT. However, as aminoacyl-tRNA synthetases are closely connected to mRNA translation and defects in hGARS causes neurodegeneration, mutant hGARS proteins might possibly lead to defective protein synthesis in motor and sensory neurons of the reported *Drosophila* CMT model [23]. Here, cell-type selective protein labeling might be useful to provide data about the protein synthesis rate in motor and sensory neurons *in vivo* giving rise to the cause of this disease.

1.4.2 FMRP and its role in protein synthesis

The fragile X syndrome (FXS) is the most common monogenic cause of inherited mental disability [87]. FXS is an inherited X-chromosomal-linked disease associated with a variety of pathologies including facial abnormalities, developmental delay, autism, and mental retardation [88-92]. The disease is caused by a methylation of a triplet CGG expansion in the 5' untranslated region of the human fragile X mental retardation (*Fmr1*) gene [93, 94]. This leads to the inhibition of *Fmr1* transcription resulting in a loss of function of fragile X mental retardation protein (FMRP) [95]. FMRP is an mRNA-binding protein with three RNA-binding domains [96], known to be involved in various processes in the brain including mRNA shuttling between the nucleus and cytoplasm [97], dendritic mRNA localization [98] and synaptic protein synthesis [99, 100]. A mouse model of FXS suggests a role of FMRP in synaptic plasticity [101] by functioning as a key regulator of mRNA translation [101-105]. Furthermore, it was shown, that the absence of FMRP results in deregulation of protein translation leading to accumulation or reduction of certain synaptic proteins [87]. FMRP was found to act as a negative regulator of protein translation by inhibiting the initiation and elongation of mRNA translation [87, 106, 107]. Thus, mutations of FMRP are accompanied with the inability to inhibit translation *in vitro* and *in vivo* [103, 104], probably leading to an increased protein translation. In *Drosophila* it was shown that treatment of *Fmr1* mutant flies with the protein synthesis inhibitors cycloheximide and puromycin resulted in an improved protein synthesis-dependent LTM formation [108], suggesting that mutations in the *Drosophila* homolog of FMRP (dFMR1) lead to an increased protein synthesis [109]. Nevertheless, there is also evidence that the protein synthesis rate is reduced in synaptoneuroosomes of *Fmr1* knockout mice, when FMRP is absent [110, 111].

However, the exact function of FMRP is not fully understood yet as the literature is contradictory about FMRP's function in local (e.g. dendritic spines) and in global protein synthesis. To investigate the role of FMRP on global protein translation in *Drosophila melanogaster* in a cell-type specific manner, the here introduced cell-type selective metabolic labeling approach using ANL (see 1.3) can be used to determine protein translation rates in a dFMR1 mutant or knockdown background cell-type selectively.

1.4.3 The Rsh learning mutant

Researchers have been trying to unravel the underlying processes of learning and memory formation for the last decades in many different organisms. They could show that proteins encoded by genes such as *dunce* [112, 113], *rutabaga* [114-116], *amnesiac* [117-120], or the protein CREB [121] contribute to the formation of short- (STM), middle- (MTM) and long-term memory (LTM). Interestingly, the Radish (Rsh) protein, encoded by the *rsh* gene [122, 123], seems to contribute to all stages of learning and memory formation. It was shown that the *rsh*¹ mutant has deficits in short-term processes that are relevant for selective attention [22]. *Rsh*¹ mutant flies showed responses characteristic of a reduced attention span, including a reduced optomotor response, induced oscillatory and periodic hyperactivity, defects in responsiveness to turn stereotypy and increased distractibility compared to *wild type* (*wt*) flies [22]. As these phenotypic defects are similar to symptoms of patients suffering from attention-deficit hyperactivity disorder (ADHD), *rsh*¹ mutant flies were treated with methylphenidate (MPH). This treatment produced a significant increase in optomotor response comparable to *wt* flies. Thus, MPH-treatment rescued the deficits in processes that are relevant for selective attention [22]. In contrast to its deficits in short-term processes, initial learning rates of *rsh*¹ mutant flies are normal, however, several hours after training with a classical learning paradigm the memory decays rapidly [122]. In the classical olfactory conditioning paradigm, the flies are trained to associate an odor with an electrical shock (punishment, aversive olfactory conditioning) or with sucrose (reinforcement, appetitive olfactory conditioning). Memory is then tested in a T-maze, where flies need to choose between the two odors [121, 124-126]. The formation of STM, MTM and LTM is tested at specific time points after training. One training session of aversive olfactory conditioning forms STM and MTM but no LTM. Formation of LTM in turn requires repetitive spaced training sessions with rest intervals in between the single training sessions. MTM can be separated into an anesthesia-sensitive form (ASM) and an anesthesia-resistant form (ARM) [122, 127, 128]. Both, ARM and LTM are formed one day after repetitive spaced training, whereas repetitive massed training without rest intervals in between the training sessions induces only ARM [121, 129]. The *rsh*¹ learning mutant was tested in appetitive and aversive olfactory paradigms for its memory formation. The formation of aversive anesthesia-resistant memory (ARM) after single or massed training and the formation of appetitive olfactory LTM is impaired in *rsh*¹ mutant flies, leading to the suggestion that both ARM and protein-synthesis dependent components of appetitive LTM depend on Rsh function [22, 130]. These findings indicate that the mechanisms that underlie appetitive olfactory memory formation are linked; meaning that appetitive LTM and *rsh*¹-dependent ARM do not represent two separable memory phases as previously assumed [129, 131]. However, the formation of aversive olfactory LTM after spaced training is not impaired in *rsh*¹ mutant flies [130].

Different studies gave rise to diverse pathways that are influenced by Rsh or depend on Rsh function, respectively. For instance, the induction of MaPKM ζ (mouse atypical protein kinase M ζ) was found to enhance memory performances in *Drosophila* flies *per se* [132]. Thus, the expression of MaPKM ζ in *rsh*¹ mutant flies rescued the defective ARM formation after massed training. This leads to two assumptions, either (i) MaPKM ζ acts downstream of Rsh or (ii) MaPKM ζ activates a parallel pathway independent of Rsh [132]. Other studies have shown, that serotonin (5-hydroxytryptamine, 5HT) and its receptor d5HT1A act via the Rsh pathway for ARM formation in α/β neurons of mushroom bodies (MBs) and that 5HT from the dorsal paired medial (DPM) neurons, which innervate the MBs, is necessary for ARM formation [133]. MBs are known to be the center of olfactory learning in *Drosophila*. Thus, the localization of Rsh within the peduncle and lobes of the MBs underlines the findings that Rsh plays a role in olfactory learning and memory [123]. On the cellular level it was shown, that Rsh is present in the cell bodies and in the nucleus of the CNS, muscle cells and salivary glands [134].

The behavioral phenotype of the *rsh*¹ mutant flies is rather well characterized. However, the molecular function of the Rsh protein is still rather elusive. Due to an apparent lack of homologies to any other proteins with known function, so far it has been difficult to predict a possible function of Rsh within *Drosophila melanogaster* [123]. Previously, the mutant *rsh*¹ gene could be characterized by a single nucleotide difference, converting a glutamine codon into an amber stop codon, resulting in a truncated protein [123]. The published amino acid sequence of Rsh had only 23 predicted PKA, 14 predicted PKC phosphorylation sites and 5 nuclear localization sites (NLS). Each PKA site overlaps with a NLS site [123]. The overlap of NLS sites with several PKA sites suggested that the phosphorylation state of Rsh might be responsible for the subcellular transition of Rsh between cytoplasm and nucleus. It was hypothesized that activated PKA (cAMP-bound PKA) could phosphorylate Rsh at synapses, initiating Rsh translocation into the nucleus with a subsequent impact on transcription or RNA processing [134]. Additionally it was shown, that several transcripts involved in synaptic transmission, membrane excitability, cell adhesion, cytoskeleton regulation and signaling were up- or down-regulated in *rsh*¹ mutant flies [134]. Taken these facts together, it can be assumed that Rsh might act as a transcription factor in *Drosophila melanogaster* flies. Initial experiments in our lab revealed that the Rhinoceros (Rno) protein is differently expressed in *rsh*¹ mutant and *wt* (Canton-S) flies, underlining the assumption of Rsh to be involved in transcription (Figure 5) [135].

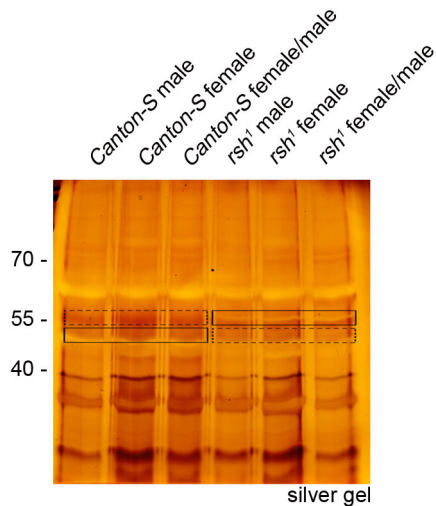


Figure 5: Comparison of total protein expression pattern between *wt* (CS) and *rsh*¹ mutant flies. Protein lysates of *wt* and *rsh*¹ mutant flies were analyzed on silver gel. Remarkably, a missing band was found in *wt* flies at 50 kDa and in *rsh*¹ mutant flies at 55 kDa (black boxes). The corresponding bands (dashed lined boxes) were analyzed with mass spectrometry and both revealed the PHD finger protein Rhinoceros (Rno). Meaning, that this protein might be different expressed between *wt* and *rsh*¹ mutant flies. Modified from Erdmann, 2011 [135].

Rno is a plant homeodomain (PHD) class zinc-finger motif-containing protein, which is located in the nucleus [136]. The N-terminus, containing the PHD domain, is highly conserved across several species including zebrafish, rodents and humans with 39% identity and 61% similarity to aa 1-203 of JADE-1 [136]. Thus, the closest mammalian homolog of Rno is JADE-1. JADE-1 is an interaction partner of the von Hippel-Lindau tumor suppressor and is mainly localized in the nucleus [137]. Despite its PHD motif, JADE-1 was shown to have histone-acetyl transferase activity (HAT) towards histone 4. Rno restricts cell fates within the *Drosophila* eye by regulating the EGFR signaling pathway negatively. *Rno* mutant flies showed excess cone cells, photoreceptors and pigment cells [136]. These findings suggest a role of Rno as a transcription factor by regulating the transcription of key pathway regulators, maybe through histone acetylation like its mammalian homolog JADE-1 [136, 138]. Furthermore, the PHD domain suggests a role in chromatin remodeling and in protein degradation of Rno [139].

The here presented facts, suggest that the Rsh protein might act as a transcriptional regulator in the brain of *Drosophila melanogaster*. Thus, the impact of Rsh on protein synthesis, on the level of transcription and/or translation, needs to be determined. Here again, determination of protein translation rates in *rsh*¹ mutant and wild type flies by using the cell-type selective metabolic labeling approach (see 1.3) might provide valuable insights on the impact of Rsh on protein synthesis, giving rise to potential protein functions.

1.5 Objectives

In the last years a variety of metabolic labeling approaches were developed to investigate protein dynamics underlying synaptic plasticity. However, cell-type selective resolution of activity-induced alteration of a cell's proteome was troublesome so far, as several cell types share a variety of identical proteins. Thus, one was not able to differentiate which protein from which cell-type was altered upon signal transduction. The possibility to unravel such changes in a cell-type selective manner would provide a tremendous progress to solve this problem and would help to understand the molecular mechanisms that e.g. underlie the signal transduction at the tripartite synapse. Therefore, the objective of this thesis was to establish a cell-type specific metabolic labeling approach *in vivo* in *Drosophila melanogaster* using ANL (FlyNCAT - fly non-canonical amino acid tagging, including GIN-/FUN-/BONCAT). A mutant variant of the murine methionyl-tRNA synthetase, mMetRS^{L274G}, had previously been validated by Dr. Anke Müller and Prof. Dr. Daniela C. Dieterich for its ability to incorporate ANL cell-specifically into proteins *in vitro* using primary neuron-glia co-cultures and astrocytic mono-cultures [140, 141]. Prof. Dr. Daniela Dieterich, Oliver Kobler and Dr. Ulrich Thomas generated constructs for transgenic flies, able to express either a mutant murine or *Drosophila* variant of the MetRS in a cell-type specific manner using the Gal4/UAS-system [8, 9]. These mutant variants were used in this study for the cell-type specific introduction of the mutated MetRS into distinct cell types, called GINCAT (genetically introduced non-canonical amino acid tagging). In the following, we established feeding protocols for chronic and acute ANL exposure in *Drosophila melanogaster* larvae and flies (Figure 1) to investigate bulk ANL incorporation into (low-abundant) proteins (chronic feeding) or to investigate protein synthesis-dependent processes (acute feeding). In conjunction with FUNCAT [49-51] and BONCAT [52, 53], the appropriate cell-type selective labeling of protein needed to be validated. Additionally, we evaluated if ANL has toxic effects towards *Drosophila* larvae and flies. These results were published in the following paper: "Cell-selective metabolic labeling of proteomes in *Drosophila melanogaster*" [11]. Cell-type specific metabolic labeling of proteins *in vivo* expands the toolbox of metabolic labeling approaches to study protein synthesis-dependent processes like synaptogenesis, synaptic plasticity, memory formation *in vivo* or the cause of pathological events. Thus, the here established FlyNCAT method was used hereafter to investigate the relative protein translation rates in (i) a Charcot-Marie-Tooth- (CMT-) associated *Drosophila* model [23] (in collaboration with Dr. Erik Storkebaum and Dr. Sven Niehues, Max-Planck Institute for Molecular Biomedicine, Molecular Neurogenetics, Münster), (ii) in *Fmr1*-knockdown larvae and (iii) *rsh*¹ learning mutant flies. As we observed a tremendous reduction of the protein synthesis rate in *rsh*¹ mutant flies, we used 2D gel electrophoresis to investigate the protein expression in *rsh*¹ mutant flies in more detail. Moreover, we repeated the sequence analysis

of the *rsh*¹ gene and Rsh protein as a data bank update from June 2014 suggested that the Rsh protein is far bigger than initially expected by Folkers and colleagues [122, 123]. To get more insights in the molecular function of Rsh on the cellular level, we started to generate and characterized an antibody against Rsh in the scope of this thesis. These findings and tools will provide new insights in the putative molecular function of Rsh in *Drosophila melanogaster*, thereby enhancing our understanding of the underlying molecular mechanisms of learning and memory formation in *Drosophila melanogaster* and in mammals as well.

2 Material and Methods

2.1 Material

2.1.1 Chemicals

All chemicals used were obtained from Roth, Sigma Aldrich, Roche, Thermo Scientific, Invitrogen, Serva or Merck in ACS grade quality. The source of other chemicals or solutions is described in the respective paragraph of the methods section. For molecular biological and protein biochemical experiments molecular biology-graded water from Roth was used. Buffers and solutions were prepared using bi-deionized water (Milli-Q[®] Direct 8, Millipore). The noncanonical amino acids azidonorleucine (ANL) and azidohomoalanine (AHA) were synthesized by Prof. Dr. Daniela C. Dieterich and Dr. Peter Landgraf as described previously via copper-catalyzed diazo transfer [142, 143]. Briefly, in this synthesis *N*_α-(*tert*-Butoxycarbonyl)-L-lysine for ANL or Boc-Dab for AHA is converted in one step to Boc-protected ANL or AHA using the azidofication reagent triflic azide. The biotin-alkyne tag (biotin-PEO-propargylamide) was synthesized by Dr. Peter Landgraf as described previously [50]. The primary and secondary antibodies, used throughout this study for western blot (WB) or immune fluorescent staining (IF), are listed in Table 1 and Table 2.

Table 1: Primary antibodies

antibody	species, clone	dilution	application	Vendor/company
anti-biotin	rabbit, polyclonal	1:10,000	WB	Bethyl Laboratoies Inc.
anti-disc large 4F3	mouse, monoclonal	1:500	WB, IF	Developmental Studies Hybridoma Bank (DSHB)
anti-SYNORF1 3C11	mouse, monoclonal	1:500	WB	DSHB
anti-Draper 8A1	mouse, n/s	1:500	WB	DSHB
anti-Notch C17.9C6	mouse, n/s	1:500	WB	DSHB
anti-dFmr1 5A11	mouse, n/s	1:100	WB	DSHB
anti-GFP (ab290)	rabbit, polyclonal	1:10,000	WB	abcam
anti-Rsh (generated)	guinea pig, polyclonal	1:250	WB	Biogenes, Berlin
anti-Rsh (generated)	rabbit, polyclonal	1:1,000/2,500 1:500	WB IF	Biogenes, Berlin
anti-Brp NC82	mouse, monoclonal	1:100	IF	DHSB
anti-HRP-Cy5	goat, n/s	1:200	IF	Jackson ImmunoResearch Laboratories, Inc.

Table 2: Secondary antibodies

antibody	species, clone	dilution	application	company
anti-rabbit IgG(H+L)-HRP	donkey, polyclonal	1:7,500	WB	Dianova
anti-mouse IgG(H+L)-HRP	goat, polyclonal	1:7,500	WB	Dianova
anti-guinea pig IgG(H+L)-HRP	donkey, polyclonal	1:7,500	WB	Dianova
anti-rabbit IgG(H+L)-680RD	donkey	1:15,000	DB	LI-COR Bioscience
anti-mouse IgG(H+L)-Cy5	goat, polyclonal	1:200	IF	Dianova
anti-rabbit IgG(H+L)-Cy3	donkey, polyclonal	1:1,000	IF	Invitrogen
anti-rabbit IgG(H+L)-Alexa488	donkey, polyclonal	1:1,000	IF	Invitrogen
DAPI (1mg/ml)	-	1:1,000	IF	Sigma

2.1.2 Laboratory animals

Larvae and flies of *Drosophila melanogaster* were raised and crossed in the Institute of Pharmacology and Toxicology of the Otto-von-Guericke University (OvGU) of Magdeburg, Germany), in the Leibniz Institute for Neurobiology (Magdeburg, Germany) and in the Max-Planck Institute for Molecular Biomedicine (Münster, Germany). For an overview of the used fly strains throughout this study see section 2.2.3.2.

2.2 Methods

2.2.1 Molecular biological methods

2.2.1.1 Extraction of genomic DNA of *Drosophila melanogaster*

Squeezing buffer: 10 mM Tris-HCl pH 8.2, 1 mM EDTA, 25 mM NaCl, Protein kinase K (200µg/µl, New England BioLabs® Inc.)

Genomic DNA of *Drosophila melanogaster* was prepared by squishing a single fly in 50 µl squeezing buffer with a pipette tip. The suspension was incubated for 30 min at 37°C with a subsequent inactivation step of the protein kinase K for 2 min at 95°C. DNA concentration was determined using a NanoDrop Lite Spectrophotometer (Thermo Scientific/peqlab).

2.2.1.2 Polymerase chain reaction (PCR)

Phusion DNA Polymerase 2 U/µl (Fermentas)
 Phusion Buffer 5x HF Buffer (Fermentas)
 Primer 10 mM (Biomers, Microsynth)
 dNTP Mix 10 mM (Fermentas)

The appropriate DNA-fragments used for cloning into expression vectors were amplified using specific primers (Supplementary Table 1). Primers were designed using the *rsh*¹ sequence (*radish*¹, transcript variant I, NCBI reference sequence NM_001298247.1) as a

template. A 50 µl PCR reaction contained 0.5 µM primer each, 50-250 ng DNA, 1x HF-Buffer, 1 U Phusion Polymerase and 200 µM deoxynucleotide-triphosphate d(A, C, G, T)TPs each. PCR-reaction was performed using a TProfessional thermocycler (Biometra). A PCR procedure comprised of a single denaturation step at 98°C for 30 s, 35 cycles of denaturation step (98°C, 30 s), primer binding (57°C-72°C, depending on primer sequence) and DNA elongation (72°C, 30 s), followed by a final DNA elongation step (72°C, 10 min). When the annealing temperature was at 72°C a two-step PCR was performed by connecting the primer annealing and the elongation step into one.

2.2.1.3 Restriction digest of DNA

Restriction enzymes	10 U/µl, Fermentas
Buffer	Fermentas

The restriction of DNA fragments and plasmid-DNA was performed according to the manufacturer's protocols for 2 h at 37°C.

2.2.1.4 Agarose gel electrophoresis

Agarose	Serva
1x TAE	40 mM Tris-Acetate, 1 mM EDTA
Midori Green Advanced	0.006 %, Biozym Scientific GmbH
6x DNA loading buffer	30 % (v/v) glycerol, 0.25 % (w/v) xenylcyanol, 50 mM EDTA, pH 8.0
GeneRuler™1kb DNA Ladder	Fermentas
GeneRuler™100bp DNA Ladder	Fermentas

Separation of DNA fragments for analytical and preparative purposes was performed using 1% (w/v) agarose gels with 6 µl Midori Green Advanced (Biozym) per 100 ml in 1x TAE running buffer at 75 V in Compact electrophoresis system M (Biometra). The documentation of the agarose gels was performed by excitation of fluorescence using UV-light of the Viber Lourmat E-Box-VX2-20MX.

2.2.1.5 DNA extraction from agarose gels

Gel extraction kit	Nucleo-Spin® Extract (Macherey Nagel)
---------------------------	--

DNA fragments were visualized after separation using a UV light table (Bachhofer). The desired DNA fragments were cut out using a scalpel and the DNA was extracted according to manufacturer's protocols.

2.2.1.6 Cloning of expression vectors

Ligase	5 U/µl (Fermentas)
Buffer	10x ligase buffer (Fermentas)
LB-agar	15 g agar per 1l
antibiotics	ampicillin (final concentration: 100 µg/ml), kanamycin (final

	concentration: 25 µg/ml)
SOC-medium	20 g/l Bacto-Trypton, 5 g/l yeast extract, 10 mM NaCl,
	2.6 mM KCl, 10 mM Mg ₂ SO ₄ , 10 mM MgCl ₂ , 20 mM glucose
competent <i>E. coli</i> (<i>Escherichia coli</i>)	
XL-10 Gold	endA1 glnV44 recA1 thi-1 gyrA96 relA1 lac The Δ(mcrA)183 Δ(mcrCB-hsdSMR-mrr)173 tet ^R F' [proAB lacI ^q ZΔM15 Tn10(Tet ^R Amy Cm ^R)]
BL-21	<i>E. coli</i> B F ⁻ dcm ompT hsdS(r _B ⁻ m _B ⁻) galλ(DE3) [pLysS Camr]

The ligation of DNA fragments with the appropriate plasmid-DNA was performed in a 3:1 ratio by incubating 5 U ligase per 10 µl reaction mixture at 22°C for 2 h. Subsequently, ligation mixture was transformed into chemical competent *E. coli* XL-10 Gold for plasmid-DNA preparation (2.2.1.7) or in chemical competent *E. coli* BL-21 for the generation of fusion proteins (2.2.4.11). Ligation reaction mixture was incubated with bacteria on ice for 5 min. After a 45 s head shock at 42°C, the bacteria were incubated for 1 h in SOC-medium at 37°C, 600 rpm before they were plated onto LB-agar plates with the appropriate antibiotics. Bacterial colonies were then used for bacterial over night cultures to isolate plasmid-DNA (2.2.1.7).

2.2.1.7 Plasmid-DNA preparation from *E. coli*

LB-medium	5 g/l yeast-extract, 10g/l Bacto-Trypton, 5 g/l NaCl
antibiotics	ampicillin (final concentration: 100 µg/ml), kanamycin (final concentration: 25 µg/ml)
P1-buffer	50 mM Tris-HCl pH 8.0, 10 mM EDTA, 100 µg/ml RNase A (Fermentas)
P2-buffer	200 mM NaOH, 1 % (w/v) SDS
P3-buffer	3 M CH ₃ CO ₂ K, pH 5.5
Kit for Midi-preparation	Macherey Nagel

Isolation of plasmid-DNA was performed using 2 ml of over night *E. coli* XL-10 Gold bacterial cultures, which were grown in 2 ml LB-medium with the appropriate antibiotics over night at 37°C under permanent agitation (Certomat[®] IS, Satorius Stedim Biotech). Extraction of plasmid DNA was performed using alkaline lysis after a modified protocol from Birnboirn & Doly (1979) [144]. Bacteria were spun down at 20,000x g for 1 min at 4°C. The resulting pellet was resuspended in 200 µl P1-buffer. After adding 200 µl P2-buffer and mixing, the suspension was incubated for 5 min at room temperature (RT). After addition of 200 µl ice-cold P3-buffer, mixing and an incubation for 5 min on ice, the samples were spun down at 20,000x g, for 15 min at 4°C. The supernatant was washed with 400 µl of isopropanol for 12 min at RT, following another centrifugation step at 20,000x g for 15 min at 4°C. After another washing step with 70% ice-cold ethanol at 20,000x g for 15 min at 4°C, the DNA pellet was dried and subsequently solved in 50 µl of bi-deionized water.

Isolation of plasmid DNA for Hek293T cells transfections (2.2.2.2) was performed using a Midi-preparation kit. For this, plasmid DNA was isolated from 100 ml of transformed over-night cultures of *E. coli* XL-10 Gold according to manufacturer's protocols.

2.2.2 Cytological Methods

2.2.2.1 Culturing of Hek293T cells

Culture medium	DMEM, 10 % (v/v) fetal calf serum (FCS), 2 mM L-Glutamine, 100 U/ml penicilline, 100 µg/ml streptomycine (all Gibco)
TrypLE™ Express	1x (Gibco)
Poly-D-Lysine	100 mg/ml in 0.15 M boracic acid, pH 8.4
HBSS	Gibco
Culturing plates	6- or 24-well plates (TPP)

A human embryonic kidney cell line (Hek293T) was used for overexpression studies. Maintenance of cultures was done in cell incubators (Heraeus or Thermo Scientific) at 37°C, 5 % CO₂ and 95 % humidity. The cultures were sub-cultured twice a week. Therefor, the cells were washed twice with 37°C warm HBSS containing 1x TrypLE for 3 min and one tenth was transferred into new culture medium. For immunocytochemistry (2.2.5.1) the cells were cultured in 24-well plates on poly-D-lysine treated cover slips. For western blot (2.2.4.8) analysis in turn the cells were cultured in 6-well plates.

2.2.2.2 Transient transfection of Hek293T cells

Solution A	500 mM CaCl ₂
Solution B	140 mM NaCl, 50 mM HEPES, 1.5 mM Na ₂ PO ₄ , pH 7.05
Culture medium	DMEM, 10 % (v/v) fetal calf serum (FCS), 2 mM L-Glutamine, 100 U/ml penicilline, 100 µg/ml streptomycine (all Gibco)

Overexpression of constructs was performed by transfection of Hek293T cells at 80% confluency with the appropriate expression vector using calcium-phosphate-precipitates. For that Hek293T cells were diluted 1:12 one day before transfection.

Transfection of Hek293T cells in 24-well plates via calcium-phosphate-precipitation was performed by mixing 25 µl of solution A thoroughly with 1 µg plasmid-DNA. After adding 25 µl of solution B, the mix was incubated for 1 min at RT. For transfection of Hek293T cells in 6-well plates 150 µl of solutions A and B were mixed with 4 µg of plasmid-DNA respectively. 50 µl using 24-well plates or 300 µl using 6-well plates of the precipitate was added to the cells. The cells were incubated for 4 h at 37°C, 5 % CO₂ and 95 % humidity. After adding 0.5 ml of new media, the transfected cell were incubated for 24 h at 37°C, 5 % CO₂ and 95 % humidity. Transfected Hek293T cells were either used for immunocytochemistry (2.2.5.1) or processed (2.2.4.1.1) for western blot analysis (2.2.4.8).

2.2.3 *Drosophila melanogaster* handling

2.2.3.1 *Drosophila melanogaster* farming

Unless stated otherwise stocks and crosses were grown in incubators (MIR-554-PE, Panasonic) at 25°C in a 14h/10h dark-light cycle on Otto-Normal-Medium (ONM). ONM contained Agar-Agar (0.83% w/v), mashed raisins (4% w/v), yeast (6% w/v), semolina (5%

w/v), sugar beet syrup (2.6% w/v), honey (2.6% w/v) and Nipagin (0.13% v/v). Metabolic labeling was performed as described in 2.2.3.3.

2.2.3.2 *Drosophila melanogaster* fly strains

For experiments either brains or body walls of 3rd instar larvae or fly heads (age as indicated) were used. The fly strains and their origin used in this study are depicted in Table 3. The transgenic MetRS flies were generated as described previously by Erdmann *et al.*, 2015 [11]. Gene expression of mutant hGARS proteins was induced as described by Niehues *et al.*, 2015 [23].

Table 3: Fly strains

Fly strain	Origin	Reference
Driver strains		
<i>elav</i> ^{C155} - <i>Gal4</i> (pan-neuronal)	Bloomington Stock Center, Indiana University (458)	Lin <i>et al.</i> , 1994 [145]
<i>repo-Gal4</i> (glial)	Bloomington Stock Center, Indiana University (4162)	Halter <i>et al.</i> , 1995 [146]
<i>C57-Gal4</i> (muscular)	Prof. Dr. Vivian Budnik	Thomas <i>et al.</i> , 1997 [147]
<i>ubi-Gal4</i> (ubiquitous)	Bloomington Stock Center, Indiana University (32551)	Chen & Megraw, 2014 [148]
<i>OK371-Gal4</i> (motorneuronal)	Bloomington Stock Center, Indiana University (26160)	Mahr <i>et al.</i> , 2006 [149]
<i>ptc</i> ^{559.1} - <i>Gal4</i> (subregional in imaginal disc)	Bloomington Stock Center, Indiana University (2017)	Hinz <i>et al.</i> , 1994 [150]
<i>ppk-Gal4</i> (class IV multidendritic sensory neurons)	Bloomington Stock Center, Indiana University (32079)	Ainsley <i>et al.</i> , 2003 [151]
<i>tubGal80^{TS}; tub-Gal4</i>	Bloomington Stock Center, Indiana University (5138)	McGuire <i>et al.</i> , 2013 [10]
Transgenic strains		
<i>UAS-dMetRS</i> ^{L262G} - <i>EGFP/(TM6b, Tb Hu)</i> (line 2.1)	Dr. Ulrich Thomas, Oliver Kobler, Prof. Dr. Daniela C. Dieterich	Erdmann <i>et al.</i> , 2015 [11]
<i>UAS-mMetRS</i> ^{L274G} - <i>EGFP/(TM6b, Tb Hu)</i> (line 6202-2)	Dr. Ulrich Thomas, Oliver Kobler, Prof. Dr. Daniela C. Dieterich	Erdmann <i>et al.</i> , 2015 [11]
<i>UAS-dMetRS</i> ^{L262G} - <i>3xmyc/(CyO)</i> (line 3.4)	Dr. Ulrich Thomas, Oliver Kobler, Prof. Dr. Daniela C. Dieterich	Erdmann <i>et al.</i> , 2015 [11]
<i>UAS-mMetRS</i> ^{wt} <i>EGFP/(CyO)</i> (line 6202-1)	Dr. Ulrich Thomas, Oliver Kobler, Prof. Dr. Daniela C. Dieterich	Erdmann <i>et al.</i> , 2015 [11]
<i>2x UAS-hGARS</i> ^{G240R}	Dr. Georg Steffes	Niehues <i>et al.</i> , 2015 [23]
<i>2x UAS-hGARS</i> ^{G526R}	Dr. Georg Steffes	Niehues <i>et al.</i> , 2015 [23]
<i>2x UAS-hGARS</i> ^{E71G}	Dr. Georg Steffes	Niehues <i>et al.</i> , 2015 [23]
<i>2xUAS-hGARS</i> ^{wt}	Dr. Georg Steffes	Niehues <i>et al.</i> , 2015 [23]
RNAi strain		
<i>UAS-TRiPFmr1</i>	Bloomington Stock Center, Indiana University (34944)	

Others		
<i>rsh</i> ¹	Prof. Dr. Björn Brembs	Folkers, Drain & Quinn, 1993 [122]
<i>Canton-S (CS)</i>	Prof. Dr. Björn Brembs	Folkers, Drain & Quinn, 1993 [122]
<i>UAS-Fmr1</i>	Bloomington Stock Center, Indiana University (6931)	
<i>w1118</i>	Bloomington Stock Center, Indiana University (3605)	
Recombinant strains		
<i>rsh</i> ¹ ; <i>UAS-dMetRS</i> ^{L262G} - <i>EGFP/(TM6b, Tb Hu)</i> (line 2.1)	Dr. Ulrich Thomas, Ines Erdmann	
<i>bsg</i> ^{CA06978} / <i>CyO</i> ^{GFP} ; <i>C57-Gal4/TM6</i>	Dr. Ulrich Thomas	

2.2.3.3 Metabolic labeling of proteins

ANL was supplied at 2 mM, 4 mM, or 8 mM in the fly food (ONM). For long-term labeling (chronic feeding), crosses were reared continuously on ANL-containing ONM until larvae and flies reached the requested developmental stage (late larval stage L3 or adults, Figure 1). To assess shorter labeling time windows *Drosophila* larvae and flies were fed acutely with ANL depending on the experimental proposes (described below).

Short-term labeling in *Drosophila* larvae for BONCAT: Dr. Kathrin Marter (Institute for Pharmacology and Toxicology, Neural Plasticity and Communication, Otto-von-Guericke University Magdeburg) performed short-term labeling of *Drosophila* larvae for BONCAT experiments. The crosses were reared on ONM for 1-2 days and transferred onto fresh ONM for 4-6 h before removing the parental generation. After 72 ± 2 h at 25°C the 3rd instar larvae (Figure 1) were washed out of the food with warm tap water and rinsed into a mesh basket before they were transferred onto ONM or 4 mM ANL-containing ONM. Larvae were allowed to feed on ANL-containing medium for 24 h.

Dr. Sven Niehues (Max-Planck Institute for Molecular Biomedicine, Molecular Neurogenetics, Münster) performed short-term labeling of hGARS mutant larvae (Figure 1). A two-hour egg collection was performed to obtain larvae of the same age. The eggs were transferred onto 4 mM ANL-containing Jazz-Mix *Drosophila* medium (Fisher Scientific) for 120 h after egg laying.

Short-term labeling in adult *Drosophila* flies for BONCAT: Crosses were reared on ONM w/o ANL. Adult offspring (Figure 1) were transferred onto 4 mM ANL-containing ONM 0 to 3 days post-eclosion and analyzed for ANL incorporation after 24 h and 48 h.

Pulse-chase labeling for BONCAT: Larvae were allowed to feed on ANL-containing ONM until they reached the late L3 wandering state (Figure 1). Half of wandering L3 stage larvae was transferred onto ONM w/o ANL (chase group) until eclosion, whereas their siblings remained on ANL-containing ONM.

Labeling of proteins with AHA: Julia Bussmann (Max-Planck Institute for Molecular Biomedicine, Molecular Neurogenetics, Münster) performed AHA labeling of *w1118* and hGARS mutant *Drosophila* flies (Figure 1) for BONCAT experiments. For this baker's yeast was labeled with AHA or Met (methionine) by incubating 1 g of baker's yeast with 4 mM AHA or Met for 42 h at 30°C, 200 rpm. After a centrifugation step (7,000x g, 30 s, RT), the yeast pellet was resuspended in water. *Drosophila* flies were fed with 200 µl of AHA- or Met-fed baker's yeast on filter paper for 24 h or 48 h.

2.2.3.4 Toxicity of ANL towards *Drosophila* larvae and flies

The body weight of wandering L3 stage larvae was determined to exclude any putative toxicity of ANL towards *Drosophila* larvae. For this, 10 male flies of the UAS-strain (*UAS-dMetRS^{L262G}-EGFP* or *UAS-mMetRS^{L274G}-EGFP*) were crossed to 10 female virgin flies of the *C57-Gal4* strain. Body weights of either *dMetRS^{L262G}-EGFP* or *mMetRS^{L274G}-EGFP* expressing larvae were determined using an ultra fine scale (Sartorius) and compared between larvae reared on ONM with 2 mM, 4 mM, 8 mM ANL, or without ANL. Data was analyzed using ONE-way ANOVAs with Dunnett post hoc tests. Additionally, linear regression analyses were performed to test for a linear relationship between ANL incorporation and larval body weight.

Any putative toxicity of ANL towards adult *Drosophila* flies was analyzed by determining the hatching rate of *MetRS^{LtoG}*-expressing flies exposed to different ANL concentrations (2 mM, 4 mM, 8 mM ANL or w/o ANL). For this five male flies of the UAS-strain (*UAS-dMetRS^{L262G}-EGFP* or *UAS-mMetRS^{L274G}-EGFP*) were crossed to five virgin female flies of the driver strain (either *elav^{C155}-Gal4* or *repo-Gal4*) and reared on ONM containing 2 mM, 4 mM, 8 mM ANL or without ANL (chronic ANL exposure). Parental flies were removed before the offspring reached the pupal stage. After hatching of the first offspring generation flies (approx. 10-11 days after the crossing was started) the number of offspring was counted every second day over a time period of 10 days. The metamorphosis and eclosion rate was determined by comparing the total number of *dMetRS^{L262G}-EGFP*- or *mMetRS^{L274G}-EGFP*-expressing flies to the group size relative to the segregation after Mendel's law. Statistical analysis was performed using one sample t-test against a theoretical mean of 1.0. A linear regression analysis was performed to investigate the correlation between ANL incorporation and eclosion rate of adult flies. All statistical analyses were performed using GraphPad Prism Version 5.0b.

Additionally, the survival rate of *MetRS^{LtoG}-EGFP* expressing flies was investigated to exclude any toxic effect of ANL towards *Drosophila* flies. For this, neuronal or glial *dMetRS^{L262G}-EGFP*-expressing flies that were chronically exposed to ONM containing 2 mM, 4 mM or 8 mM ANL, or without ANL, were transferred either to ONM with the same ANL

concentration as previously (e.g. 2 mM ANL – 2 mM ANL) or to ONM without ANL (e.g. 2 mM ANL – w/o ANL). Over a period of 14 days the number of living flies was determined every other day.

2.2.4 Biochemical methods

2.2.4.1 Protein extractions

2.2.4.1.1 Protein extraction from Hek293T cells

1x PBS	137 mM NaCl, 2.7 mM KCl, 4.3 mM Na ₂ HPO ₄ • 7 H ₂ O, 1.4 mM KH ₂ HPO ₄ , pH 7.8
1x PBS-MC	1x PBS, pH 7.4, 0.5 mM CaCl ₂ , 5 mM MgCl ₂
Protease inhibitor (PI)	complete EDTA-free Protease Inhibitor cocktail tablets
Triton-X-100	20% (v/v)
SDS	20% (w/v)
Benzonase®	≥ 250 U/μl
4x SDS protein sample buffer	250 mM Tris, 20% (v/v) β-mercaptoethanol, 1% (w/v) SDS, 40% (v/v) Glycerol, 0.004% bromphenolblue, pH 6.8

Transfected Hek293T cells grown in 6-well plates (2.2.2.2) were washed once with 1 ml 1x PBS-MC before harvesting. The harvest of cells was performed in 1 ml of 1x PBS pH 7.8. The cells were spun down at 3,000x g for 5 min at 4°C. The supernatant was discarded and the pellet was resuspended in 150 μl 0.05% SDS in 1x PBS pH 7.8 – 1x Protease Inhibitor (PI) w/o EDTA. After adding 0.5 μl Benzonase®, the cells were incubated for 7 min at 95°C. After cooling down on ice 50 μl of 4x SDS-sample buffer was added and again the suspension was incubated for 7 min at 95°C. Afterwards the lysates were used for SDS-PAGE (2.2.4.6) and western blot analysis (2.2.4.8).

2.2.4.1.2 Protein extraction from larval body walls, larval brains and adult fly heads of *Drosophila melanogaster*

HL-3 (hemolymph-like solution)

	70 mM NaCl, 5 mM KCl, 20 mM MgCl ₂ • 6 H ₂ O, 10 mM NaHCO ₃ , 115 mM sucrose, 5 mM trehalose, 5 mM HEPES, 0.1 mM CaCl ₂
1x PBS	137 mM NaCl, 2.7 mM KCl, 4.3 mM Na ₂ HPO ₄ • 7 H ₂ O, 1.4 mM KH ₂ HPO ₄ , pH 7.8
Homogenization buffer	0.5% (w/v) SDS in 1x PBS pH 7.8 – 2x PI w/o EDTA supplemented with 1 μl Benzonase® (≥ 250 U/μl) per 100 μl homogenization buffer
Triton-X-100	20% (v/v)
SDS	20% (w/v)
Protease inhibitor	complete EDTA-free Protease Inhibitor Cocktail Tablets

Protein extraction was performed either from larval body walls (final amount of 2.5-3.5 mg wet tissue), from 60-200 larval brains, or from 20 heads of adult *Drosophila* flies. Body walls or larval brains were dissected in HL-3 solution with 0.1 mM Ca²⁺. *Drosophila* heads were collected after anesthetizing flies with CO₂ by cropping heads from the body using a fine scissor. Body walls, larval brains, or fly heads were transferred to glass homogenizers

(Wheaton). Protein extraction was done from 2.5-3.5 mg of body wall material, 60-200 larval brains, or 20 fly heads in 100 µl homogenizing buffer. Homogenates were incubated for 20 min at RT under permanent agitation before incubation at 95°C for 7 min. After cooling down on ice 20% (v/v) Triton-X-100 was added to a final concentration of 1% (v/v), and homogenates were diluted with 1x PBS, pH 7.8 - 2x PI w/o EDTA to a final concentration of 0.1% (w/v) SDS and 0.2% (v/v) Triton-X-100. After an incubation for 1 h at 4°C under permanent agitation, the suspension was spun down at 3.000x g, 5 min, 4°C. The resulting supernatants ('lysates') were transferred to new 1.5 ml Eppendorf tubes. Lysates were either used for BONCAT (see 2.2.4.2) or were directly subjected to SDS-PAGE (2.2.4.6) and western blot analysis (2.2.4.8).

2.2.4.2 Bio-orthogonal non-canonical amino acid tagging (BONCAT)

Biotin-PEO ₃ -alkyne-Tag	25 mM in 1x PBS pH 7.8
Copper(I)Bromide-Suspension	10 mg/ml in ultrapure water
Triazol-Ligand	Tris[(1-benzyl-1H-1,2,3-triazo-4-yl)methyl]amine) 200 mM in DMSO
Zeba [®] desalting columns	Thermo Scientific
1x PBS	137 mM NaCl, 2.7 mM KCl, 4.3 mM Na ₂ HPO ₄ • 7 H ₂ O, 1.4 mM KH ₂ HPO ₄ , pH 7.8
1x PBS-SDS	0.05 % (w/v) SDS in 1x PBS pH 7.8,
Protease inhibitor	complete EDTA-free Protease Inhibitor Cocktail Tablets

A modified BONCAT protocol according to Dieterich *et al.* (2007) was used to detect AHA- or ANL-labeled proteins in *Drosophila* larvae and flies [52]. For this, AHA- or ANL-labeled protein lysates were tagged by adding triazol ligand (1:1,000), biotin-PEO₃-alkyne tag (1:1,000) and copper(I)bromide suspension (1:100) as described previously [52]. The samples were incubated over night at 4°C under permanent agitation. Precipitates were removed in a subsequent centrifugation step (3,000x g, 5 min, 4°C). The resulting supernatant was subjected to a desalting procedure to remove excess reagents. For this, desalting columns were washed three times with 1 ml 1x PBS-SDS with a subsequent centrifugation step (1,000x g, 2 min, 4°C). Afterwards, samples were added to the columns and spun down at 1,000x g, 2 min, 4°C. Samples were supplemented with 50x PI w/o EDTA (final concentration: 2x).

2.2.4.3 Determination of protein concentrations with amido black assay

Standard	0.5 mg/ml BSA
Staining solution	14.4 g/l amido black 10B
Washing solution	90 % (v/v) methanol, 10 % (v/v) acetic acid
Resolving solution	0.1 M NaOH

Determination of protein concentration was performed using the amido black assay according to Becker (1966) [152]. For this, the protein concentration was determined by means of a BSA-calibration series. This BSA-calibration series was then used to determine

the protein concentration, which was calculated as a mean of three measured single values. The absorption was determined using a microplate reader (Biochrome Asys) at 620 nm.

2.2.4.4 NeutrAvidin purification of ANL- or AHA-labeled biotin-tagged proteins

NeutrAvidin™ Agarose-Resin	Thermo Scientific
1x PBS	137 mM NaCl, 2.7 mM KCl, 4.3 mM Na ₂ HPO ₄ • 7 H ₂ O, 1.4 mM KH ₂ HPO ₄ , pH 7.8
Igepal - 630	Sigma
1x PBS-Igepal-630	1x PBS, pH 7.8, 1% (v/v) Igepal-630
2x SDS sample buffer	125 mM Tris, 10% (v/v) β-mercaptoethanol, 0.5% (w/v) SDS, 20% (v/v) Glycerol, 0.002% bromphenolblue, pH 6.8

Purification of ANL-labeled biotin-tagged proteins derived from neuronal expression was performed using 100 µl of high-capacity NeutrAvidin agarose, whereas ANL-labeled biotin-tagged proteins derived from muscular and glial expression or AHA-labeled biotin-tagged proteins derived from adult fly heads were purified using 150 µl of high-capacity NeutrAvidin agarose. The NeutrAvidin agarose suspension was equilibrated with three washes of 1 ml 1x PBS-Igepal-630 each by inverting the tube several times followed by a centrifugation step (3,000x g, 5 min, 4°C). Tagged lysates with equal protein concentrations (2.2.4.3) were incubated with 1% Igepal for at least 20 min at 4°C under permanent agitation. Lysates were then incubated with NeutrAvidin agarose over night at 4°C, again under permanent agitation. After another centrifugation step (3,000x g, 5 min, 4°C) the supernatants were transferred to new Eppendorf tubes. NeutrAvidin agarose was washed five times for 5 min each with 1x PBS-Igepal-630 and three times for 5 min each with 1x PBS, pH 7.8, each washing step (at RT) was followed by a centrifugation step (3,000x g, 5 min, 4°C). AHA- or ANL-labeled biotin tagged proteins were eluted with 2x SDS sample buffer (0.5x volume of the suspension volume) for 7 min at 95°C. Eluates were collected after a centrifugation step (3,000x g, 5 min, 4°C), transferred to new tubes and processed SDS-PAGE (2.2.4.6) following western blot analysis (2.2.4.8) or dot blot analysis (2.2.4.9).

2.2.4.5 Purification of GFP-tagged proteins and mass spectrometry analysis

HL-3 (hemolymph-like solution)	70 mM NaCl, 5 mM KCl, 20 mM MgCl ₂ • 6 H ₂ O, 10 mM NaHCO ₃ , 115 mM sucrose, 5 mM trehalose, 5 mM HEPES, 0.1 mM CaCl ₂
µMACS GFP isolation kit Mylteni	Biotec
Protease inhibitor	complete EDTA-free Protease Inhibitor Cocktail Tablets
Elution buffer	50 mM Tris-HCl, pH 6.8, 50 mM DTT, 1% (w/v) SDS, 0.005% bromphenolblue, 10% glycerol
Destaining solution	50 mM Na ₂ S ₂ O ₅ • 5H ₂ O, 15 mM C ₆ FeK ₃ N ₆

Body walls of 16 *Bsg*^{CA06978}; *C57-Gal4/UAS-dMetRS*^{L262G}-EGFP, ANL-fed (ONM with 4 mM ANL, chronic feeding) 3rd instar larvae were dissected in ice-cold HL-3 solution as described (see 2.2.4.1.2). The µMACS GFP isolation kit (Mylteni Biotec) was used in combination with µMACS anti-GFP micro beads according to the manufacturer's instructions. Briefly, proteins

were isolated using 400 μ l lysis buffer (2x PI w/o EDTA) provided in the kit and mixed with 80 μ l μ MACS anti-GFP beads. Following incubation on ice for 1 h the suspension was loaded onto a μ MACS column, pre-equilibrated with 200 μ l lysis buffer. The flow through was collected as a control. After five washing steps, the EGFP-tagged proteins were eluted in two elution steps (50 μ l each) using the elution buffer recommended in the manufacturer's protocol but without EDTA. The pooled eluted fractions (100 μ l) were separated on 10% Tris-Glycine PAA gels (1.5 mm) and silver stained (see 2.2.4.7, protocol for mass spectrometry). Corresponding bands at 130 kDa were cut out and destained using 50 mM sodiumthiosulfatepentahydrate ($\text{Na}_2\text{S}_2\text{O}_5 \cdot 5\text{H}_2\text{O}$) and 15 mM potassiumcyanoferrate ($\text{C}_6\text{FeK}_3\text{N}_6$) and send to Dr. Tamar Ziv (Smoler Proteomics Center, Faculty of Biology, Technion, Haifa, Israel), who performed the mass spectrometry (MS) analysis of GFP-tagged proteins according to Erdmann *et al.* (2015) [11].

2.2.4.6 Sodium dodecyl sulfate polyacrylamide gel electrophoresis (SDS-PAGE)

Tris-Glycine Gels

4x separation gel buffer (homogen)	1.5 M Tris-HCl, 0.4 % (w/v) SDS, pH 8.8
4x stacking gel buffer (homogen)	0.5 M Tris-HCl, 0.4 % (w/v) SDS, pH 6.8
4x separation gel buffer (gradient)	1.8 M Tris-HCl, pH 8.8
4x stacking gel buffer (gradient)	0.5 M Tris-HCl, pH 6.8
Rotiphorese 30	30 % (v/v) acrylamide, 0.8 % (v/w) bis-acrylamide
Rotiphorese 40	40 % (v/v) acrylamide, 0.8 % (v/w) bis-acrylamide
25 ml 9.5% separation gel solution for 5 gels (homogenous):	6.25 ml 4x separation gel buffer, 7.92 ml Rotiphorese 30, 8.75 ml bidest. water, 10.42 μ l 0.5 % (w/v) bromphenolblue, 1.88 ml 87% (v/v) glycerol, 166.67 μ l 10 % (w/v) APS, 16.67 μ l TEMED (AppliChem)
13 ml 5% stacking gel solution for 5 gels (homogenous):	3.25 ml 4x stacking gel buffer, 2.14 ml Rotiphorese 30, 4.53 ml bidest. water, 11.56 μ l phenolred (2000x), 2.96 ml 87 % (v/v) glycerol, 74 μ l 10 % (w/v) APS, 18.5 μ l TEMED (AppliChem)
13.5 ml 5% separation gel solution for 5 gels (gradient):	2.85 ml 4x separation gel buffer, 1.69 ml Rotiphorese 40, 7.89 ml bidest. water, 132 μ l 10% (w/v) SDS, 132 μ l 0.2 M EDTA, 0.75 ml 87 % (v/v) glycerol, 48 μ l 10 % (w/v) APS, 9 μ l TEMED (AppliChem)
13.5 ml 20% separation gel solution for 5 gels (gradient):	2.85 ml 4x separation gel buffer, 9.11 ml Rotiphorese 40, 0.58 ml bidest. water, 132 μ l 10 % (w/v) SDS, 132 μ l 0.2 M EDTA, 0.8 μ l 0.004 % bromphenolbue, 3 ml 87 % (v/v) glycerol, 30 μ l 10 % APS, 9 μ l TEMED (AppliChem)
9.9 ml 15% stacking gel solution for 5 gels (gradient):	2.5 ml 4x stacking gel buffer, 1.6 ml Rotiphorese 30, 3.3 ml bidest. water, 100 μ l 10 % (w/v) SDS, 100 μ l 0.2 M EDTA, 5 μ l phenolred (2000x), 2.3 ml 87% (v/v) glycerol, 61.75 μ l 10 % APS, 7.6 μ l TEMED (AppliChem)
4x SDS protein sample buffer	250 mM Tris, 20 % (v/v) β -mercaptoethanol, 1 % (w/v) SDS, 40 % (v/v) glycerol, 0.004 % bromphenolblue, pH 6.8
Electrophoresis buffer	192 mM glycine, 1 % (w/v) SDS, 25 mM Tris, pH 8.3

Tris-Acetate Gels

4x gel buffer	62.5 mM Tris-Base, pH 7.0
Rotiphorese 30	30 % acrylamide, 0.8 % bis-acrylamide

13 ml 4% separating gel solution for 5 gels (gradient):	3.25 ml 4x gel buffer, 1.75 ml Rotiphorese 30, 7.25 ml bidest. water, 0.75 ml 87 % (v/v) glycerol, 50 µl 10 % (w/v) APS, 10 µl TEMED (AppliChem)
13 ml 8% separating gel solution for 5 gels (gradient):	3.25 ml 4x gel buffer, 3.5 ml Rotiphorese 30, 3.25 ml bidest. water, 50 µl 0.5 % (w/v) bromphenolblue (Merck), 3 ml 87 % (v/v) glycerol, 50 µl 10 % (w/v) APS, 10 µl TEMED (AppliChem)
10 ml 3.5% stacking gel solution for 5 gels (gradient):	2.5 ml 4x gel buffer, 1.2 ml Rotiphorese 30, 4 ml bidest. water, 25 µl phenolred (2000x), 2.3 ml 87 % (v/v) glycerol, 60 µl 10 % (w/v) APS, 10 µl TEMED (AppliChem)
4x SDS protein sample buffer	250 mM Tris-HCl, pH 8.5, 0.1 % bromphenolblue, 2 mM EDTA, 40 % (v/v) glycerol, 8 % SDS (v/v), 100 mM DTT
Electrophoresis buffer	50 mM Tris-Base, 50 mM tricine, 0.1 % (w/v) SDS, pH 8.24
PageRuler™ Plus Prestained Protein Ladder	Fermentas
PageRuler™ Prestained Protein Ladder	Fermentas

Protein separation was performed using the SDS-PAGE method described by Laemmli (1970) [153]. Protein sample buffer (4x) was added to the samples to a final concentration of 1x and incubated for 7 min at 95°C before they were loaded either onto 9.5% homogenous, 5%-20% gradient Tris-Glycine-SDS-PAGE or 4%-8% gradient Tris-Acetate-SDS-PAGE. The gel system was selected depending on protein size. In the course of this study all SDS-PAGEs were run loading equal protein concentrations. Electrophoresis was performed in Hoefer Mighty Small System SE250 (Amersham Bioscience) at 8-12 mA in 1x electrophoresis buffer. Gels were used either for gel staining (see 2.2.4.7) or for western blot analysis (see 2.2.4.8).

2.2.4.7 Silver gel staining

Silver gel staining for protein concentration adjustment

Fixative	30 % (v/v) ethanol, 10 % (v/v) acetic acid
Wash solution	10 % (v/v) ethanol
Silver solution	0.1 % (w/v) silver nitrate (Fluka)
Developer solution	3 % (w/v) sodium carbonate, 0.02 % (v/v) formaldehyde
Stop solution	1 % (v/v) acetic acid

Silver gel staining for mass spectrometry analysis

Fixative	40 % (v/v) ethanol, 10 % (v/v) acetic acid
Wash solution	30 % (v/v) ethanol
Thiosulfate reagent	0.02 % (w/v) sodium thiosulfate
Silver solution	0.2 % (w/v) silver nitrate, 0.02 % (v/v) formaldehyde
Developer solution	3 % (w/v) sodium carbonate, 0.05 % (v/v) formaldehyde, 0.0005 % (w/v) sodium thiosulfate
Stop solution	= fixative

Silver gel staining for adjustment of protein concentrations were performed according to Heukeshoven & Dernick (1985) [154] or for MS analysis according to a modified protocol after Blum *et al.* (1987) [155]. Briefly, proteins were fix in the gel over night by incubating gels in fixative at RT under gentle agitation. After several washing and sensitization steps, the gels were incubated with silver solution under gentle agitation at RT for 20-30 min.

Incubation of the gel with the developer solution visualized the protein bands. Incubating gels with stop solution finalized this reaction.

For adjustment of protein concentrations, the protein bands were compared for equal signal intensity (by eye).

For MS analysis of protein bands, the according bands were cut out and analyzed either by Dr. Thilo Kähne (Institute of Experimental Internal Medicine, OvGU Magdeburg) or Dr. Tamar Ziv (Smoler Proteomics Center, Faculty of Biology, Technion, Haifa, Israel).

2.2.4.8 Western blot analysis

Western blot buffer	192 mM glycine, 25 mM Tris-Base, 0.2% (w/v) SDS, 20% (v/v) methanol pH 8.3
Poncaeu S-staining solution	0.5% (w/v) Ponceau S in 3% (v/v) acetic acid
1x TBS	140 mM sodium chloride, 250 mM Tris-HCl, pH 7.6
TBS-T	0.1% (v/v) Tween-20 in 1x TBS
TBS-TA	0.02% (v/v) sodium-azide in TBS-T
Blocking solution I	5% milk powder in TBS-T
Blocking solution II	5% BSA in TBS-T
Nitrocellulose Membrane I	Protran[®], Whatman[®], 0.45 μm
Nitrocellulose Membrane II	Odyssey[®], LI-COR Bioscience, 0.22 μm
ECL Reagent	ECL Western Blotting Substrate or SuperSignal[™] West Dura Extended Signal Duration

This method was performed according to Twobin *et al.* (1992) [156]. Protein transfer onto a nitrocellulose membrane was performed at 200 mA at 4°C for 1.5-4 h depending on the protein size. After the blotting procedure the nitrocellulose membrane was incubated for 10 min with Ponceau-S staining solution at RT.

For immuno-detection the membrane was incubated for 1 h in blocking solution I or II at RT under permanent agitation. Incubation with primary antibody was done over night at 4°C under permanent agitation. Primary antibody dilution was done either in blocking solution I (biotin-antibody and antibodies obtained from DSHB), in blocking solution II (generated antibodies against Radish) or in TBS-TA (all other antibodies). Nitrocellulose membranes were washed three times with TBS-T for 10 min before incubation with the secondary antibody for 1.5 h at RT under permanent agitation. Following two additional washing steps with TBS-T and one with TBS, the nitrocellulose membrane was treated with ECL (electrochemiluminescence) reagent according to manufacturer's protocol before documentation. Documentation of the chemiluminescence signal was done using an Odyssey FC scanner (LI-COR Bioscience).

2.2.4.9 Dot blot analysis, immuno-detection and statistical analysis

1x TBS	140 mM sodium chloride, 250 mM Tris-HCl, pH 7.6
TBS-T	0.1% (v/v) Tween-20 in 1x TBS
Blocking solution II	5% BSA in 1x TBS
Nitrocellulose Membrane	Protran [®] , Whatman [®] , 0.45 µm

The dot blot analysis was performed according to Dieterich *et al.* (2007) [52]. For this the same eluate fractions of the NeutrAvidin purification (2.2.4.4) as for western blot analysis were used. Eluate fractions were diluted 1:200, 1:100 and 1:50 in 1x TBS and applied in triplets to the nitrocellulose membrane. The nitrocellulose membrane was incubated with blocking solution for 1 h at RT under permanent agitation before incubation with an anti-biotin antibody diluted in blocking solution II over night at 4°C under permanent agitation. After three washing steps with 1x TBS for 10 min each, the nitrocellulose membrane was probed with a fluorescence secondary antibody (Table 2) for 1.5 h under permanent agitation at RT. After another three washing steps with 1x TBS for 10 min each, signal detection was performed using an Odyssey FC scanner (LI-COR Bioscience) at a wavelength of 700 nm. For quantification, gray values of dots (1:100 dilution) of three to four independent experiments were determined using ImageJ64 software. Student's t-test with or without (as indicated) Welch's correction (two-tailed) was used for statistical analysis using GraphPad Prism[®] Version 5.0b.

2.2.4.10 2D Gel electrophoresis and mass spectrometry analysis

1x TBS	140 mM sodium chloride, 250 mM Tris-HCl, pH 7.6
Protease inhibitor	complete EDTA-free Protease Inhibitor Cocktail Tablets
Lysis buffer	1x TBS pH 8.0, 1% (w/v) deoxycholic acid, 0.5% (v/v) Igepal-630, 1% (v/v) Triton-X-100, 1x PI w/o EDTA
Benzonase [®]	≥ 250 U/µl

The 2D gel electrophoresis was performed with *rsh*¹ (*radish*¹) mutant and *wild type* (*Canton-S*) flies, which were divided into the following conditions: (a) *rsh*¹ females + males (same ratio), (b) *rsh*¹ females, (c) *rsh*¹ males, (d) wild type females + males (same ration), (e) wild type females and (f) wild type males. 500 heads (female:male, 250:250) of 0-3 day old flies were mashed in 1 ml of lysis buffer. After adding 1 µl Benzonase[®], lysates were incubated for 25 min at RT under permanent agitation. After incubating lysates for 7 min at 95°C and a subsequent cooling step for 5 min on ice, lysates were spun down at 3,000x g for 5 min at 4°C. Supernatants were transferred into a new 15 ml falcon and diluted 1:10 before subjecting them to 2D gel electrophoresis after the O'Farrell protocol (1975) [157]. 2D Gel electrophoresis was performed by Kathrin Pohlmann (Special Lab Molecularbiological Techniques, Leibniz Institute for Neurobiology, Magdeburg, Germany). Protein spots of silver gel stained 2D gels were analyzed using the PDQuest software (Biorad) together with Dr.

Karl-Heinz Smalla (Special Lab Molecular Biological Techniques, Leibniz Institute for Neurobiology, Magdeburg, Germany). The optical density (OD) of each spot was determined using PDQuest software analysis. This comparison of the ODs between *wt* and *rsh*¹ mutant flies was performed using a statistical analysis with a significance level of $p \leq 0.1$. The content of all spots that seemed to be different in their ODs were analyzed using MS analysis. For this the proteins were extracted from each spot picked, digested with trypsin and the resulting peptides were analyzed with LC-MS/MS analysis (Yvonne Ducho and Dr. Thilo Kähne, Institute for Experimental Medicine, Otto-von-Guericke University, Magdeburg). The determined spectra were organized using the ProteinScape® (Bruker Daltonics) software. The alignment of each single experimental mass spectrum was performed over the Mascot Server (Matrix Science) using the protein database UniPort (www.uniprot.org), and identified the protein content of each spot.

2.2.4.11 Generation of fusion proteins

LB medium	5 g/l yeast-extract, 10g/l Bacto-Trypton, 5 g/l NaCl
antibiotics	ampicillin (final concentration: 100 µg/ml)
IPTG	0.1 M
1x PBS	137 mM NaCl, 2.7 mM KCl, 4.3 mM Na₂HPO₄ • 7 H₂O, 1.4 mM KH₂HPO₄, pH 7.4
Protease inhibitor	complete EDTA-free Protease Inhibitor Cocktail Tablets
Amylose resin	New England BioLabs® Inc.
Washing buffer for Amylose resin	1x PBS pH 7.4
Maltose	Serva

The MPB-Rsh²³⁵⁻⁵¹⁵ fusion protein was generated using transformed *E.coli* BL-21 cells (2.2.1.6) with the appropriate expression vector (Supplementary Table 3). For this, 100 ml over-night bacterial culture were grown for 1 h at 37°C in 1 l LB-medium with the appropriate antibiotic under permanent agitation, before adding 5 ml of 0.1 M IPTG to induce protein expression. Bacteria were incubated for another 4 h at 37°C under permanent agitation. After a centrifugation step (Beckman Coulter Avanti® J-E Centrifuge; rotor: J-14) at 5,000x g for 7 min at 4°C, the bacterial pellets were resuspended in 45 ml 1x PBS pH 7.4. Bacterial suspension was frozen at -80°C at least for one day.

Protein extraction was performed using a Constant Cell Disrupter System TS 0.75kW (Constant Systems Ltd.). For this cells were disrupted with 25 KPSI at 4°C. Homogenates were collected and PI w/o EDTA was added to a final concentration of 2x. Following, the homogenates were spun down at 12,000x g for 20 min at 4°C (Beckman Coulter Optima XPN-80 Ultracentrifuge, rotor: SW 32Ti). The pellet was resuspended in 1 ml 1x PBS pH 7.4 and frozen at -20°C. The supernatant i.e. protein extract was used for purification of MPB-Rsh²³⁵⁻⁵¹⁵ fusion protein.

For purification of MPB-Rsh²³⁵⁻⁵¹⁵ fusion protein 2 ml of amylose resin were equilibrated by two washing steps using 10 ml washing buffer for 5 min under permanent agitation at 4°C

with a following centrifugation step at 600x g for 5 min at 4°C. Protein extracts were incubated with the amylose resin for 1 h under permanent agitation at 4°C. After another three washing steps as described above, the MPB-Rsh²³⁵⁻⁵¹⁵ fusion protein was eluted from the amylose resin using 600 µl of a 20 mM maltose elution buffer for 10 min under permanent agitation at 4°C. After another centrifugation step (600x g, 5 min 4°C), the supernatant was transferred into a new Eppendorf tube. The elution step was repeated another 2 times. The MPB-Rsh²³⁵⁻⁵¹⁵ fusion protein was used for the antibody generation against Radish (see 2.2.6).

2.2.5 Fluorescent staining methods

2.2.5.1 Immunocytochemistry of transfected Hek293T cells

4 % PFA	4 g in 1x PBS pH 7.5-8.0
B-Block	1x PBS pH 7.4, 10 % (w/v) normal horse serum, 5 % (w/v) saccharose, 2 % (w/v) BSA
B-Block-T	B-Block, 0.1% (v/v) Triton-X-100
1x PBS	137 mM NaCl, 2.7 mM KCl, 4.3 mM Na ₂ HPO ₄ • 7 H ₂ O, 1.4 mM KH ₂ HPO ₄ , pH 7.4
1x PBS-T	1x PBS pH 7.4, 0.3 % (v/v) Triton-X-100
DAPI	see Table 2
Mowiol	10 % mowiol, 25 % glycerol, 100 mM Tris-HCl pH 8.5, 2.5% (DABCO)

Transfected Hek293T cells were fixed for 5 min at RT with 4 % paraformaldehyde (PFA), following three washing steps with 1x PBS pH 7.4 at RT. To block unspecific binding sites, cells were incubated for 1.5 h with B-Block-T under gentle agitation at RT. Cover slips were then transferred into a humid, dark chamber and incubated with the primary antibody (Table 1), diluted in B-Block-T, over night under gentle agitation at 4°C. Cover slips were washed three times with 1x PBS-T for 10 min at RT before incubation with the appropriate secondary antibody (Table 2) for 1.5 h at RT. After another two washing steps with 1x PBS-T and one with 1x PBS for 10 min at RT, cell nuclei were stained with DAPI (Table 2) for 10 min at RT. Cover slips were washed once more with 1x PBS for 10 min at RT and mounted in Mowiol.

2.2.5.2 Fluorescent non-canonical amino acid tagging (FUNCAT) and immunocytochemistry of larval body walls

HL-3 (hemolymph-like solution)

	70 mM NaCl, 5 mM KCl, 20 mM MgCl ₂ • 6 H ₂ O, 10 mM NaHCO ₃ , 115 mM sucrose, 5 mM HEPES, 0.1 mM CaCl ₂
PB	solution A: 0.1 M Na ₂ HPO ₄ •2 H ₂ O pH 8.8, solution B: 0.1 M NaH ₂ PO ₄ •H ₂ O pH 4.1 → mix solution A with solution B until pH 7.2
PBT	0.2% (v/v) Triton-X-100 in 0.1 M PB pH 7.2
4% PFA	4 g in 100 ml 0.1 M PB pH 7.2
TAMRA-alkyne tag	200 mM in DMSO
Coppersulfate	200 mM in ultrapure H ₂ O
Triazol-Ligand	200 mM in DMSO
TCEP	Tris[(1-benzyl-1H-1,2,3-triazol-4-yl)methyl]amine, 400 mM in ultrapure H ₂ O
1x PBS	137 mM NaCl, 2.7 mM KCl, 4.3 mM Na ₂ HPO ₄ • 7 H ₂ O, 1.4 mM KH ₂ HPO ₄ ,

PBS-Tw	pH 7.4
Antibodies	1% (v/v) Tween-20 in 1x PBS pH 7.4
VectaShield™	see Table 1
Mounting Medium	Vector Laboratories
Nail polish	p2, dm

Larval Body walls were dissected in HL-3 solution with 0.1 mM Ca²⁺ and pre-fixed with 2-3 drops of 4% PFA for 1 min. All following incubation steps were performed in darkness. After exchanging the solution to 4% PFA in PB pH 7.2 body walls were incubated for 20 min at RT under gentle agitation. Following fixation, body walls were washed three times with PBT and another three times with 1x PBS pH 7.8 both for 15 min each at RT under gentle agitation. ANL-labeled proteins were tagged by mixing triazole ligand (1:1,000), TAMRA-alkyne tag (1:5,000), TCEP solution (1:1,000) and CuSO₄ solution (1:1,000) in 1x PBS pH 7.8. After each addition the solution was mixed thoroughly for 10 s using a high-speed vortexer. Body walls were incubated with 200 µl of this mixture over night at 4°C under gentle agitation. Subsequently, body walls were washed three times with PBS-Tw and PBT for 15 min each at RT under gentle agitation before incubation with primary and secondary antibodies. Primary antibodies were diluted as depicted in Table 1 in PBT and incubated over night at 4°C under permanent agitation in the dark. After another three washing steps with PBT for 15 min each under permanent agitation at RT, body walls were incubated with the appropriated secondary antibodies (Table 2) in PBT for 2 h at RT under permanent agitation. After immunostaining body walls were washed once more three times for 15 min each with PBT at RT under gentle agitation in the dark. Finally body walls were mounted in VectaShield, cover slips were sealed with a thin layer of nail polish and stored at 4°C until imaging.

2.2.5.3 Microscopy

Images of larval body wall muscles and CNS were acquired on a Leica-SP5 confocal microscope. Hek293T cells were imaged using a microscope from Axioplan 1 imaging (Zeiss).

2.2.6 Data Bank analysis

DNA and protein sequence analysis of Radish (*rsh/Rsh*) and Rhinoceros (*rno/Rno*) were performed using ensemble.org, flybase.org, uniprot.org, Interpro (ebi.ac.uk) and Clustal Omega 1.2.1 data basis. DNA sequences of *rsh* were investigated using the following NCBI accession numbers: NM_001298247.1, NM_001298248, NM_001298249, NM_001298250, NM_001298251 and NM_132622.4. For protein sequence analysis (uniprot.org & Interpro) of Rsh the following accession numbers were used: X2DJH0, X2JJU0, X2JEQ0, X2JF15, X2JBI1 and Q9I7S4.

For investigation of *rno* DNA sequences the following NCBI accession numbers were used: NM_206222.3, NM_138163.2 and NM_001259599.2. For protein sequence analysis (uniprot.org & Interpro) of Rno the accession number Q7YZH1 was used.

Clustal Omega 1.2.1 multiple sequence alignment was performed using the protein accession numbers of uniprot.org.

2.2.7 Antibody generation

Generation of Rsh antisera in guinea pig and rabbit was performed by BioGenes GmbH (Berlin) using a MPB-Rsh²³⁵⁻⁵¹⁵ fusion protein (5 mg/ml, 2.2.4.11) for immunization. The MPB-Rsh²³⁵⁻⁵¹⁵ fusion protein consists of a MBP-tag (maltose binding protein) and a part of the Rsh protein covering amino acids 235-515 (Supplementary Figure 2). Two Guinea pigs and two rabbits were injected with the MPB-Rsh²³⁵⁻⁵¹⁵ fusion protein (boost) and test bleedings were performed as depicted in Table 4.

Table 4: Immunization of guinea pigs and rabbits with MPB-Rsh²³⁵⁻⁵¹⁵ fusion protein

Guinea pig		Rabbit	
day	works	day	works
0	Pre-serum/Immunization	0	Pre-serum/Immunization
14	boost	7	boost
28	boost	14	boost
42	test bleding	28	bleeding/boost
56	boost	35	bleeding
70	final bleeding	56	boost
		63	boost
		70	test bleeding
		91	boost
		98	boost
		105	test bleeding
		126	boost
		133	boost
		140	final bleeding

Each test bleeding during Rsh antibody generation was tested for the ability of the antisera to specifically detect Rsh on western blot (2.2.4.8) and in immunofluorescent stainings (2.2.5.1).

3 Results

3.1 Endogenous wild-type Methionyl-tRNA synthetase (MetRS) incorporates AHA, but not ANL into proteins of *Drosophila melanogaster*

Previous studies showed that the non-canonical amino acid azidohomoalanine (AHA) is incorporated into proteins using the endogenous wild type MetRS and the endogenous protein synthesis machinery. Several studies have shown that AHA can be used to visualize and identify newly synthesized proteins in bacteria [54], mammalian cell culture [49, 50, 56, 57] and larval zebrafish [58] by previously introduced techniques FUNCAT [49-51] and BONCAT [52, 53].

To test whether living *Drosophila melanogaster* larvae and flies can utilize AHA for metabolic protein labeling as well, *w1118* larvae and flies were fed with AHA-containing food (4 mM, feeding and head preparation performed by Julia Bussmann, Max-Planck Institute for Molecular Biomedicine, Molecular Neurogenetics) and analyzed using BONCAT (Figure 6). Head lysates of *w1118* flies, acutely fed with 4 mM AHA-labeled yeast for 48 h, were subjected to BONCAT-mediated coupling of the azide group of AHA to the alkyne group of a biotin-alkyne affinity tag resulting in AHA-labeled biotin-tagged proteins, prospectively referred to as biotin-tagged proteins. Biotin-tagged proteins were then analyzed on western blot using an antibody against biotin. Samples from AHA-fed flies showed a robust signal for biotin on western blot covering the whole molecular weight range, demonstrating that AHA is incorporated by the endogenous MetRS into proteins of any size (Figure 6). As expected, the biotin signal for smaller proteins is weaker than for proteins of greater size, because the former have fewer methionines (Met) that can be potentially replaced by AHA. Western blots of head lysates of Met-fed flies (Met-labeled yeast, 4 mM Met, acute feeding) were devoid of any biotin signal, except for a band at 130 kDa (Figure 6), which is most likely derived from one of the endogenously biotinylated proteins [158]. As the 130 kDa band in AHA-labeled samples is not only composed of endogenous biotinylated proteins but contains also biotin-tagged proteins, the signal intensity for this band was stronger in AHA-fed flies compared to Met-fed flies. FUNCAT analysis of body wall preparations of L3 stage larvae using the red-fluorescent dye tetramethylrhodamine (TAMRA) revealed that larvae fed chronically with AHA-containing (4 mM) Otto-Normal-Medium (ONM) showed a robust incorporation of AHA into larval body walls and any tissues attached to it [11]. In contrast, chronic ANL feeding to *w1118* larvae showed no TAMRA-signal [11], demonstrating that the endogenous MetRS is unable to use ANL as a substrate. The reason behind that is that ANL harbors an enlarged side chain (Figure 4a) leading to an exclusion from the binding pocket of the endogenous MetRS. Thus, the endogenous MetRS fails to load ANL onto its cognate Met-tRNA and prevents ANL incorporation into proteins.

These first experiments showed that *Drosophila melanogaster* larvae and flies are amenable to use AHA as a Met substrate for incorporation into proteins. AHA incorporation is sufficient to detect AHA-labeled proteins either using western blot analysis (BONCAT) or fluorescent microscopy (FUNCAT, [11]). Due to the highly selective click reaction, only low background staining was observed in Met-controls.

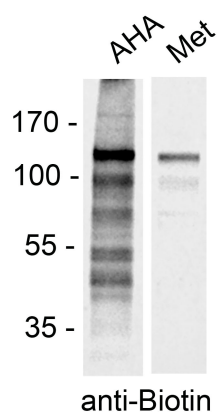


Figure 6: *Drosophila* larvae are able to use AHA as a substrate to label proteins for their detection using click chemistry (BONCAT). Western blot analysis of biotin-tagged proteins derived from head lysates of AHA-fed (48 h) *w1118* flies revealed a strong biotin signal for AHA-labeled proteins across the whole molecular range. In contrast, head lysates of Met-fed flies lacked the biotin signal. Only a band at 130 kDa composed of endogenously biotinylated proteins was detected here. n=3 independent experiments. Modified after Erdmann *et al.* (2015)

3.2 Generation of transgenic MetRS^{LtoG} flies

Since the binding pocket of the endogenous MetRS of *Drosophila melanogaster* is unable to use ANL as a substrate [11], the construction of mutant MetRS variants with an enlarged amino acid binding pocket, which is able to efficiently incorporate ANL into *Drosophila* proteins, was necessary.

Previous studies uncovered several mutations within the MetRS binding pocket of *Escherichia coli* (*E. coli*) enabling the activation of ANL by the mutant MetRS, and, therefore, allowing its incorporation into proteins during protein synthesis [66-69, 159]. Among them the single amino acid mutant EcMetRS^{L13G} showed efficient incorporation of ANL into newly synthesized proteins. A leucine to glycine substitution at position 13 within the amino acid sequence results in an enlarged MetRS binding pocket (Figure 4b). Consequently, ANL can be loaded onto its cognate tRNA for its incorporation into proteins [66, 67]. The MetRS binding pocket is evolutionary well conserved (Figure 7) [160], which led to the construction of an enhanced green fluorescent protein (EGFP)-tagged murine mutant MetRS variant. Prof. Dr. Daniela C. Dieterich generated the mutant mMetRS^{L274G}-EGFP construct with the respective leucine to glycine substitution at position 274 within the amino acid sequence [11, 161]. Prof. Dr. Daniela C. Dieterich and Dr. Anke Müller showed that this mutant MetRS^{LtoG} variant is able to efficiently incorporate ANL cell-type selectively into newly synthesized proteins in mammalian cell culture assays [161]. Additionally, a *Drosophila* MetRS variant (dMetRS^{L262G}-EGFP) was generated by substituting leucine with glycine at the respective position 262 within the amino acid sequence (Prof. Dr. Daniela C. Dieterich, Dr. Ulrich

Thomas and Oliver Kobler, Figure 7) [11]. In order to drive this mutant enzymes cell-type specifically in *Drosophila* larvae and flies, the following Gal4-inducible UAS-constructs were generated: *UAS-mMetRS^{L274G}-EGFP*, *UAS-dMetRS^{L262G}-EGFP*, *UAS-dMetRS^{L262G}-3xmyc* and a *UAS-mMetRS^{wt}-EGFP* construct, functioning as a control. The generated UAS-constructs were used for germline injections at BestGene Inc. (CA, USA) to establish individual lines for each construct. The following lines were used throughout this study: *UAS-mMetRS^{wt}EGFP/(CyO)* (line 6202-1), *UAS-mMetRS^{L274G}-EGFP/(TM6b, Tb Hu)* (line 6202-2) and *UAS-dMetRS^{L262G}-EGFP/(TM6b, Tb Hu)* (line 2.1).

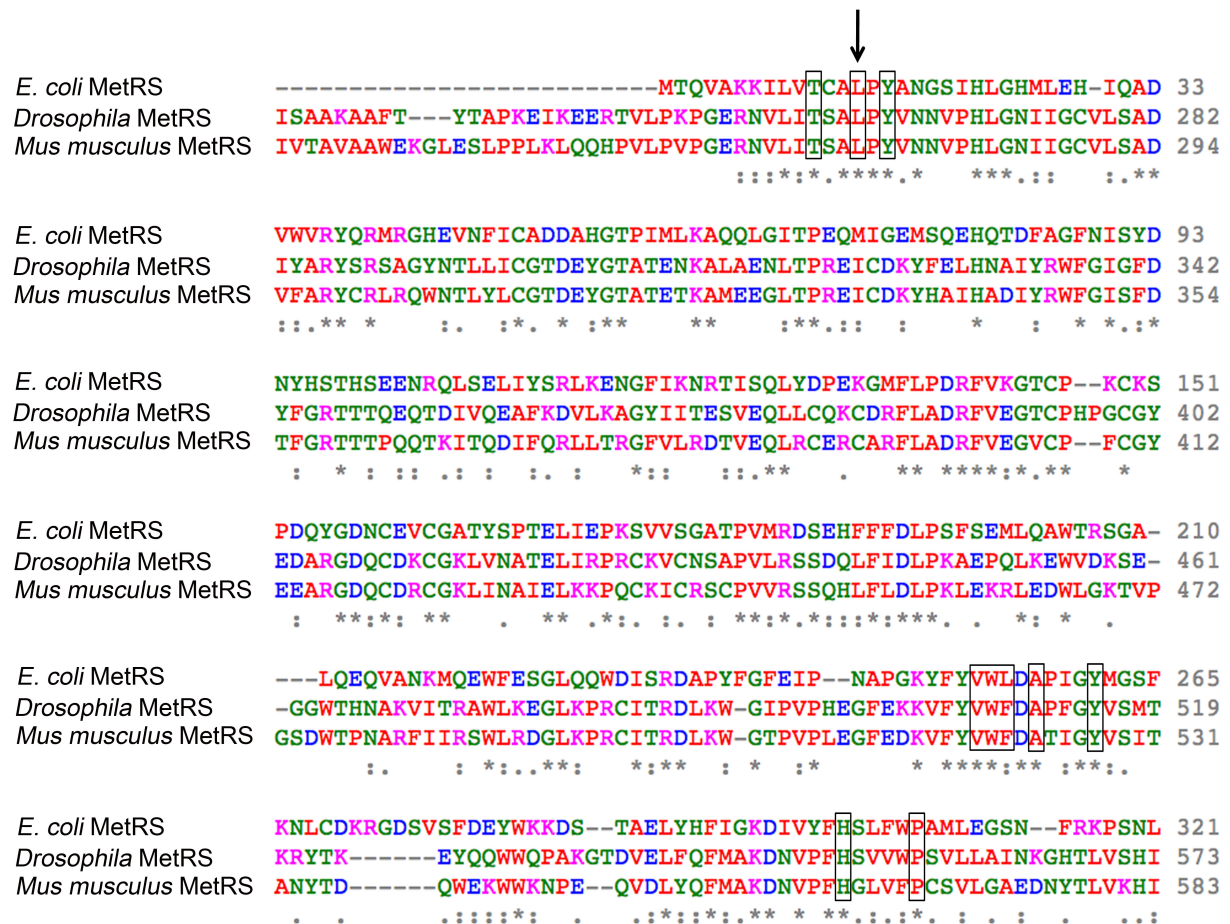


Figure 7: Sequence alignment of orthologous MetRS. Clustal O (1.2.0) multiple sequence alignment of *E. coli* MetRS (K02671), *Drosophila* MetRS (CG15100), and *Mus musculus* MetRS (BC079643). Conserved residues that are critical for the binding pocket architecture are framed [160]. The arrow indicates the respective position of the leucine to glycine substitution in mMetRS^{L274G} and dMetRS^{L262G} variants. Positions of amino acids within the respective sequence are depicted at the right. Modified after Erdmann *et al.* (2015)

3.3 Visualization of cell-type specific protein labeling with ANL using FUNCAT

The generated mutant MetRS variants were tested for their ability to incorporate ANL into newly synthesized proteins *in vivo*. For this, the different UAS-strains were crossed to various cell-type restricted Gal4-driver lines to express the mutant MetRS-variants specifically in respective cell types of *Drosophila* larvae and flies [8, 9]. The cell-type specific

expression of either MetRS variant should lead to a cell-type specific incorporation of ANL into proteins, enabling the investigation of cell-type specific proteome dynamics.

Here, FUNCAT was used to investigate whether the expression of the mutated MetRS variants leads to successful ANL incorporation into proteins using the fluorescent alkyne-tag (TAMRA-tag) via click chemistry. For this, parental flies of either UAS-strain (*UAS-dMetRS^{L262G}-EGFP*, *UAS-mMetRS^{L274G}-EGFP*) were crossed to a neuronal (*elav^{C155}-Gal4*) or to a glial specific driver (*repo-Gal4*) to restrict MetRS expression to neurons or glia cells respectively. Crossings were reared on ANL-containing (4 mM) ONM throughout life (chronic ANL feeding). Control crossings were reared on ONM without ANL. The fluorescent TAMRA-tag showed a strong fluorescent signal for ANL-labeled proteins in neurons of larval brains (Figure 8a) or in glia cells at larval neuromuscular junction (NMJ; Figure 8b) of body wall preparations from *dMetRS^{L262G}-EGFP*- or *mMetRS^{L274G}-EGFP*-expressing larvae. Remarkably, no TAMRA-signal was found in any other tissue or cell type of these preparations. Thus, ANL incorporation was restricted to the *dMetRS^{L262G}-EGFP*- or *mMetRS^{L274G}-EGFP*-expressing cell type; even when different cell types were present in close contact within the specimen (Figure 8a, b). Body wall preparations of the control crossings showed no TAMRA-signal (Figure 8a), showing the specificity of both ANL incorporation and the click reaction. Additionally, expression of either *MetRS^{LtoG}* variant was tested in other tissues and confirmed that only larvae expressing either mutant MetRS variant were able to use ANL as a substrate leading to an effective and cell-type specific ANL incorporation into proteins [11]. Magnification of *dMetRS^{L262G}-EGFP*-expressing muscle cells showed, that TAMRA-tagged proteins are found throughout the cell [11]. Meaning, that ANL incorporation was abundant in the cytosol, nuclei and in the area of the bouton surrounding subsynaptic reticulum [11]. This indicates, that ANL-harboring proteins belong to different protein categories, including soluble and membrane-associated proteins.

These first experiments showed that monitoring ANL incorporation with FUNCAT upon target expression of either type of *MetRS^{LtoG}* variant is restricted to *MetRS^{LtoG}-EGFP*-expressing cell types. Thus, the here reported *MetRS^{LtoG}* variants are able to use ANL as a substrate for cell type specific protein incorporation to track proteome dynamics cell-type specifically. Fluorescent tagging of ANL-labeled proteins in larval brains revealed that ANL-labeled proteins could be visualized in complex and tightly organized structures.

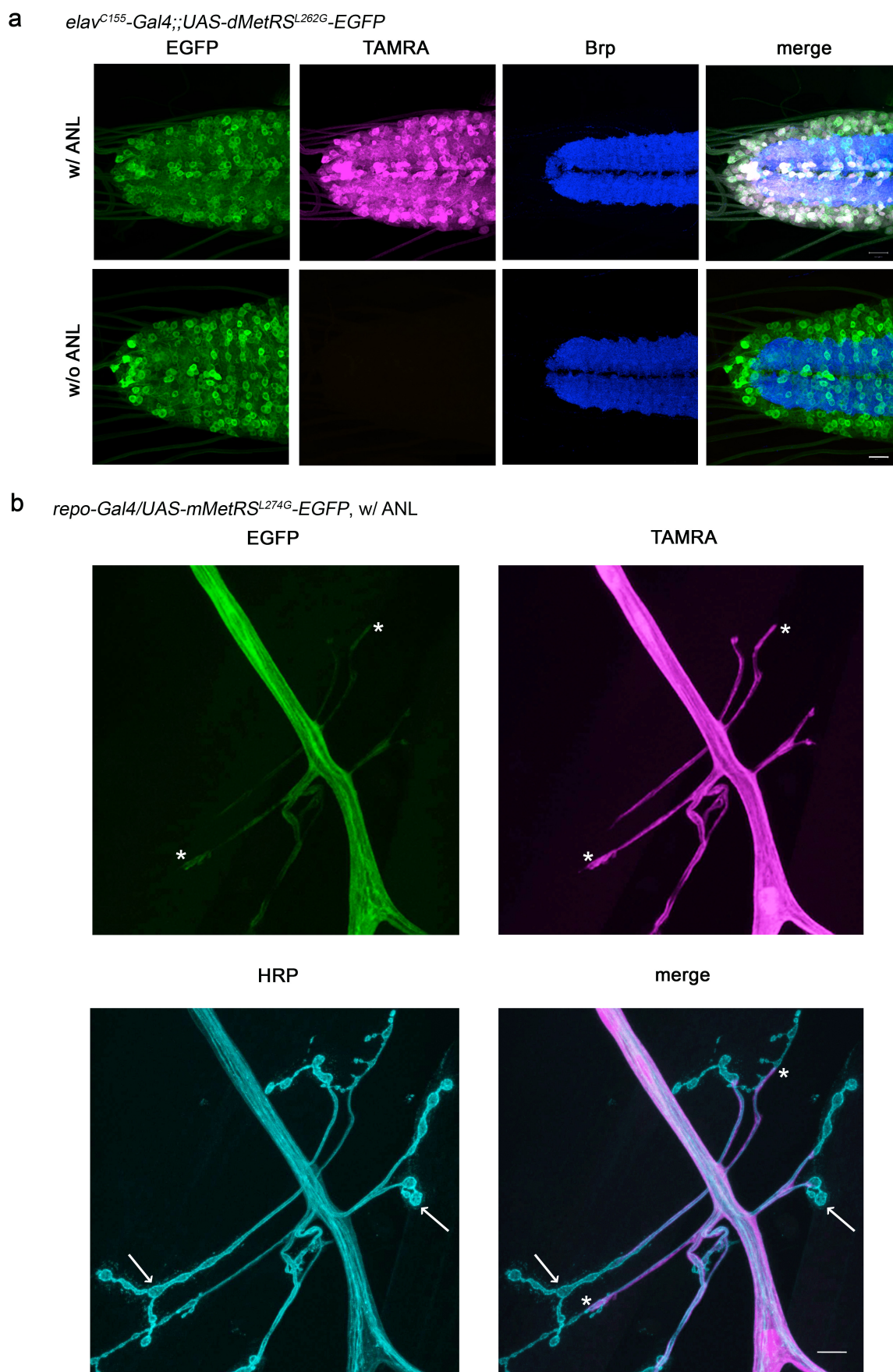


Figure 8: ANL incorporation upon target expression of MetRS^{LtoG}-EGFP in neurons and glia cells of *Drosophila* larvae. Target expression of dMetRS^{L262G}-EGFP in neurons of larval brains (a) and mMetRS^{L274G}-EGFP in glia cells at larval NMJs (b) resulted in a cell-type specific ANL

incorporation, reflected by the signal of the TAMRA-tag. This incorporation was restricted to MetRS^{LtoG}-EGFP-expressing tissues (*b*, asteriks and arrows). Control groups showed no ANL-incorporation (*a*, lower panel). arrow = synaptic boutons, asteriks = end of glial process. Scale bars (*a*) 20 μ m, (*b*) 10 μ m. Experiments (*a*) Ines Erdmann, Dr. Kathrin Marter, Julia Abele; Experiment (*b*) image taken by Oliver Kobler. Modified after Erdmann *et al.* (2015).

3.4 Identification of cell-type specific protein labeling with ANL using BONCAT

FUNCAT visualizes ANL-labeled proteins but one is not able to distinguish whether ANL is incorporated into just a few abundantly expressed proteins or into many different proteins. To discriminate, which of these categories of proteins and how many are labeled with ANL, the mMetRS^{L274G}-EGFP variant was expressed either in larval muscle cells (*C57-Gal4*) and in neurons (*elav^{C155}-Gal4*) or in glia cells (*repo-Gal4*) of *Drosophila* flies. Crosses were reared on ANL-containing ONM (4 mM, chronic ANL-feeding), whereas control groups were raised on non-ANL-containing ONM expressing the mMetRS^{L274G}-EGFP. Body wall or head lysates were then subjected to BONCAT. After a desalting step, protein concentrations were adjusted using an amido black assay. This was done for all western blot analyses shown in this study. ANL-labeled biotin-tagged proteins were affinity purified to separate ANL-labeled biotin-tagged proteins from non-labeled/-tagged ones. Different fractions (input, unbound and eluate fraction) of ANL-labeled and biotin-tagged proteins were analyzed on western blot using either an antibody against biotin or against cell-type specific candidate proteins. Protein lysis, BONCAT, desalting of samples, adjustment of protein concentration, NeutrAvidin purification and western blot analysis are hereupon referred to as the 'BONCAT-protocol' (see section 2.2.4.1.2, 2.2.4.2 – 2.2.4.4, 2.2.4.6, 2.2.4.8).

The alkyne-affinity tag enables the purification of ANL-labeled biotin-tagged proteins. The biotin-tagged input (I) fraction consists of ANL-labeled, ANL-labeled and biotin-tagged proteins as well as non-ANL-labeled proteins (before affinity purification). Affinity purification separated ANL-labeled biotin-tagged proteins from non-labeled/-tagged ones resulting in two fractions: the unbound (U) fraction consisting of no ANL-containing and non-biotin-tagged proteins, and the eluate (E) fraction consisting of enriched ANL-labeled biotin-tagged proteins (referred to as biotin-tagged proteins). Western blot analysis depicted in Figure 9a-c ('anti-Biotin') revealed a strong signal for biotin in muscle cells of *Drosophila* larvae (Figure 9a), and in neurons (Figure 9b) and glia cells (Figure 9c) of *Drosophila* flies in the input and eluate fractions, when mMetRS^{L274G}-EGFP-expressing larvae or flies were fed chronically with ANL. Affinity purification of proteins leads to an enrichment of biotin-tagged proteins, resulting in an increased biotin signal of the eluate fractions. Notably, ANL was efficiently incorporated into muscle, neuronal and glial proteins across the entire molecular weight range. As for AHA-labeled proteins (Figure 6), the biotin signal intensity for smaller proteins is not as strong as for proteins of higher molecular weight, most likely reflecting fewer Met replacement sites available in smaller proteins. Additionally, as the *UAS-MetRS^{LtoG}-EGFP-*

expressing larvae/flies are knock-in animals and the endogenous MetRS is still expressed, the endogenous and the mutant MetRS compete for Met versus ANL incorporation into the same proteins. In control groups only a few distinct bands were detected, reflecting most likely endogenously biotinylated proteins (Figure 9a-c, 'anti-Biotin') [158]. Using specific antibodies against selected proteins revealed biotin-tagged proteins specific for each cell type tested in ANL-fed mMetRS^{L274G}-EGFP-expressing larvae and flies (Figure 9a-c, 'anti-candidate protein'). Using an antibody against the protein Discs-Large (Dlg) on western blot of protein lysates of larval body walls expressing the mMetRS^{L262G}-EGFP, revealed two distinct bands (Figure 9a, 'anti-Dlg'), representing the isoforms DlgA and DlgS97 in muscle cells of *Drosophila* larvae. Both isoforms were detectable at about equal quantities in the eluted fraction; thus, both Dlg isoforms are expressed in comparable amounts in muscle cells as indirectly indicated previously [162]. By expressing the single-pass transmembrane protein Basigin (Bsg) endowed with EGFP in larval body wall lysates from *Bsg*^{CA0698/+;C57-Gal4/UAS-mMetRS^{L274G}-EGFP-expressing animals, biotin-tagged EGFP-Bsg was detected in eluate fractions (Figure 9a, 'anti-GFP'). This indicates that ANL becomes incorporated into transmembrane proteins. Other ANL-labeled candidate proteins detected were the synaptic vesicle protein Synapsin (Figure 9b, 'anti-Synapsin') in neurons of head lysates as well as the glial engulfment receptor Draper (Figure 9c, 'anti-Draper8A1') and again Dlg (Figure 9c, 'anti-Dlg') in glia cells of head lysates. Control groups showed no specific bands for biotin-tagged candidate proteins in the eluate fractions (Figure 9a-c, 'anti-candidate protein'). Larvae and flies expressing the dMetRS^{L262G}-EGFP variant showed very similar signals for bulk ANL-labeling of overall proteins and for cell-type specific proteins (Figure 10).}

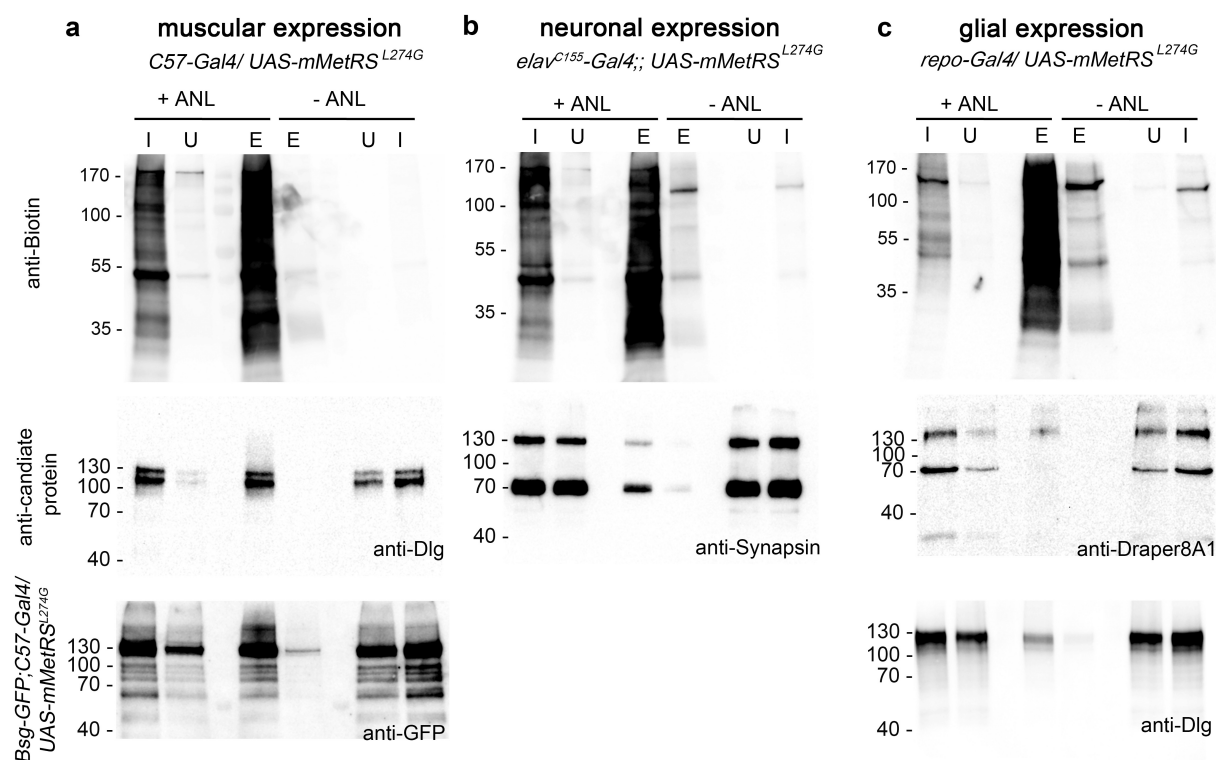
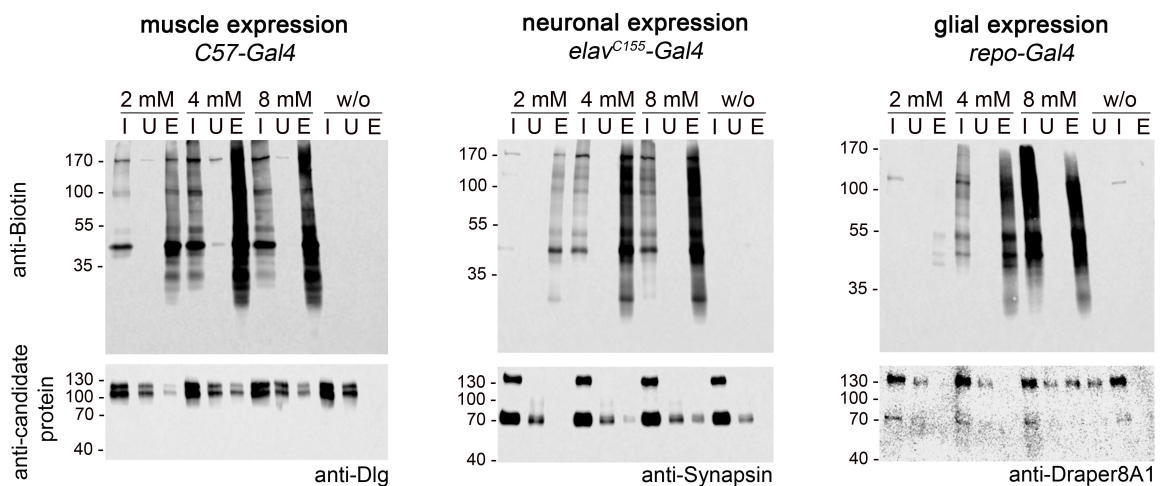


Figure 9: Detection of affinity purified biotin-tagged proteins in *Drosophila* larvae and flies using BONCAT. Protein lysates of L3 stage larval body walls (a) or protein lysates of fly heads (b, c) were subjected to BONCAT, using a biotin-alkyne affinity tag, and subsequent affinity purification. Depicted are representative western blots run in mirror-image order showing the tagged input (I, before purification), unbound (U, non-biotin tagged proteins and no ANL-containing proteins) and eluted (E, enriched ANL-labeled proteins after NeutrAvidin purification) fractions of ANL-labeled and control samples. Western blots of either cell type showed an intense signal for biotin (upper panel), proving that ANL is efficiently incorporated into proteins of muscle cells (a), neurons (b) and glial cells (c) in mMetRS^{L274G}-EGFP-expressing larvae (a) or flies (b, c) after chronic ANL treatment. After affinity purification biotin-tagged proteins were enriched in the eluate fractions. Control groups showed no biotin signal for ANL-labeled proteins (a-c). Aside from bulk labeling of overall proteins, ANL-labeling was verified for selected marker proteins specific for each cell type tested. Efficient ANL-labeling was shown for Dlg (a, medial panel) and Bsg (a, lower panel) in muscle cells, for neuronal Synapsin (b, medial panel), as well as for Draper (c, medial panel) and Dlg (c, lower panel) in glia cells. n=3-4 independent experiments. Modified after Erdmann *et al.* (2015).

After establishing the general BONCAT-protocol in *Drosophila* larvae and flies, different ANL concentrations were applied to check if lower or higher concentrations of ANL resulted in higher incorporation rates. For this, flies carrying either the *UAS-dMetRS*^{L262G}-EGFP or the *UAS-mMetRS*^{L274G}-EGFP construct were crossed again to a muscle- (*C57-Gal4*), a neuron- (*elav*^{C155}-*Gal4*) or a glial-specific (*repo-Gal4*) driver line. Crosses were reared on ONM containing 2 mM, 4 mM or 8 mM ANL (chronic feeding). When larvae or flies expressed the dMetRS^{L262G}-EGFP variant, the biotin signal intensity for biotin-tagged protein increased from 2 mM to 4 mM to 8 mM ANL (Figure 10a, 'anti-Biotin'). The same increase of the signal intensity was detectable for any of the tested candidate proteins. The signal intensity for biotin-tagged Dlg, Synapsin or Draper increased with higher ANL concentrations (Figure 10a, 'anti-candidate protein'). Investigation of ANL incorporation mediated by the mMetRS^{L274G}-EGFP for different ANL concentrations revealed a slightly different result. Upon

mMetRS^{L274G}-EGFP expression in muscle cells of *Drosophila* larvae, the biotin signal intensity for global proteins and for the candidate protein Dlg increased from 2 mM to 4 mM ANL (Figure 10b, first column). Higher ANL concentrations resulted in larval lethality (see 3.7) and, hence, could not be analyzed on western blot. Expression of mMetRS^{L274G}-EGFP in neurons and glial cells of adult flies led to an intense ANL-labeling of global proteins and of respective candidate proteins at 2 mM ANL compared to higher concentrations of 4 mM or 8 mM ANL (Figure 10b, 'anti-Biotin' and 'anti-candidate protein'). This might be due to massive ANL incorporation at higher concentrations, which in turn could influence the epitope accessibility for the antibodies in a negative manner.

a UAS-dMetRS^{L262G}-EGFP



b UAS-mMetRS^{L274G}-EGFP

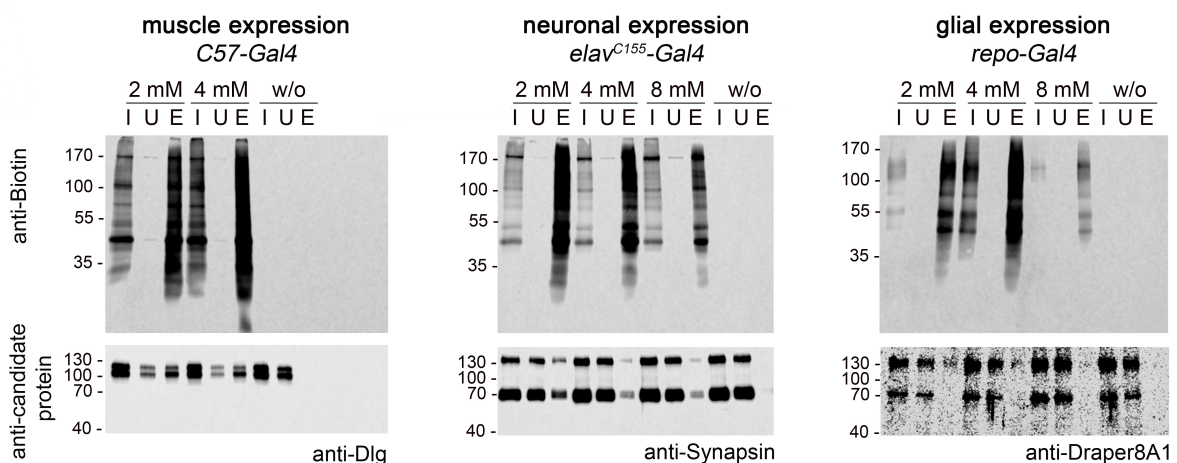


Figure 10: Chronic ANL incorporation into muscle, neuronal and glial proteins using differing ANL concentrations. Protein lysates of L3 stage larval body walls (a, b, first column) and of fly heads (a, b, second and third column) were subjected to BONCAT-protocol after chronic ANL feeding using different ANL concentrations as indicated. Depicted are representative western blots showing input (I, before NeutrAvidin purification), unbound (U, non-biotin tagged proteins and no ANL-containing proteins), and eluted fractions (E, enriched ANL-labeled proteins after NeutrAvidin purification) at the global protein level ('anti-Biotin') and for selected candidate proteins ('anti-candidate protein'). (a) ANL

incorporation mediated by the dMetRS^{L262G}-EGFP variant resulted in an elevated signal intensity for ANL-harboring proteins with increasing ANL concentrations on both the global protein level ('anti-Biotin') and on the level of cell-type specific candidate proteins ('anti-candidate protein') in all three tissues tested. (b) In contrast mMetRS^{L274G}-EGFP mediated ANL incorporation already resulted in an intense biotin signal after 2 mM ANL administration for both bulk labeling of proteins ('anti-Biotin') and for Dlg, Synapsin and Draper8A1 for the respective cell type expressing the mMetRS^{L274G}-EGFP variant ('anti-candidate protein'). n=3 independent experiments. Modified after Erdmann *et al.* (2015).

FUNCAT labeling of larval muscle cells, neurons and glial cells already showed that ANL incorporation into proteins is restricted to MetRS^{LtoG}-EGFP-expressing cells (Figure 8) [11]. To demonstrate the specificity of ANL-labeling using BONCAT, head lysates of ANL-fed (4 mM) flies, expressing either type of MetRS^{LtoG}-EGFP in glia cells, were analyzed on western blot using an antibody against the neuron-specific protein Synapsin. Eluate fractions of affinity-purified samples derived from glia cells should contain only ANL-labeled proteins specific for glia cells. Anti-Synapsin treated western blots revealed no signal for biotin-tagged Synapsin in the eluate fractions of head lysates of *Drosophila* flies, expressing either MetRS^{LtoG} variant in glia cells (Figure 11a, b). The Synapsin-signal was absent even when high concentrations of ANL were applied (Figure 11a, b). Head lysates of *Drosophila* flies consist of neurons and glia cells, on this account a signal for Synapsin was detect in the input and unbound fraction, since here the protein lysates consist of both biotin-tagged (glial) and non-tagged (neuronal and glial) proteins (input fraction) or consist only of non-tagged (neuronal) proteins (unbound fraction). Figure 10a and b (third column) demonstrate that the purification of biotin-tagged proteins in glia cells was successful.

Thus, the here presented experiments prove the cell-specificity of the metabolic ANL-labeling of proteins in *Drosophila melanogaster* (Figure 11a, b).

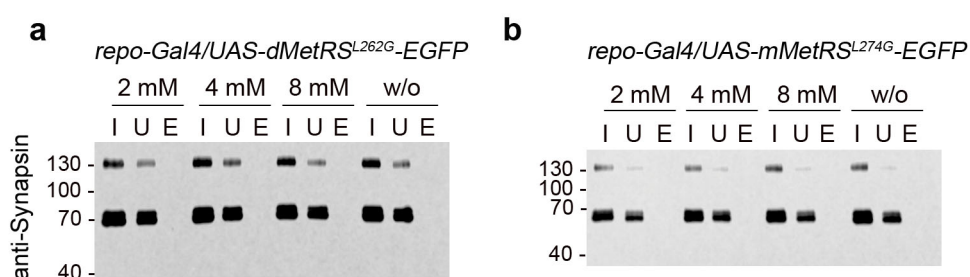


Figure 11: Cell-type specificity of ANL-labeling. Head lysates of (a) dMetRS^{L262G}-EGFP- and (b) mMetRS^{L274G}-EGFP- expressing flies were subjected to the BONCAT-protocol. After NeutrAvidin purification no ANL-containing Synapsin could be detected in any of the eluate fractions (enriched ANL-labeled proteins) of samples derived from flies expressing either MetRS^{LtoG} variant in glial cells demonstrating the specificity of this metabolic labeling approach. Depicted are representative western blots showing input (I, before NeutrAvidin purification), unbound (U, non-biotin tagged proteins and no ANL-containing proteins), and eluate fractions (E, enriched ANL-labeled proteins after NeutrAvidin purification). n=3 independent experiments. Modified after Erdmann *et al.* (2015).

In summary, BONCAT analysis of metabolically ANL-labeled proteins enables the identification of proteins on the global protein level and on the level of a single cell-type

specific protein, including cytosolic and transmembrane proteins. Thus, BONCAT analysis is sensitive enough to investigate protein dynamics biochemically in a complex and behaving organism, like *Drosophila melanogaster*.

3.5 ANL-labeling correlates with the duration of ANL exposure

Chronic ANL feeding to *Drosophila* larvae and flies results in massive labeling of proteins (Figure 9, 10). However, using chronic ANL labeling is not useful to investigate protein dynamics during different more rapid behavioral processes such as memory formation. Hence, in the following experiments *Drosophila* larvae and flies were exposed to ANL for shorter time periods and tested for sufficient ANL incorporation in conjunction with BONCAT. *Drosophila* larvae were exposed to ANL for 24 h (performed by Dr. Kathrin Marter, Institute for Pharmacology and Toxicology, Neural Plasticity and Communication, Otto-von-Guericke University Magdeburg). Body wall lysates of mMetRS^{L274G}-EGFP-expressing larvae were subjected to the BONCAT-protocol and analyzed on western blot for ANL incorporation into overall proteins (Figure 12a) and into the candidate protein Dlg (Figure 12a'). Figure 12 shows that ANL labeling for 24 h is sufficient enough to label muscle proteins of *Drosophila* larvae with ANL, covering the whole molecular weight range, and to detect ANL-labeled Dlg in the eluate fraction of affinity purified biotin-tagged proteins (Figure 12a, a'). The efficiency of ANL-labeling for shortend time periods in adult flies was tested as well. For this, one to three days old flies expressing the mMetRS^{L274G}-EGFP variant pan-neuronally (*elav^{C155}-Gal4*) were exposed to 4 mM ANL for 24 h and 48 h. Head lysates were subjected to the BONCAT-protocol. A biotin signal was detected after 24 h for overall protein incorporation (Figure 12b) and for incorporation into Synapsin (Figure 12b'). These signal intensities increased when flies were exposed to ANL for 48 h (Figure 12b, b'). FUNCAT experiments confirmed this finding that the longer *Drosophila* larvae were exposed to ANL the higher the observed signal intensity of the TAMRA-signal [11]. Additionally, FUNCAT experiments revealed that the variations of labeling intensities increase with longer ANL exposure, possibly due to inter-individual translation rates [11]. Hence, shortened ANL exposure enables to detect ANL-labeled proteins using FUNCAT and BONCAT to investigate protein dynamics *in vivo*.

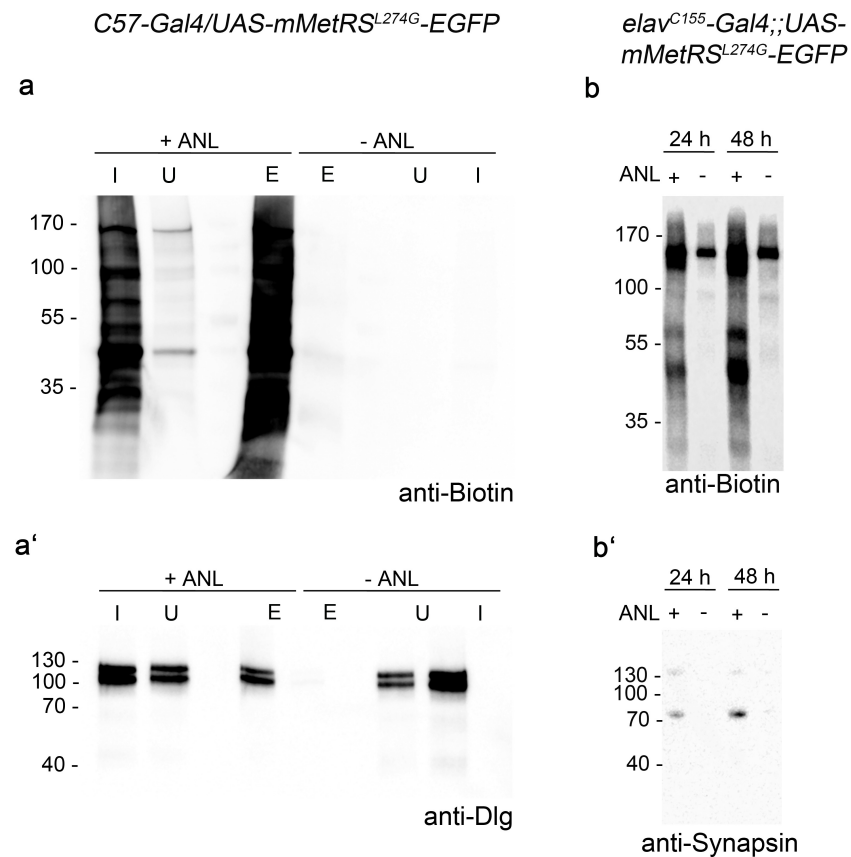


Figure 12: Short-term labeling of proteins with ANL. ANL exposure for 24 h led to a sufficient mMetRS^{L274G}-EGFP-mediated ANL incorporation into muscle proteins of L3 stage larvae to detect newly synthesized proteins (*a*, *a'*). Adequate signals for biotin (*a*) and the candidate protein Dlg (*a'*) were detectable in representative western blot after affinity purification of biotin-tagged proteins. Monitoring newly synthesized proteins in adult flies with BONCAT revealed that 24 h of exposure to 4 mM ANL was sufficient enough to detect globally ANL-labeled proteins (*b*) as well as the candidate protein Synapsin (*b'*). Prolonging the exposure time to 48 h even increased the signal intensity (*b*, *b'*). I = input (before NeutrAvidin purification), U = unbound (non-biotin tagged proteins and no ANL-containing proteins), and E = eluate fractions (enriched ANL-labeled proteins after NeutrAvidin purification). '+' represents ONM with 4 mM ANL and '-' represents ONM w/o ANL. (*a*) Dr. Kathrin Marter performed ANL labeling of *Drosophila* larvae. (*a-b'*) n=3 independent experiments. Modified after Erdmann *et al.* (2015).

The nervous system of *Drosophila melanogaster* undergoes drastic changes and reorganizations during metamorphosis [163]. To determine if ANL-labeled proteins outlast this phase, wandering late L3 stage *elav*^{C155}-Gal4;;UAS-mMetRS^{L274G}-EGFP-expressing larvae were subjected to metabolic pulse-chase experiments. For this larvae were reared on 4 mM ANL-containing ONM until they reached the late larval wandering L3 stage. Now, half of the larvae were put onto ONM without ANL (chase group), whereas the other half remained on ANL-containing ONM, until both groups reached the adult stage. Subsequently, head lysates of these flies were subjected to the BONCAT-protocol before they were analyzed on western blot for ANL-labeled proteins after metamorphosis. Interestingly, although the labeling intensities for overall proteins (Figure 13a) and for the candidate protein Synapsin (Figure 13a') were clearly reduced between groups, the signal intensity was rather high in animals that were not allowed to remain on ANL-containing ONM. However, the origin

of the ANL-labeled proteins, derived either from rescued apoptotic material or from survived 'larval' cells and proteins, need to be addressed by further experiments.

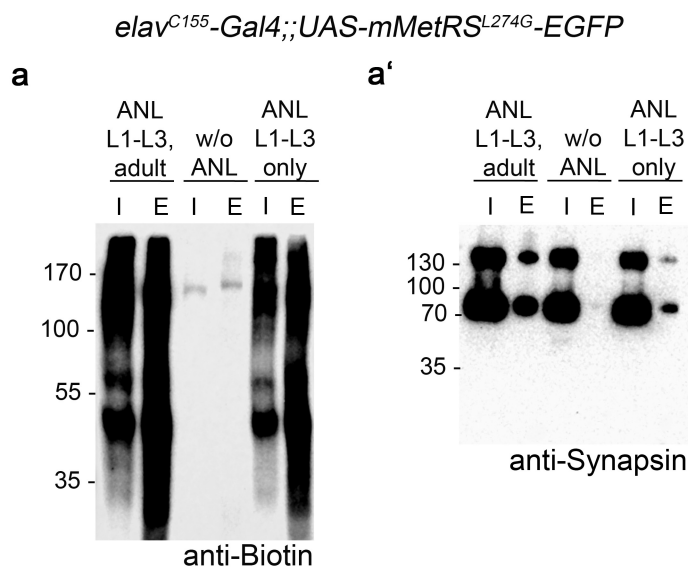


Figure 13: Fate of larval ANL-labeled neuronal proteins after metamorphosis in adult *Drosophila* flies. Metabolic pulse-chase-labeling experiments revealed that a substantial amount of ANL-labeled proteins is transmitted from larval neurons throughout pupal to adult neurons of *elav^{C155}-Gal4;;UAS-mMetRS^{L274G}-EGFP*-expressing animals. I = input (before NeutrAvidin purification), U = unbound (non-biotin tagged proteins and no ANL-containing proteins), and E = eluate fractions (enriched ANL-labeled proteins after NeutrAvidin purification). (a-a') n=3 independent experiments. Modified after Erdmann *et al.* (2015).

3.6 Methionine is replaced by ANL at internal amino acid positions within a protein

Tirrell and co-workers reported cell-type specific labeling with ANL in a mammalian cell culture system mediated by a mutated *E. coli* MetRS^{NLL}-variant, which leads to the loading of ANL onto the methionine initiator tRNA, allowing for the incorporation of ANL only at the N-terminus of proteins [69]. As 80% of proteins undergo proteolytic cleavage at their N-terminus most of the ANL-labeled proteins cannot be readily analyzed by this mutant, reflecting a severe limitation for the applicability of this method to investigate protein dynamics [164-166]. There is evidence that the here reported MetRS^{LtoG} variants do incorporate ANL throughout a proteins' entire sequence as the transmembrane proteins Bsg (Figure 9a, 'anti-GFP') and Draper I (Figure 9c, 10b, 'anti-Draper8A1') were detected after affinity purification in the eluate fractions. To substantiate that the here reported MetRS^{LtoG} variants replace internal Met residues rather than only at the very N-terminal of proteins, two independent assays were performed.

The transmembrane protein Notch is activated upon binding to one of its ligands, Delta or Serrate, leading to a proteolytic cleavage at its intramembraneous site, releasing the intracellular domain of Notch [167, 168]. The released intracellular domain of Notch then associates directly with the nuclear transcription factor Suppressor of Hairless [Su(H)] and regulates target expression of specific genes [167, 168]. Brain lysates of ANL-fed ubiquitously dMetRS^{L262G}-EGFP- (*ubi-Gal4*) expressing larvae were subjected to the BONCAT-protocol and analyzed on western blot using a specific antibody recognizing the intracellular fragment of Notch. The full-length Notch protein has a molecular weight of \approx 300 kDa (Figure 14a, arrow head), thereof 120 kDa belong to the intracellular domain (Figure 14a,

asteriks). The intracellular fragment was clearly detectable as a smear at around 120 kDa on western blot after affinity purification (Figure 14a). As the intracellular Notch harbors 32 methionine residues, the smear is likely to represent the different levels of ANL incorporation into the intracellular domain.

Furthermore, anti-GFP immunoprecipitates of dMetRS^{L262G}-EGFP-expressing larvae were subjected to mass spectrometry analysis (performed by Dr. Tamar Ziv, Smoler Proteomics Center, Faculty of Biology, Technion, Haifa, Israel) and revealed the replacement of two internal methionine residues by ANL (Supplementary Figure 1). The internal peptides found in MS analysis replaced Met by ANL at position 544 aa and 1036 aa. Dr. Anke Müller observed that the mMetRS^{L274G}-EGFP variant incorporates ANL along a proteins' length as well [140]. Consequently, ANL is incorporated into proteins at their internal sides by either type of MetRS^{LtoG} variant with an eucaryotic background, rather than only at the N-terminus of a protein as previously reported [69].

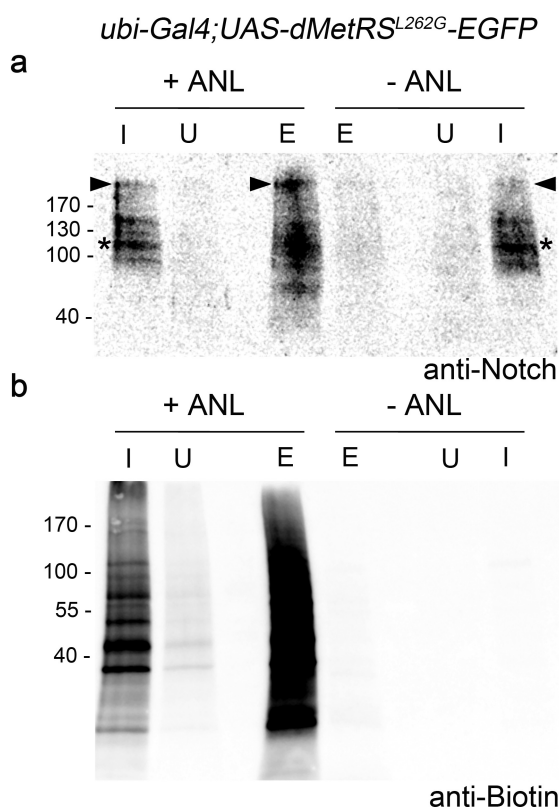


Figure 14: ANL is incorporated at internal amino acid positions within a protein. L3 stage larval brains of dMetRS^{L262G}-EGFP-expressing larvae were subjected to the BONCAT-protocol after chronic ANL feeding (4 mM ANL). (a) A representative western blot showed efficient incorporation of ANL into the intracellular domain of Notch (\approx 120 kDa, asteriks) upon ubiquitous expression of dMetRS^{L262G}-EGFP. Arrow head = full length Notch, asteriks = intracellular Notch fragment (b) The biotin signal verified ANL incorporation and affinity purification of biotin-tagged proteins. Protein lysates of the control group, reared on ONM w/o ANL, showed no signal for biotin. I = input (before NeutrAvidin purification), U = unbound (non-biotin tagged proteins and no ANL-containing proteins), and E = eluate fractions (enriched ANL-labeled proteins after NeutrAvidin purification). Modified after Erdmann *et al.* (2015). n=3 independent experiments.

3.7 Limited side effect upon chronic ANL incorporation

Chronic ANL feeding of *Drosophila* larvae and flies results in abundant incorporation of ANL into proteins (Figure 8-10, 12-14). However, the enlarged side chain of ANL (Figure 4a) might possibly lead to misfolding of proteins harboring ANL, consequently resulting in possible malfunctioning of essential proteins associated with misbehavior. For this, the vitality of MetRS^{LtoG}-EGFP-expressing ANL-treated larvae and flies was investigated for such

putative negative side effects resulting from ANL incorporation. Consequently, MetRS^{LtoG}-EGFP-expressing larvae were investigated regarding their body weight and motor performances after chronic ANL-feeding. MetRS^{LtoG}-EGFP-expressing flies in turn were tested for their eclosion and survival rates, their geotactic behavior, sensitivity to intoxication and locomotion after chronic ANL-treatment.

Determining the larval body weight assessed possible side effects of ANL incorporation into the muscle proteome mediated by the MetRS^{LtoG}-EGFP variants in larvae. For this, either MetRS^{LtoG} variant was expressed under the control of the muscle specific *C57-Gal4* driver in larvae chronically exposed to ONM w/ different ANL concentrations (2 mM, 4 mM, 8 mM) or to ONM w/o ANL. The larval body weight of wandering 3rd instar larvae was significantly reduced when mMetRS^{L274G}-EGFP-expressing larvae were fed either with 2 mM or 4 mM ANL (Figure 15a'). Feeding 8 mM ANL to mMetRS^{L274G}-EGFP-expressing animals resulted in embryonic lethality (Figure 15a'). Additionally, feeding ANL to mMetRS^{L274G}-EGFP-expressing larvae regardless of its concentration resulted in a high larval lethality. Furthermore, larval crawling behavior was significantly impaired when ANL was incorporated into proteins mediated by the mMetRS^{L274G}-EGFP [11]. Remarkably, much less pronounced deficits in larval growth (Figure 15a) and no impairment in larval locomotion [11] were observed when ANL was incorporated by the dMetRS^{L262G}-EGFP into muscle proteomes of *Drosophila* larvae. The larval body weight correlated negatively with the applied ANL concentrations (Figure 15a, a').

Putative side effects of chronic ANL incorporation into neuronal and glia proteins of adult flies, was assessed by determining the eclosion rate of flies, expressing one of the MetRS^{LtoG}-EGFP variants either in glia cells (*repo-Gal4*) or neurons (*elav^{C155}-Gal4*). Neuronal ANL incorporation mediated by either type of MetRS^{LtoG} variant resulted in a reduced eclosion rate (Figure 15b, b'). The number of eclosed progeny was significantly reduced compared to the expected eclosion rate of 1.0 when 2 mM, 4 mM or 8 mM ANL was fed chronically. When the mMetRS^{L274G}-EGFP variant was expressed in glia cells the number of eclosed progeny was significantly reduced when treated with either 2 mM or 8 mM ANL chronically (Figure 15c'). In contrast, no such effects were observed when ANL was incorporated by the dMetRS^{L262G}-EGFP variant into glial proteins (Figure 15c). Additionally, a negative correlation between ~~impairment~~ of the eclosion rate and the administered ANL concentration was found in MetRS^{LtoG}-EGFP-expressing flies with one exception (*repo-Gal4/UAS-dMetRS^{L262G}-EGFP*, Figure 15b-c').

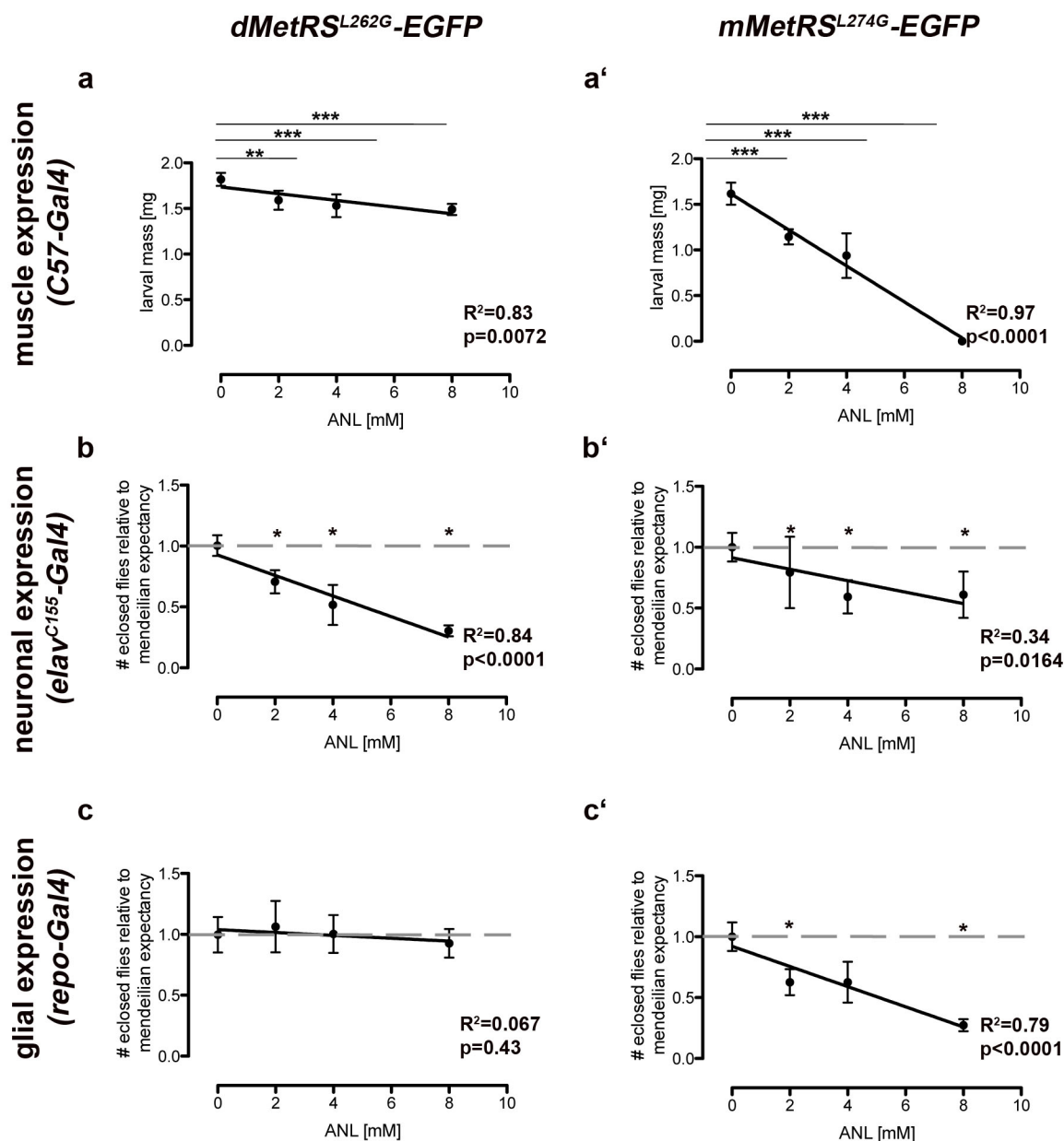


Figure 15: Limited toxic side effects on $MetRS^{LtoG}$ -expressing larvae and flies after chronic ANL exposure. (a, a') Putative side effects of ANL incorporation into muscle proteomes were determined by measuring the body weight of 3rd instar larvae expressing either $MetRS^{LtoG}$ variant under the control of the muscle-specific *C57-Gal4* driver. ANL incorporation mediated by the $dMetRS^{L262G}$ -EGFP led to a moderate reduction of larval body weight (a), whereas severe reduction of the larval body weight was observed for $mMetRS^{L274G}$ -EGFP-mediated ANL incorporation. Feeding 8 mM ANL to $mMetRS^{L274G}$ -EGFP-expressing larvae resulted in embryonic lethality (a'; ONE-way ANOVA with Dunnett post hoc test, ***: $p<0.001$, $n=3$, 4-12 larvae/condition). Body weights of $dMetRS^{L262G}$ -EGFP or $mMetRS^{L274G}$ -EGFP-expressing larvae correlated negatively with the applied ANL concentration (a, a', *C57-Gal4/UAS-dMetRS^{L262G}-EGFP*: $R^2=0.83$, $p=0.0072$; *C57-Gal4/UAS-mMetRS^{L274G}-EGFP*: $R^2=0.97$, $p<0.0001$, $n=3$). (b-c') Possible side effects of ANL incorporation into neuronal and glial proteomes on fly development were addressed by determining eclosion rates of adult flies upon *elav^{C155}*- or *repo-Gal4*-driven $MetRS^{LtoG}$ expression (number of progeny: 51-183; theoretical mean of 1.0 indicated by dashed line). Neuronal ANL incorporation led to a significantly reduced eclosion rate of $dMetRS^{L262G}$ -EGFP (b) and $mMetRS^{L274G}$ -EGFP (b') expressing flies when ANL was applied with 2 mM, 4 mM and 8 mM ANL (one sample t-Test, *: $p<0.05$, *elavC155-Gal4/UAS-dMetRS^{L262G}-EGFP*: 2 mM ANL: $p=0.0374$, 4 mM ANL: $p=0.0351$, 8 mM ANL: $p=0.0017$, *elavC155-Gal4/UAS-mMetRS^{L274G}-EGFP*: 2 mM ANL: $p=0.0369$, 4 mM ANL: $p=0.0099$, 8 mM ANL: $p=0.0262$, $n=3$). Reduced eclosion rates of neuronal $dMetRS^{L262G}$ -EGFP or $mMetRS^{L274G}$ -EGFP-expressing flies correlated with increasing ANL concentration (b, b', *elav^{C155}-Gal4;;UAS-dMetRS^{L262G}-EGFP*: $R^2=0.84$, $p<0.0001$,

elav^{C155}-Gal4;;UAS-mMetRS^{L274G}-EGFP: $R^2=0.34$, $p=0.0164$, $n=4$). However, eclosion rates of glial *MetRS^{LtoG}* expression was only significantly reduced in the case of *mMetRS^{L274G}-EGFP*-mediated ANL incorporation at 2 mM ANL and 8 mM ANL (c' , one sample t-Test, *: $p<0.05$, $p=0.002$, $n=3$; $R^2=0.79$, $p<0.0001$). Again, the reduced eclosion rate correlated with increasing ANL concentrations (c' , *repo-Gal4/UAS-mMetRS^{L274G}-EGFP*: $R^2=0.79$, $p<0.0001$, $n=3$). Normal eclosion rates were observed when ANL incorporation was mediated by the *dMetRS^{L262G}-EGFP* into glial proteins, showing no correlation between the number of eclosed flies and the applied ANL concentration (c , *repo-Gal4/UAS-dMetRS^{L262G}-EGFP*: $R^2=0.067$, $p=0.43$, $n=3$). ($a-c'$) Mean \pm SD. ($a-a'$) $n=3$ independent experiments with 4-12 larvae/experiment, ($b-b'$) $n=3$ independent experiments, ($c-c'$) $n=4$ independent experiments. Modified after Erdmann *et al.*, (2015)

In addition, the influence of chronic ANL incorporation on the survival rate of *dMetRS^{L262G}-EGFP*-expressing adult flies was investigated. For this, the number of alive flies, expressing the *dMetRS^{L262G}-EGFP* variant in neurons (Figure 16a) or in glia cells (Figure 16b), was evaluated every second day for 17 days. Crosses were reared on ONM containing 2 mM, 4 mM or 8 mM ANL until progeny flies were one to three days old. Five female and five male were transferred into ONM with or without ANL (ANL concentrations during larval/pupal development until post-eclosion as indicated). Control groups were reared on ONM without ANL during the whole experiment. Long-term exposure of ANL to *dMetRS^{L262G}-EGFP*-expressing flies had no discernible effects on the survival rate (Figure 16a, b).

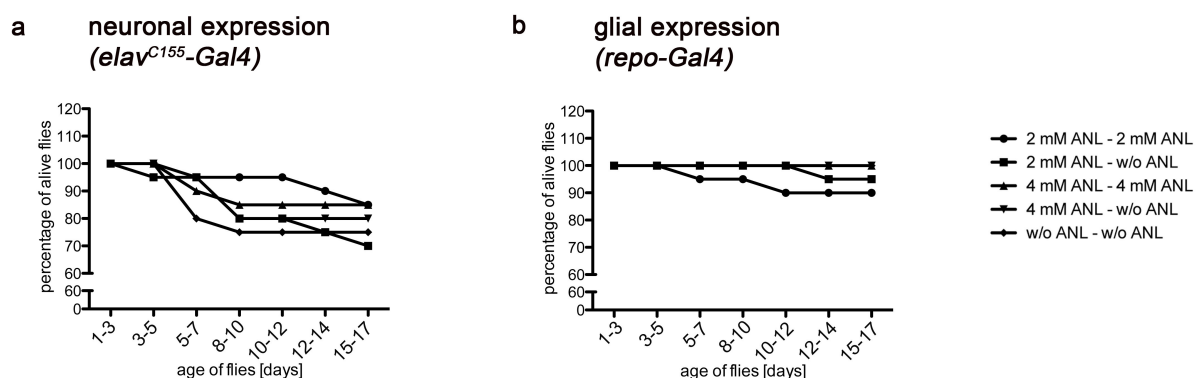


Figure 16: Normal survival rate of *dMetRS^{L262G}-EGFP*-expressing flies after chronic ANL exposure. Assessing the survival rate of adult flies during neuronal (a) or glial (b) ANL incorporation mediated by the *dMetRS^{L262G}-EGFP*. Crosses of *elav^{C155}*- or *repo-Gal4*-driver lines with *UAS-dMetRS^{L262G}-EGFP* strains were reared on ONM containing either 0, 2 mM, or 4 mM ANL. One to three days old adult progeny flies were transferred onto ONM with or without ANL (ANL concentrations during larval/pupal development to post-eclosion as indicated). The control group was reared on ANL-free ONM during the whole duration of the experiment. No obvious ANL effects on the survival rates of adults became evident under these conditions. ($a-b$) $n=2$ independent experiments. (d, d') Average of flies. Modified after Erdmann *et al.* (2015).

ANL incorporation into the neuronal proteome did not result in enhanced pupal lethality, thus *MetRS^{LtoG}* expressing animals might be affected at the larval phase. Confocal microscopy at the larval neuromuscular junction (NMJ) of larvae expressing the *dMetRS^{L262G}-3xmyc* variant pan-neuronally (*elav^{C155}-Gal4*) showed that the distribution of the common marker proteins, like the homophillic cell adhesion molecule Fasciclin II (FasII), the active zone marker Bruchpilot (Brp) or the postsynaptic subsynaptic reticulum visualized by the

plasma membrane Ca^{2+} ATPase (PMCA), showed no obvious differences between ANL- and non-ANL fed animals [11]. Consistently, larvae subjected to the larval crawling assay showed normal locomotion after chronic ANL incorporation mediated by either type of MetRS^{LtoG}-EGFP variant [11], concluding, that chronic ANL incorporation into neuronal proteins does not cause one major effect rather than multiple small side effects leading to a reduced eclosion rate of MetRS^{LtoG} expressing flies.

The effects of ANL incorporation into neuronal proteins on fly behavior were investigated in more detail by subjecting MetRS^{LtoG}-EGFP-expressing flies to the following fundamental behavioral assays: rapid iterative negative geotaxis assay (RING) [169], the island assay [170] and the ethanol sensitivity assay [171]. In general, *wt* flies (*Canton-S*) tested in any of the behavioral experiments after chronic ANL exposure showed no impairment of their behavioral performances [11]. Chronic ANL exposure to MetRS^{LtoG}-EGFP-expressing flies resulted in an indistinguishable behavior from MetRS^{LtoG}-EGFP-expressing flies not exposed to ANL [11]. Impaired behaviors were only observed in the negative geotaxis assay for both MetRS^{LtoG} variants and for mMetRS^{L274G}-EGFP-expressing flies in delayed platform clearance in the island assay [11]. However, no behavioral deficits were observed when ANL was fed acutely to adult flies [11], despite efficient ANL incorporation (see 3.5).

Although, the chronic application of ANL to *Drosophila* larvae and flies resulted in a reduction of larval body weight and in a reduced eclosion rate of adult flies, the behavior of adult *Drosophila* flies was impaired only in two behavioral assays [11]. Nevertheless, these effects were rescued when ANL was applied acutely for a defined time period [11]. Only the defects in larval locomotion could not be rescued in mMetRS^{L274G}-EGFP-expressing larvae [11]. Therefore, the type of MetRS^{LtoG} variant, the ANL concentration and the duration of ANL exposure need to be chosen carefully according to the experimental procedure.

In summary, in the first section of this thesis, the cell-type specific labeling of proteins with the non-canonical amino acid ANL upon targeted expression of MetRS^{LtoG} variants (GINCAT) was established *in vivo* using *Drosophila melanogaster* flies and larvae. The visualization and detection of ANL-labeled proteins was achieved with the previously introduced FUNCAT [49-51] and BONCAT [52, 53] techniques either after chronic or acute ANL exposure revealing that ANL is incorporated cell-type specifically into global proteins and into single ANL-labeled candidate proteins. Both MetRS^{LtoG}-EGFP variants are able to incorporate ANL at internal Met-sites. Thus, the here established FlyNCAT (GIN-/FUN-/BONCAT) technique represents a useful tool to investigate protein synthesis dependent processes cell-type specifically in various tissues of living organisms.

3.8 Investigation of protein synthesis rates in different mutant backgrounds applying cell-type selective amino acid tagging

In the following sections cell-type specific FlyNCAT was used to investigate the influence of pathological conditions on protein synthesis demonstrating the broad applicability of this method. To do so, relative protein translation rates were determined (i) in a GARS-associated *Drosophila* model for Charcot-Marie-Tooth neuropathy, (ii) in dFMR1 knockdown larvae and (iii) in *rsh*¹ mutant flies.

3.8.1 Reduced protein synthesis in a *Drosophila* model for GARS-associated Charcot-Marie-Tooth (CMT) neuropathy

As Charcot-Marie-Tooth (CMT) is known to be associated with mutations in five different aminoacyl-tRNA synthetases [78-83], the relative protein translation rate in motor and sensory neurons was determined in a GARS-associated CMT *Drosophila* model [23] using the FlyNCAT technique.

In collaboration with Dr. Erik Storkebaum and Dr. Sven Niehues (Max-Planck Institute for Molecular Biomedicine, Molecular Neurogenetics, Münster) global protein translation rates in CMT flies were evaluated using BONCAT analysis in the scope of this thesis. For this, the respective mutant hGARS proteins were co-expressed with the dMetRS^{L262G}-EGFP in motor neurons of *Drosophila* larvae. The mutant hGARS proteins were expressed in dual copies to achieve higher expression levels. *Drosophila* larvae were exposed to 4 mM ANL for 120 h before larval brains were subjected to the BONCAT-protocol. Dr. Sven Niehues performed crossing, ANL-labeling procedures and larval brain dissection for these BONCAT experiments. Larval brain lysates were analyzed using the biotin-alkyne affinity tag to determine the relative protein translation rates using the biotin-BONCAT signals in motor neurons of larvae expressing either the mutant or the *wt* hGARS protein together with the dMetRS^{L262G}-EGFP. BONCAT experiments revealed that the signal intensity for the biotin-tag, reflecting the relative protein translation rate, was significantly reduced in motor neurons of hGARS^{G240R} mutant larvae compared to larvae expressing the hGARS^{wt} protein (Figure 17a). Evaluation of the biotin signal intensity revealed that the protein synthesis rate of hGARS^{G240R} mutant larvae was significantly reduced to ≈68 % compared to hGARS^{wt}-expressing larvae (Figure 17b). Interestingly, there was no obvious difference of ANL-labeled proteins in terms of protein expression pattern between hGARS^{G240R} or hGARS^{wt} larvae suggesting an overall reduced protein translation rate (Figure 17a). Additionally, FUNCAT experiments were performed with all three reported hGARS mutations (hGARS^{E71G}, hGARS^{G240R}, hGARS^{G526R}) and revealed a reduction of the relative protein translation rate as well, but with one exception [23]. TAMRA-signal intensity in hGARS^{E71G} was not different from hGARS^{wt} larvae. However, TAMRA signal intensities in hGARS^{G240R} and hGARS^{G526R}

mutant larvae were reduced to $\approx 40\%$ compared to hGARS^{wt} expressing larvae [23]. Thus, BONCAT and FUNCAT results lead to the conclusion that the protein synthesis rate is impaired in motor neurons of their hGARS-associated CMT-model. As the CMT-*Drosophila* model showed deficits in sensory neurons as well [23], the protein translation rate was evaluated in class IV multidendritic sensory neurons too. FUNCAT experiments showed again that the expression of any of the three mutant hGARS proteins in sensory neurons resulted in a significant reduction of protein synthesis rate in these neurons of mutant hGARS-associated CMT larvae [23].

OK371-Gal4/UAS-hGARS;UAS-dMetRS^{L262G}-EGFP/
UAS-hGARS

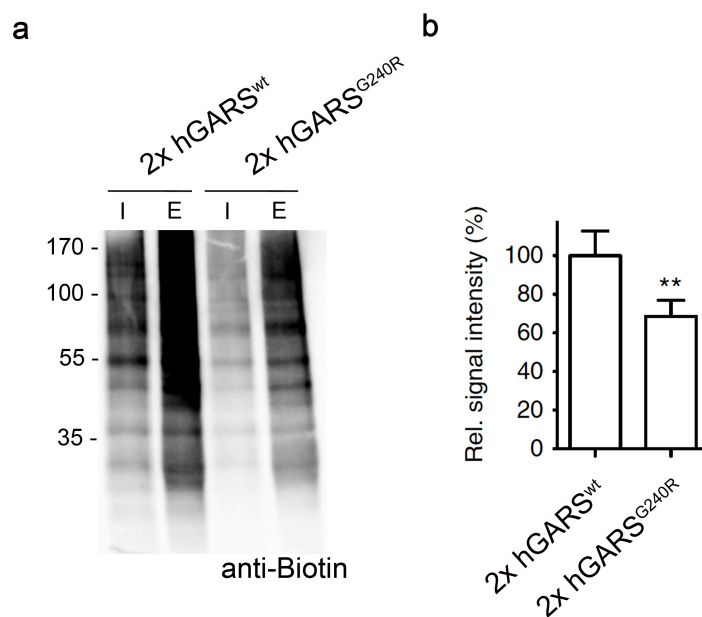


Figure 17: Reduced protein translation rate in GARS-associated CMT larvae. Co-expressing dMetRS^{L262G}-EGFP and mutant hGARS larvae were exposed to ANL for 120 h to monitor protein translation rate with BONCAT in larval motor neurons. (a, b) BONCAT analysis revealed that the relative protein translation rate is significantly reduced in motor neurons of mutant hGARS^{G240R} larvae. Depicted is a representative western blot of biotin-tagged proteins displaying samples before purification (I, input fraction) and after purification, containing enriched ANL-labeled proteins (E, eluted fraction). Average \pm SEM relative to hGARS^{wt} (100%). Statistical significance was determined by an unpaired t-Test with Welch's correction (b). (a, b) n=4 independent experiments. (a, b) Dr. Sven Niehues performed ANL-labeling and dissecting.

In addition, the impaired protein synthesis in adult flies was evaluated on western blot level. As any of the three mutant hGARS proteins caused developmental lethality [23], the mutant hGARS proteins were expressed ubiquitously from the adult stage onwards using the GAL80^{ts} target system [10]. Three days after inducing the gene expression, adult flies were exposed for 48 h to AHA-labeled yeast (4 mM; induction of protein expression, AHA-labeling and head dissection were performed by Julia Bussmann, Max-Planck Institute for Molecular Biomedicine, Molecular Neurogenetics, Münster). Head lysates were then subjected to the BONCAT-protocol. Ubiquitous expression of either hGARS mutation resulted in a diminished protein synthesis rate, whereas hGARS^{wt} and control (*w1118*) flies showed normal protein synthesis rates (Figure 18). The signal intensity for biotin was barely discernible in mutant hGARS flies (Figure 18).

These results indicate that the protein synthesis rate *per se* is impaired in this GARS-associated CMT-*Drosophila* model, giving a new leverage point to predict a possible cause of this particular type of CMT.

UAS-hGARS/tubulin-Gal80^{ts};UAS-hGARS/tubulin-Gal4

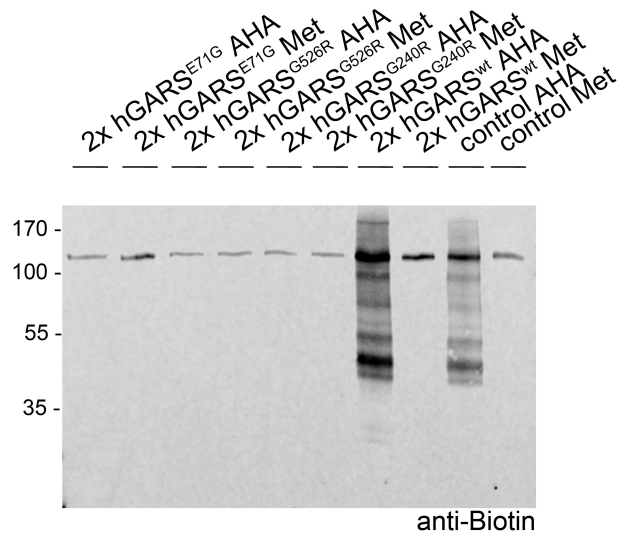


Figure 18: Reduced protein translation rate in GARS-associated CMT flies. Monitoring protein synthesis in hGARS mutant flies revealed that the biotin signal intensities were severely reduced in mutant hGARS flies compared to hGARS^{wt} or control (*w1118*) flies, reflecting a drastic reduction of protein translation rates. n=3 independent experiments. Julia Bussmann performed induction of gene expression, AHA-labeling and head dissecting. Modified after Niehues *et al.*, 2015.

3.8.2 Reduced protein synthesis rate in dFMR1 knockdown larvae

Fragile X mental retardation protein (FMRP) is known to influence various crucial synaptic plasticity- and protein translation-related processes in the brain including mRNA shuttling between the nucleus and cytoplasm [97], dendritic mRNA localization [98] and synaptic protein synthesis [99, 100]. As the literature on the role of FMRP in terms of generally elevated or diminished protein translation is contradictory [87, 99, 100, 103-107, 110, 111], the impact of global dFMR1 knockdown or overexpression was determined in neurons of *Drosophila* larvae using FlyNCAT.

For this, the previously published fly strains *UAS-TRiP-Fmr1* (Bloomington Stock Center, Indiana University, 34944) and *UAS-Fmr1* (Bloomington Stock Center, Indiana University, 6931) were used to either knockdown or overexpress dFMR1, respectively, in neurons (*elav^{C155}-Gal4*) of larvae expressing the *UAS-dMetRS^{L262G}-EGFP* construct. First, larval brain lysates were tested for correct expression or knockdown of dFMR1. As demonstrated in Figure 19a ('anti-dFmr1') lysates derived from dFMR1 knockdown larvae showed no signal for dFMR1, whereas larval brain lysates of larvae overexpressing dFMR1 revealed elevated signal intensities compared to larvae expressing dFMR1 on *wt* level. Western blot analysis showed no difference in dMetRS^{L262G}-EGFP expression of all genotypes tested (Figure 19a, 'anti-GFP'). To track changes in protein synthesis, larvae were chronically fed with 4 mM ANL before BONCAT analysis. Notably, the biotin signal of affinity-purified fractions (=eluate fractions) was decreased in dFMR1 knockdown larvae compared to the biotin signal of larvae

expressing dFMR1 on the *wt* level (Figure 19b). In contrast, overexpression of dFMR1 resulted in a slightly increased biotin signal for ANL-labeled proteins compared to the biotin signal of *wt* larvae (Figure 19b).

Thus, applying the here established FlyNCAT technique revealed that the protein synthesis rate seemed to be reduced in neurons of dFMR1 knockdown larvae, implying that dFMR1 might play a different role on global protein synthesis than previously assumed. Further experiments including the identification of proteins that are differently expressed across the different genotypes are necessary to investigate the putative role of dFMR1 during protein synthesis. Additionally, distinct global versus local protein synthesis should be addressed as well.

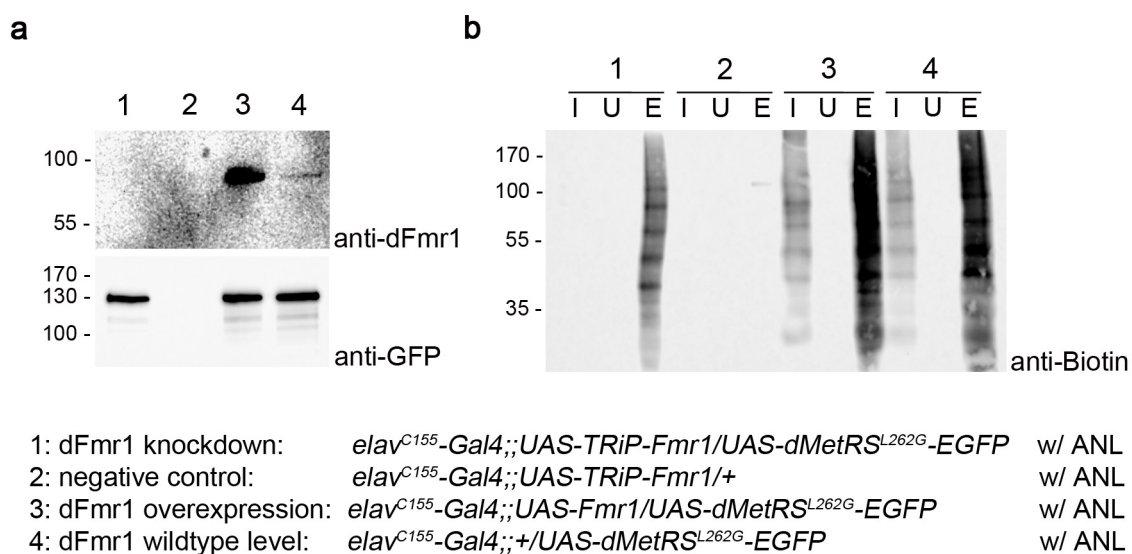


Figure 19: Reduced protein synthesis rate in dFMR1 knockdown larvae. (a) Western blot analysis confirmed that dFmr1 was knocked down (1, 2), overexpressed (3) or expressed at *wt* levels (4) according to the respective genotype ('anti-dFmr1'). Expression of the dMetRS^{L262G}-EGFP was identical between genotypes ('anti-GFP'). (b) Knock down of dFMR1 (1) in neurons of *Drosophila* larvae results in reduced biotin signal for ANL-harboring proteins compared to *wt* larvae (4), whereas dFMR1 overexpression (3) led to an elevated biotin signal compared to *wt* larvae (4). The negative control (w/o dMetRS^{L262G}-EGFP expression) showed no biotin signal (2). Depicted is a representative western blot of two independent experiments with the tagged input (I, before purification), unbound fraction (U, non-biotin tagged proteins and no ANL-containing proteins) and eluted (E, enriched ANL-labeled proteins after NeutrAvidin purification) fractions of ANL-labeled and control samples. n=2 independent experiments.

3.8.3 Reduced protein synthesis in *rsh*¹ mutant flies

The *rsh*¹ learning mutant displays normal initial learning rates but impaired formation of memory [122]. However, little is known about the putative molecular and cellular function of the Rsh protein [123]. Previously, 1D gel analysis and western blot analysis of lysates from *wt* and *rsh*¹ mutant flies in our lab revealed, that the transcription factor Rno is differently expressed or processed in *wt* compared to *rsh*¹ mutant flies [135, 172]. Furthermore, it has been shown that a protein-synthesis-dependent component during LTM formation depends

on proper Rsh function [130] and Guan *et al.* (2011) proposed that Rsh plays a role during transcription and/or translation [134]. Taken together, these facts point towards the hypothesis that protein synthesis rates might be affected in *rsh*¹ mutant flies.

Here, the FlyNCAT technique was applied to investigate the protein synthesis rate in *rsh*¹ mutant flies. For this, recombinant flies carrying the *rsh*¹ mutation and the dMetRS^{L262G}-EGFP variant were generated. The recombinants were crossed to the pan-neuronal driver *elav*^{C155}-*Gal4* to investigate the protein synthesis rate in neurons of heterozygous *rsh*¹ mutant flies. As controls *UAS-dMetRS*^{L262G}-*EGFP*-expressing flies were crossed to *elav*^{C155}-*Gal4* driver alone to determine *wt* protein expression levels. Both genotypes expressed the dMetRS^{L262G}-EGFP heterozygous. One to three days old progeny flies were exposed to 4 mM ANL-containing ONM for 24 h. Negative controls were kept on ONM without ANL for the same duration. Subsequently, head lysates were subjected to the BONCAT-protocol. The biotin-signal of affinity purified fractions (=eluate fractions) of *elav*^{C155}-*Gal4/rsh*¹::*UAS-dMetRS*^{L262G}-*EGFP* flies was clearly reduced compared to *elav*^{C155}-*Gal4/+*::*UAS-dMetRS*^{L262G}-*EGFP* flies (Figure 20a). Quantification of biotin signal intensities using dot blot analysis revealed that the global neuronal protein expression rate of *elav*^{C155}-*Gal4/rsh*¹::*UAS-dMetRS*^{L262G}-*EGFP* co-expressing flies was significantly reduced to 54.9 % of that in *elav*^{C155}-*Gal4/+*::*UAS-dMetRS*^{L262G}-*EGFP*-flies (Figure 20b). Furthermore, western blot analysis of head lysates showed that the dMetRS^{L262G}-EGFP expression itself seemed to be reduced in head lysates of heterozygous *rsh*¹ mutant flies (Figure 20c). This indicates that the reduced protein expression rate might result from a general reduction of the protein translation rate including the dMetRS^{L262G}-EGFP.

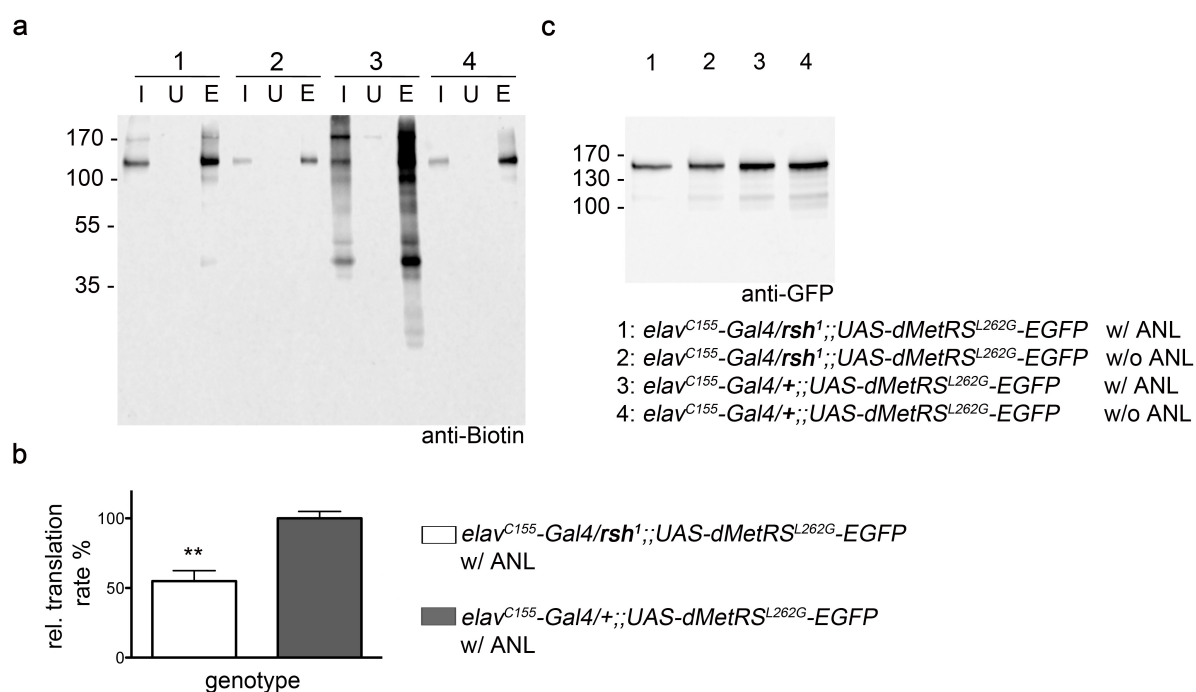


Figure 20: Reduced protein synthesis rate in neurons of heterozygous *rsh*¹ mutant flies. (a) A representative western blot of affinity purified biotin-tagged proteins uncovered a reduction of the biotin signal of the eluate fractions in *elav*^{C155}-*Gal4*/*rsh*¹; *UAS-dMetRS*^{L262G}-*EGFP* flies compared to the biotin signal of *elav*^{C155}-*Gal4*/+; *UAS-dMetRS*^{L262G}-*EGFP* flies. (b) Protein synthesis rates in neurons of *rsh*¹/+ mutant and +/+ flies. Student's t-Test, $p=0.0074$, $n=3$ independent experiments, Average \pm SEM relative to *elav*^{C155}-*Gal4*/+; *UAS-dMetRS*^{L262G}-*EGFP* (100%). (c) Reduced dMetRS^{L262G}-EGFP expression in *rsh*¹/+ mutant flies in the input fraction. I = input (before NeutrAvidin purification), U = unbound (non-biotin tagged proteins and no ANL-containing proteins), and E = eluted fractions (enriched ANL-labeled proteins after NeutrAvidin purification), (a-c) $n=3$ independent experiments.

3.9 Analysis of global protein expression pattern in *rsh*¹ mutant flies

The aforementioned FlyNCAT analysis suggests that other proteins other than Rno are differently expressed in *rsh*¹ mutant flies [135], too. To identify such proteins, a two-dimensional gel electrophoresis was performed with head lysates of *wt* (*Canton-S*) and *rsh*¹ mutant flies. This allows for the separation of proteins according to their isoelectric point (first dimension) and their molecular weight (second dimension) [157]. Protein spots were visualized using silver gel staining (Figure 21) and subsequently digitized. PDQuest software analysis selected all spots whose OD were different between the two conditions were tagged with a number and a red spot and picked for subsequent MS analysis (Figure 21, Figure 22, see 2.2.4.9.). Figure 22 exemplary shows one of these spots, number 1306, chosen for MS analysis. As shown in figure 22b the mean OD was significant different between the *rsh*¹ mutant and the *wt* group ($p \leq 0.1$). Furthermore, the ratio between the mean OD of the *rsh*¹ and *wt* group was determined to obtain a statement about the regulation of each spot referring to the control group (regulation = mean OD of *wt* group divided by the mean OD of the *rsh*¹ group, Table 7).

Figure 21: Silver stained 2D-gels of *rsh*¹ mutant and *wt* head lysates. Separation according to the isoelectric point (pI) and molecular weight (kDa) are indicated. Spots with different ODs ($p \leq 0.1$) after PDQuest analysis are marked with a red dot and a number. Green rectangle marks the spot magnified in Figure 22.

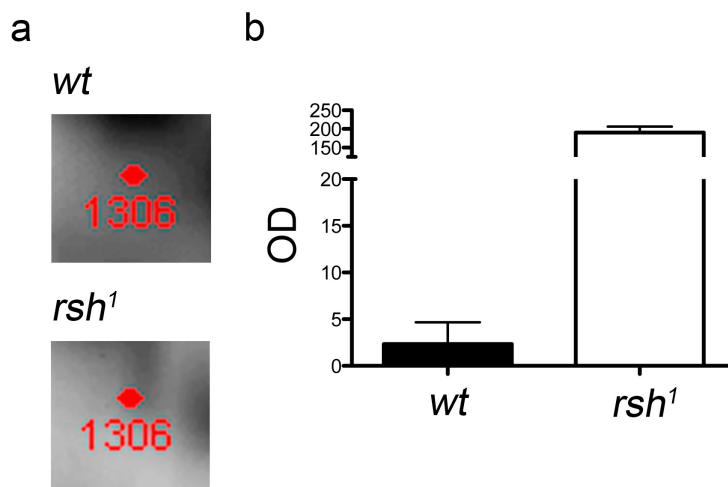


Figure 22: Example for 2D gel analysis. The mean OD of spot 1306 was significantly different ($p \leq 0.1$) in *rsh*¹ mutant flies compared to the *wt* group. (a) Magnification of the silver stained 2D gel with spot 1306. (b) Comparison of mean ODs + SEM of spot 1306 in both groups.

The MS analysis was performed by Yvonne Ducho and Dr. Thilo Kähne (Institute for Experimental Medicine, Otto-von-Guericke University, Magdeburg) and reveals the protein composition of each spot. In each spot a variety of proteins with different 'score' values (Mascotscore) were identified (Table 7) determining the quality of the identified proteins within a spot. Only proteins with a minimum 'score' value of 80 and greater were included for further analysis. The 'score' value gives the likelihood that the identified peptides of the MS analysis correspond to a certain protein. Table 5 shows the number of spots that were used for the MS analysis. In total 35 spots from the *rsh*¹ mutant group and 36 spots of the control group were identified to be different between the groups. Using MS analysis 41 proteins were identified in each group. However, not all found proteins within a spot were identical between the groups (Table 7).

Table 5: Number of spots identified by PDQuest software and their respective protein fraction in *rsh*¹ mutant and *wt* flies

	Number of spots	Number of proteins
<i>rsh</i> ¹	35	41
CS	36	41

For further analysis an additional statistical test was performed to compare the single OD-values between *rsh*¹ mutant and *wt* flies using a student's T-test with a significance level of $p \leq 0.05$. Spots with a significant difference in their OD-values are listed in table 7 (green spot number). In total 16 spots in each group were significant different. Again, there was no obvious difference in the number of proteins identified in these spots between *rsh*¹ mutant

and *wt* flies (Table 6), but the type of proteins identified between groups were different (Table 7, black protein labels). On the one hand, one has to consider that not all proteins identified within one regulated spot are regulated in the same manner (up or down). On the other hand, proteins can indeed be significantly expressed between the two genotypes in a given regulated spot that is not statistically secured, because other regulated proteins within this spot might weaken the overall difference. Thus, determining the significance interval to 0.05 could possibly exclude potential candidate proteins, which are differently expressed between *wt* and *rsh*¹ mutant flies. However, the main goal of this proteomic study was to identify a number of candidate proteins that are differently regulated/expressed between *rsh*¹ mutant and *wt* flies serving as a basis to investigate the influence of the *rsh* mutation in *Drosophila* flies. For this reason the significance level was elevated to 0.1 to identify proteins from spots that showed a significant difference between the two groups but without statistical security. This increased the number of spots in *rsh*¹ mutant group to 26 containing 34 proteins and in the *wt* group to 27 spots containing 31 proteins (Table 6, Table 7, green und blue spot number). Again, the number of spots and the number of identified proteins did not marginally differ between *rsh*¹ mutant and *wt* flies. One has to state that for later analyses of these possible candidates, proteins with a molecular weight greater than 150 kDa and with an isoelectric point smaller than 3 or greater than 11 should not be considered as these proteins are excluded *per se* by the experimental procedure used here. Moreover, proteins with experimental molecular weight being different more than 15 kDa from their theoretical molecular weight should be excluded for further analysis (Table 7, red protein label) as far as there is no plausible explanation for this apparent difference such as high degrees of posttranslational modifications or posttranslational cleavage. The remaining candidates (Table 7, black protein label) can be used for further analyses, including quantitative western blot analysis, to determine the actual regulation of each protein found in the regulated spots. This will then provide data to perform an Ingenuity pathway analysis to investigate if Rsh influences important networks or pathways within *Drosophila melanogaster*.

Interestingly, the Rno protein was found in the 2D-gel analysis in spots that showed a difference of $p \leq 0.1$ (Table 7). MS analysis of spot 1113 in *rsh*¹ mutant flies contained Rno and spot 1113 and 2506 in *wt* flies contained Rno peptides. All spots were upregulated in *rsh*¹ mutant flies. The Rsh protein itself, however, was not found using the 2D gel analysis, possibly for reasons named above.

Table 6: Number of spots per genotype after verification using student's T-Test.

	genotype	Number of spots	Number of proteins
$p \leq 0.05$	<i>rsh</i> ¹	17	21
	CS	16	23
$p \leq 0.1$	<i>rsh</i> ¹	27	34
	CS	27	31
$p \leq 0.1$, MW experimental \approx theoretical	<i>rsh</i> ¹	17	17
	CS	15	14

Table 7: 2D gel analysis of protein fraction from *rsh*¹ mutant and *wt* (CS) flies***Legend:**

black protein label: proteins that are considered for further analysis (regulated spots with significant ODs $p \leq 0.1$ and correct MW)

red protein name: proteins are excluded from further analysis as the theoretical and experiment MW differ more than 15 kDa

green spot number: ODs were different between *wt* and *rsh*¹ mutant flies with a significance level of $p \leq 0.05$

blue spot number: ODs were different between *wt* and *rsh*¹ mutant flies with a significance level of $p \leq 0.1$.

red spot number: ODs were not significant different between *wt* and *rsh*¹ mutant flies ($p > 0.1$).

Protein name	Geno- type	Accession (Uniprot)	Spot no.	Mr theor	Mr exp	pl theor	pl exp	Mascotscore (<80)	no. peptides	OD1 (CS)	OD2 (rsh)	OD1/OD2	t- Test
<i>no protein found in MS analysis</i>	<i>rsh</i> ¹		7811							6,67	60,37	0,11	0,004
Protein dopey-1 homolog	CS	DOP1_DROME		291.0	73	6.1	6,5	109.3 (M:109.3)	2				
Troponin T, skeletal muscle	<i>rsh</i> ¹	TNNT_DROME	3604	47.4	45	4.5	4,8	351.7 (M:351.7)	9	4,83	23,50	0,21	0,055
ATP synthase subunit beta, mitochondrial	<i>rsh</i> ¹	ATPB_DROME		54,1		5.0		466.1 (M:466.1)	7				
Glutamine synthetase 2 cytoplasmic	CS	GLNA2_DROME		41.3		5.3		82.0 (M:82.0)	2				
Arginine kinase	<i>rsh</i> ¹	KARG_DROME	6513	39.8	35	6.0	5,8	833.6 (M:833.6)	13	0,00	62,97	0,00	0,030
<i>no protein found in MS analysis</i>	CS												
Diacylglycerol kinase eta	<i>rsh</i> ¹	DGKH_DROSE	5408	213.7	29	6.6	5,5	114.3 (M:114.3)	2	13,53	36,87	0,37	0,040
DM7 family protein GM11958	CS	DM7B_DROSE		55.4		4.6		49.2 (M:49.2)	1				
<i>no protein found in MS analysis</i>	<i>rsh</i> ¹		7405							72,20	34,37	2,10	0,010
Microtubule-associated protein futsch	CS	FUTSC_DROME		591.7	27	4.8	6,1	139.1 (M:139.1)	3				
E3 ubiquitin-protein ligase highwire 2	CS	HIW_DROME		565.3		6.5		102.1 (M:102.1)	3				
Titin	<i>rsh</i> ¹	TITIN_DROME	2402	2064.5	25	4.8	3,25	308.0 (M:308.0)	6	5,93	26,30	0,23	0,010
Tropomyosin-1, isoforms 9A/A/B	<i>rsh</i> ¹	TPM1_DROME		39.3		4.8		132.2 (M:132.2)	2				
Protein crossbronx	<i>rsh</i> ¹	AKTP1_DROPE		28.1		4.9		83.3 (M:83.3)	1				
Tropomyosin-1, isoforms 9A/A/B	CS	TPM1_DROME		39.3		4.8		244.0 (M:244.0)	4				
Eukaryotic translation initiation factor 3 subunit J	CS	EIF3J_DROME		26.6		4.6		210.9 (M:210.9)	4				
Conserved oligomeric Golgi complex subunit 5	<i>rsh</i> ¹	COG5_DROME	5302	84.9	23	6.3	5,3	98.7 (M:98.7)	1	89,70	150,37	0,60	0,010
Catenin alpha	CS	CTNA_DROME		102.4		6.0		112.8 (M:112.8)	3				
Probable elongation factor 1-beta	<i>rsh</i> ¹	EF1B_DROME	1306	24.2	21	4.2	3,15	354.3 (M:354.3)	6	2,33	190,37	0,01	0,006
Pheromone-binding protein- related protein 2	<i>rsh</i> ¹	PBP2_DROME		16.8		4.7		128.2 (M:128.2)	2				
Myosin regulatory light chain 2	CS	MLR_DROME		23.7		4.5		618.1 (M:618.1)	8				
Probable elongation factor 1-beta	CS	EF1B_DROME		24.2		4.2		146.2 (M:146.2)	2				
Pheromone-binding protein- related protein 2	CS	PBP2_DROME		16.8		4.7		84.1 (M:84.1)	2				

E3 UFM1-protein ligase 1 homolog	CS	UFL1_DROAN		87.1		6.1		80.3 (M:80.3)	1				
Protein lethal(2)essential for life <i>no spot detected</i>	<i>rsh</i> ¹ CS	L2EFL_DROME	4208	21.3	19	5.8	5,18	105.6 (M:105.6)	2	0,00	16,67	0,00	0,040
Bipolar kinesin KRP-130 Microtubule-associated protein futsch ATP-dependent DNA helicase 2 subunit 1 Probable serine/threonine-protein kinase CG32666	<i>rsh</i> ¹ CS CS CS	KL61_DROME FUTSC_DROME KU70_DROME Y2666_DROME	6202	121.1	20	6.0	5,6	101.2 (M:101.2) 123.6 (M:123.6) 108.2 (M:108.2) 81.4 (M:81.4)	3 3 2 1	185,57	33,70	5,51	0,007
<i>no protein found in MS analysis</i> <i>no spot detected</i>	<i>rsh</i> ¹ CS		7205							0,00	4,40	0,00	0,030
Proteasome-associated protein ECM29 homolog Protein phosphatase PHLPP-like protein <i>no spot detected</i>	<i>rsh</i> ¹ <i>rsh</i> ¹ CS	ECM29_DROME PHLPP_DROME	7206	212.0	18	6.4	6,45	108.7 (M:108.7) 101.9 (M:101.9)	2 3	0,00	7,70	0,00	0,020
<i>no spot detected</i> Protein unc-80 homolog Bipolar kinesin KRP-130	<i>rsh</i> ¹ CS CS	UNC80_DROME KL61_DROME	3117	366.6	14,5	9.2	4,8	142.2 (M:142.2) 94.2 (M:94.2)	2 2	8,87	3,27	2,71	0,020
Complexin Complexin	<i>rsh</i> ¹ CS	CPLX_DROME CPLX_DROME	2009	16.4	14	4.8	4,8	252.2 (M:252.2)	3	23,37	72,80	0,32	0,030
Frequenin-1 Myosin heavy chain 95F Probable ATP-dependent RNA helicase spindle-E Myosin heavy chain 95F	<i>rsh</i> ¹ <i>rsh</i> ¹ <i>rsh</i> ¹ CS	FREQ_DROME MYS9_DROME SPNE_DROWI MYS9_DROME	2017	21.7	11	4.8	3,25	121.6 (M:121.6) 118.4 (M:118.4) 100.0 (M:100.0) 90.5 (M:90.5)	2 3 2 3	17,77	4,23	4,20	0,040
Bipolar kinesin KRP-130 Titin DDB1- and CUL4-associated factor-like 1 DNA replication licensing factor Mcm3	<i>rsh</i> ¹ CS CS CS	KL61_DROME TITIN_DROME DCAF1_DROME MCM3_DROME	7112	121.1	13	6.0	6,45	131.6 (M:131.6) 336.0 (M:336.0) 102.4 (M:102.4) 92.1 (M:92.1)	2 3 3 1	5,73	15,07	0,38	0,008
Sterile alpha and TIR motif-containing protein 1 Bipolar kinesin KRP-130	<i>rsh</i> ¹ <i>rsh</i> ¹	SARM1_DROME KL61_DROME	3304	147.8	21	6.9	4,8	113.2 (M:113.2) 102.8 (M:102.8)	4 2	7,33	37,13	0,20	0,010

Replication factor C subunit 1	<i>rsh</i> ¹	RFC1_DROME		108.5		9.9		95.4 (M:95.4)	1				
Tyrosine-protein kinase receptor torso	CS	TORSO_DROME		105.1		6.3		80.4 (M:80.4)	1				
<i>no spot detected</i>	<i>rsh</i> ¹		4019							10,17	0,00	-	0,050
Superoxide dismutase [Cu-Zn]	CS	SODC_DROME		15.7	12	5.7	5,15	173.2 (M:173.2)	2				
<i>no spot detected</i>	<i>rsh</i> ¹		8017							10,27	0,00	-	0,006
Neural-cadherin	CS	CADN_DROME		347.0	12	4.8	6,6	151.1 (M:151.1)	4				
Myosin heavy chain 95F	<i>rsh</i> ¹	MYS9_DROME	0801	143.6	75	9.5	3,2	137.6 (M:137.6)	2	6,00	20,70	0,29	0,080
Regulator of gene activity	<i>rsh</i>	RGA_DROME		59.9		5.6		93.5 (M:93.5)	2				
Glutamine synthetase 2 cytoplasmic	CS	GLNA2_DROME		41.3		5.3		74.5 (M:74.5)	2				
Nucleoplasmin-like protein	<i>rsh</i> ¹	NLP_DROME	1101	17.0	18	4.4	3,3	85.2 (M:85.2)	1	22,33	15,70	1,42	0,770
Breast cancer type 2 susceptibility protein homolog	<i>rsh</i> ¹	BRCA2_DROSE		105.4		5.4		80.8 (M:80.8)	2				
Nucleoplasmin-like protein	CS	NLP_DROME		17.0		4.4		352.7 (M:352.7)	5				
Glutamine synthetase 2 cytoplasmic	CS	GLNA2_DROME		41.3		5.3		89.8 (M:89.8)	2				
Translationally-controlled tumor protein homolog	CS	TCTP_DROME		19.6		4.5		83.0 (M:83.0)	1				
Nucleoplasmin-like protein	<i>rsh</i> ¹	NLP_DROME	1113	17.0	17	4.4	4	276.9 (M:276.9)	4	19,20	72,93	0,26	0,080
PHD finger protein rhinoceros	<i>rsh</i> ¹	RNO_DROPS		351.5		9.8		150.1 (M:150.1)	3				
Enhancer of mRNA-decapping protein 3	<i>rsh</i> ¹	EDC3_DROME		73.4		9.4		86.5 (M:86.5)	2				
PHD finger protein rhinoceros	CS	RNO_DROPS		351.5		9.8		179.8 (M:179.8)	4				
Nucleoplasmin-like protein	CS	NLP_DROME		17.0		4.4		135.8 (M:135.8)	2				
<i>no spot detected</i>	<i>rsh</i> ¹		1203							15,80	8,37	1,89	0,050
<i>no protein found in MS analysis</i>	CS												
Mediator of RNA polymerase II transcription subunit 26	<i>rsh</i> ¹	MED26_DROME	2506	165.4	30	6.8	4,8	81.1 (M:81.1)	3	15,80	25,53	0,62	0,060
PHD finger protein rhinoceros	CS	RNO_DROPS		351.5		9.8		77.8 (M:77.8)	1				
DNA-directed RNA polymerase I subunit RPA1	<i>rsh</i> ¹	RPA1_DROME	2904	185.3	75	8.2	4,8	140.2 (M:140.2)	3	10,90	21,43	0,51	0,090
Heat shock 70 kDa protein cognate 3	<i>rsh</i> ¹	HSP7C_DROME		72.2		5.1		88.6 (M:88.6)	1				
<i>no protein found in MS analysis</i>	CS												
<i>no spot detected</i>	<i>rsh</i> ¹		3006							166,40	33,27	5,00	0,070

DNA-directed RNA polymerase I subunit RPA1	CS	RPA1_DROME		185.3	10	8.2	5	89.0 (M:89.0)	1				
Actin-57B	<i>rsh</i> ¹	ACT3_DROME	3603	41.8	37	5.1	5	318.3 (M:318.3)	8	75,43	265,30	0,28	0,080
Actin-5C	<i>rsh</i> ¹	ACT1_DROME		41.8		5.2		240.1 (M:240.1)	1				
Endophilin-A	<i>rsh</i> ¹	SH3G3_DROWI		41.1		5.3		102.5 (M:102.5)	1				
Actin-87E	CS	ACT5_DROME		41.8		5.2		266.8 (M:266.8)	4				
Actin-5C	<i>rsh</i> ¹	ACT1_DROME	3611	41.8	37	5.2	5,2	608.2 (M:608.2)	11	56,40	236,70	0,24	0,070
Actin, indirect flight muscle	<i>rsh</i> ¹	ACT6_DROME		41.7		5.2		489.5 (M:489.5)	1				
Titin	<i>rsh</i> ¹	TITIN_DROME		2064.5		4.8		382.5 (M:382.5)	6				
<i>no spot detected</i>	CS												
<i>no protein found in MS analysis</i>	<i>rsh</i> ¹		5203							819,33	608,97	1,35	0,080
ATP synthase subunit d, mitochondrial	CS	ATP5H_DROME		20.2	21	6.1	5,5	232.0 (M:232.0)	4				
Myosin-VIIa	<i>rsh</i> ¹	MYO7A_DROME	6501	250.2	37	9.7	5,8	102.5 (M:102.5)	1	52,47	7,50	7,00	0,080
Myosin heavy chain 95F	<i>rsh</i> ¹	MYS9_DROME		143.6		9.5		94.4 (M:94.4)	1				
Titin	CS	TITIN_DROME		2064.5		4.8		161.4 (M:161.4)	4				
<i>no protein found in MS analysis</i>	<i>rsh</i> ¹		6622							29,87	3,40	8,78	0,100
Titin	CS	TITIN_DROME		2064.5	45	4.8	6	207.2 (M:207.2)	3				
Enolase	CS	ENO_DROME		54.3		9.4		121.6 (M:121.6)	2				
Enolase	<i>rsh</i> ¹	ENO_DROME	7609	54.3	44	9.4	6,4	74.4 (M:74.4)	1	46,03	22,73	2,02	0,090
Enolase	CS	ENO_DROME		54.3		9.4		196.7 (M:196.7)	5				
Myosin regulatory light chain 2	<i>rsh</i> ¹	MLR_DROME	1305	23,7	24	4,5	3,5	1291.5 (M:1291.5)	16	131,30	211,80	0,62	0,410
Alanyl-tRNA synthetase, mitochondrial	<i>rsh</i> ¹	SYAM_DROME		113		6,2		105.0 (M:105.0)	1				
Myosin regulatory light chain 2	CS	MLR_DROME		23,7		4,5		906.8 (M:906.8)	12				
Synaptosomal-associated protein 25	CS	SNP25_DROME		23,7		4,4		118.7 (M:118.7)	1				
Protein disulfide-isomerase	<i>rsh</i> ¹	PDI_DROME	1710	55.7	50	4.6	4,3	1023.6 (M:1023.6)	19	412,07	545,70	0,76	0,430
Down syndrome cell adhesion molecule-like protein	<i>rsh</i> ¹	DSCL_DROME		227.5		9.3		97.8 (M:97.8)	2				
Protein disulfide-isomerase	CS	PDI_DROME		55.7		4.6		1084.6 (M:1084.6)	16				
<i>no protein found in MS analysis</i>	<i>rsh</i> ¹		1718							15,27	6,80	2,25	0,270
Protein bangles and beads	CS	BNB_DROME		45.8	49	4.5	4,5	127.9 (M:127.9)	4				
Tropomyosin-1, isoforms 9A/A/B	<i>rsh</i> ¹	TPM1_DROME	2407	39.3	36	4.8	4,3	88.8 (M:88.8)	2	21,13	31,83	0,66	0,410

Tropomyosin-1, isoforms 9A/A/B	CS			39.3		4.8		134.6 (M:134.6)	2				
Bipolar kinesin KRP-130	<i>rsh</i> ¹	KL61_DROME	3823	121.1	55	6.0	5,1	113.1 (M:113.1)	1	8,57	13,03	0,66	0,600
Replication factor C subunit 1	<i>rsh</i> ¹	RFC1_DROME		108.5		9.9		93.5 (M:93.5)	1				
Regulator of telomere elongation helicase 1 homolog	CS	RTEL1_DROPS		112.1		9.6		135.3 (M:135.3)	3				
Breast carcinoma-amplified sequence 3 homolog	CS	BCAS3_DROME		117.5		5.5		81.8 (M:81.8)	2				
Titin	<i>rsh</i> ¹	TITIN_DROME	4108	2064.5	17	4.8	5,2	319.6 (M:319.6)	5	5,53	2,07	2,68	1,000
Replication factor C subunit 1	<i>rsh</i> ¹	RFC1_DROME		108.5		9.9		98.0 (M:98.0)	2				
Protein bric-a-brac 1	<i>rsh</i> ¹	BAB1_DROME		103.3		9.2		83.9 (M:83.9)	2				
<i>no spot detected</i>	CS												
<i>no spot detected</i>	<i>rsh</i> ¹		4422							7,00	4,73	1,48	0,100
Replication factor C subunit 1	CS	RFC1_DROME		108.5	25	9.9	5,3	120.1 (M:120.1)	2				
Cytosolic carboxypeptidase NnaD	CS	NNAD_DROME		133.9		8.9		115.0 (M:115.0)	1				
V-type proton ATPase subunit E	CS	VATE_DROME		26.1		5.8		88.0 (M:88.0)	2				
<i>no spot detected</i>	<i>rsh</i> ¹		4506							12,50	33,23	0,38	0,280
Regulator of gene activity	CS	RGA_DROME		59.9	30	5.6	5,5	50.2 (M:50.2)	1				
Actin-5C	<i>rsh</i> ¹	ACT1_DROME	4607	41.8	38	5.2	5,2	192.1 (M:192.1)	3	98,77	28,33	3,49	0,240
PHD finger protein rhinoceros	CS	RNO_DROPS		351.5		9.8		172.6 (M:172.6)	4				
Actin-5C	CS	ACT1_DROME		41.8		5.2		138.4 (M:138.4)	3				

3.10 Sequence analysis of Radish (Rsh) and Rhinoceros (Rno)

The reduced protein expression rate and the finding, that a number of proteins seem to be differently expressed in *rsh*¹ mutant flies, indicate that Rsh might play a more general role in protein translation than previously hypothesized. In order to understand this role it is necessary to reveal its exact molecular function. For this, the protein sequence of the Rsh protein was revisited and re-investigated in more detail to obtain insights in possible functions of Rsh derived from protein motif analysis. Gene and protein sequence analyses of Rsh were performed using uniprot.org, flybase.org and Interpro (ebi.ac.uk) databases. In 2006, Folkers and colleagues showed already that the *rsh* transcript consists of 5 exons, which results in a protein with a molecular weight of 85 kDa [123]. However, a re-assessed database analysis from June 2014 gave evidence that the *rsh*¹ gene and the Rsh protein seem to be far bigger than initially expected.

Transcript sequence analysis of the *rsh* gene with ensemble.org revealed six different mRNA transcript/splice variants (Figure 23a, Table 8). The open reading frames (ORF) of the transcript variants ranged from 3,516 bp (transcript variant N) to 5,399 bp (transcript variant I). Transcript variant I-M consist of 19 exons each, whereas transcript variant N is composed of 15 exons. The position of the *rsh* mutation is present in exon 4 of transcript variants I-M, but not in transcript variant N (Figure 23a). Translation of the transcript variants results in six different isoforms of the Rsh protein (Figure 23b, Table 8) with molecular weights ranging from 128 kDa (isoform N) to 198 kDa (isoform I). In contrast, based on old sequence data available to them, Folkers and colleagues [123] reported that the Rsh protein has a molecular weight of 85 kDa using western blot analysis [123]. The predicted molecular weight was at that time around 64 kDa (Isoform 'A', Table 8, accession number: AAF48220.1). A Clustal Omega 1.2.1 multiple sequence alignment of all six Rsh isoforms (Supplementary Figure 5) shows, that the amino acid sequence of the protein is not changed between isoforms in terms of amino acid substitution and such. However, the position of the initial Met differs between isoforms (Figure 23b, Supplementary Figure 2, Table 7). Furthermore, this analysis revealed, that isoforms K, L and M lack 145 aa (1,108-1,253 aa, Figure 23a, Supplementary Figure 2) each and that isoform K and J additionally lack 2 aa (1,429-1,430 aa, Supplementary Figure 2).

Protein sequence analysis using InterPro data basis revealed three important domains within the Rsh protein: Zinc-finger LIM type domain, RapGap domain and a BTB/POZ domain (Figure 23b, Table 8). The old isoform 'A' displayed none of the here-described domains (Figure 23b, Table 8). Five out of six isoforms show all three domains, whereas isoform N lacks the Zinc-finger LIM type domain (Figure 23b, Table 8). A protein blast (www.ncbi.nlm.nih.gov/blast) revealed that the Rsh protein is similar to proteins from three other *Drosophila* species: *Drosophila simulans* (95%, flybase-ID: GD17098), *Drosophila*

sechellia (94%, flybase-ID: GM11598) and *Drosophila busckii* (87%, flybase-ID: CG42629). Entries from flybase using the previously named flybase-IDs always lead to the *D. melanogaster rsh*. However, no remarkable homology was found to a protein in other species. Gene ontology analysis predicts molecular functions of Rsh in GTPase activator activity, protein binding and zinc ion binding being involved in ARM, olfactory learning [22, 122, 123, 129-133], activation of GTPase activity and regulation of small GTPase mediated signal transduction [173].

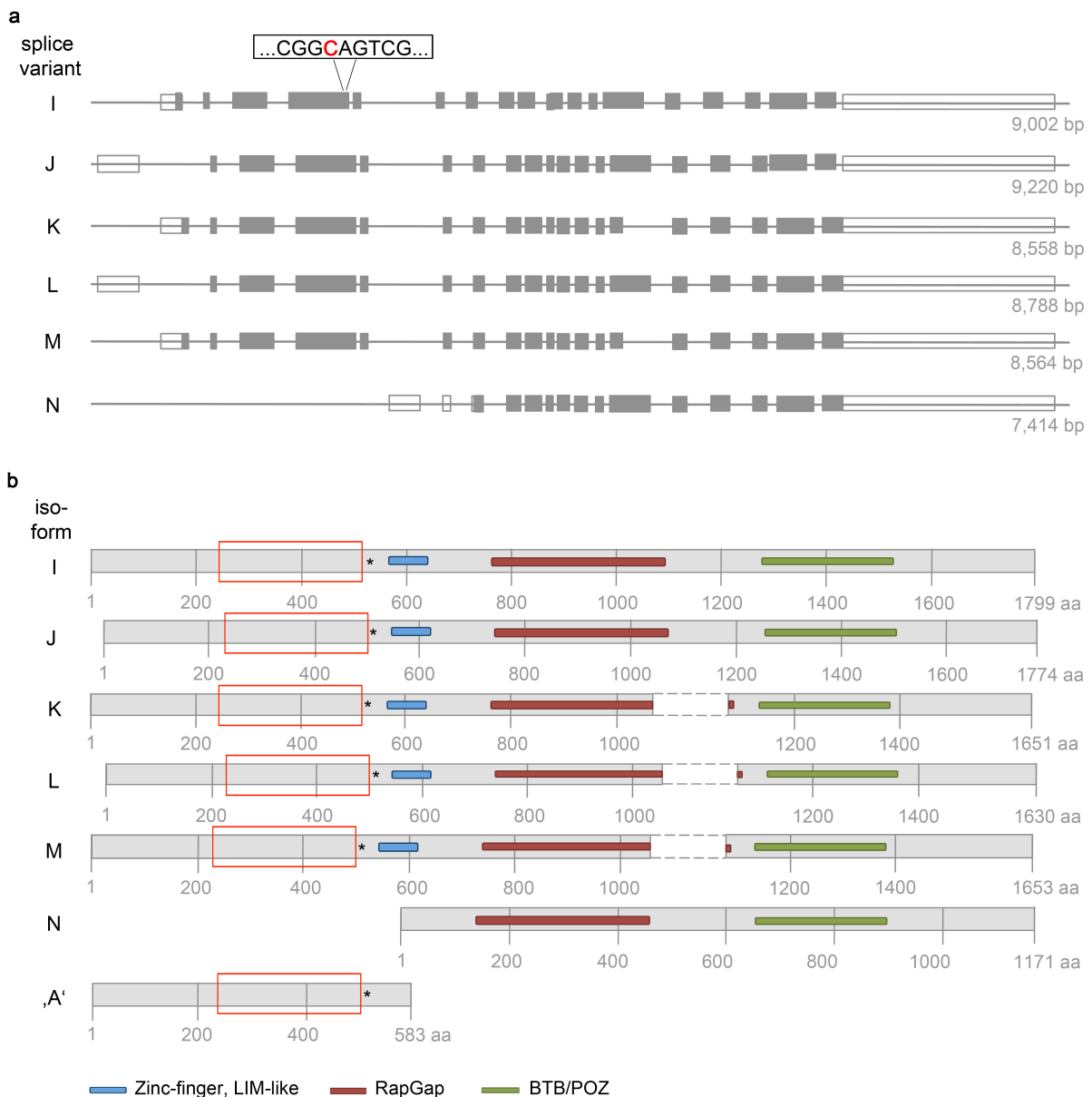


Figure 23: *rsh* splice variants and Rsh isoforms. (a) Six described splice variants of the *rsh* gene. The boxed nucleotide sequence in the 4th exon, depicted exemplarily in splice variant I, contains the cytosine (C), which is converted into a thymine (T) in the *rsh*¹ allele leading to an *amber* stop codon. This affects isoforms I-M. Empty boxes = 5' and 3' untranslated regions (UTRs), filled boxes = coding sequences, line = introns. Numbers displayed on the right represent the number of base pairs (bp) of the respective isoform. (b) Six Rsh isoforms and the originally proposed Rsh isoform ,A' [123] with their respective domains: Zinc-finger, LIM-like domain (blue), RapGap domain (red) and BTB/POZ domain (green). The asterisks mark the C-terminus of the mutated (truncated) Rsh protein. The

mutation is only absent in isoform N. red framed box = region used for immunization to generate anti-Rsh antibodies. Numbers displayed on the right represent the number of amino acids (aa) of the respective isoform.

Table 8: Sequence analysis of *rsh*¹ gene and Rsh protein

transcript variant/ isoform	accession pubmed	position start codon	length ORF	accession uniprot	amino acid number	calculated molecular weight
I	NM_001298247.1	331-333 bp	5,399 bp	X2DJH0	1,799 aa	198 kDa
J	NM_001298248	624-626 bp	5,325 bp	X2JJU0	1,774 aa	195 kDa
K	NM_001298249	331-333 bp	4,956 bp	X2JEQ0	1,651 aa	181 kDa
L	NM_001298250	624-626 bp	4,893 bp	X2JF15	1,630 aa	179 kDa
M	NM_001298251	331-333 bp	4,962 bp	X2JBI1	1,653 aa	181 kDa
N	NM_132622.4	627-629 bp	3,516 bp	Q9I7S4	1,171 aa	128 kDa
'A'	AAF48220.1		1,614 bp		538 aa	64 kDa
Isoform	domain	position	domain	position	domain	position
	Zinc-finger, LIM type		RapGAP domain		POZ domain	
I	+	aa 568-638	+	aa 863-1,081	+	aa 1,281-1,526
J	+	aa 545-615	+	aa 840-1,058	+	aa 1,258-1,501
K	+	aa 568-638	+	aa 863-1,081	+	aa 1,135-1,378
L	+	aa 545-615	+	aa 840-1,058	+	aa 1,112-1,357
M	+	aa 568-638	+	aa 863-1,081	+	aa 1,135-1,380
N	-	-	+	aa 235-453	+	aa 653-898
'A'	-	-	-	-	-	-

As Rno expression shows rather big differences between *wt* and *rsh*¹ mutant flies [135], one might suggest that the *rsh*¹ mutation has either a direct or indirect influence on Rno. However, the molecular function of Rno in the *Drosophila* brain is not fully understood yet, too. Therefore, a gene and protein sequence analysis of Rno was performed as well. The transcript sequence analysis of the Rno mRNA with ensemble.org databases revealed three mRNA transcript variants (Figure 24a, Table 9). The ORF was equal across these variants with a length of 9,723 bp. Translation of the transcript variants results in one isoform for Rno (Figure 24b, Table 9) with a molecular weight of 356 kDa. Analyzing the protein sequence with InterPro showed two different domains within the protein sequence of Rno: an enhancer polycomb-like domain and according to Bateman *et al.* (2002) a Zinc-finger RING/FYVE/PHD motif (Figure 24b, Table 9, [174]). Enhancer of polycomb-like proteins are members of a histone acetyltransferase complex, which are involved in transcriptional activation of selected genes [175]. This indicates that Rno might have a HAT activity like its mammalian homolog Jade-1 [137]. This underlines the finding, that the plant homeodomain (PHD)-containing Rno

seem to be a nuclear protein and might be involved in chromatin-mediated transcriptional regulation [139].

Together these *in silico* data support the idea that both proteins, Rsh and Rno, might be crucially involved in more general regulation of protein expression in *Drosophila melanogaster*.

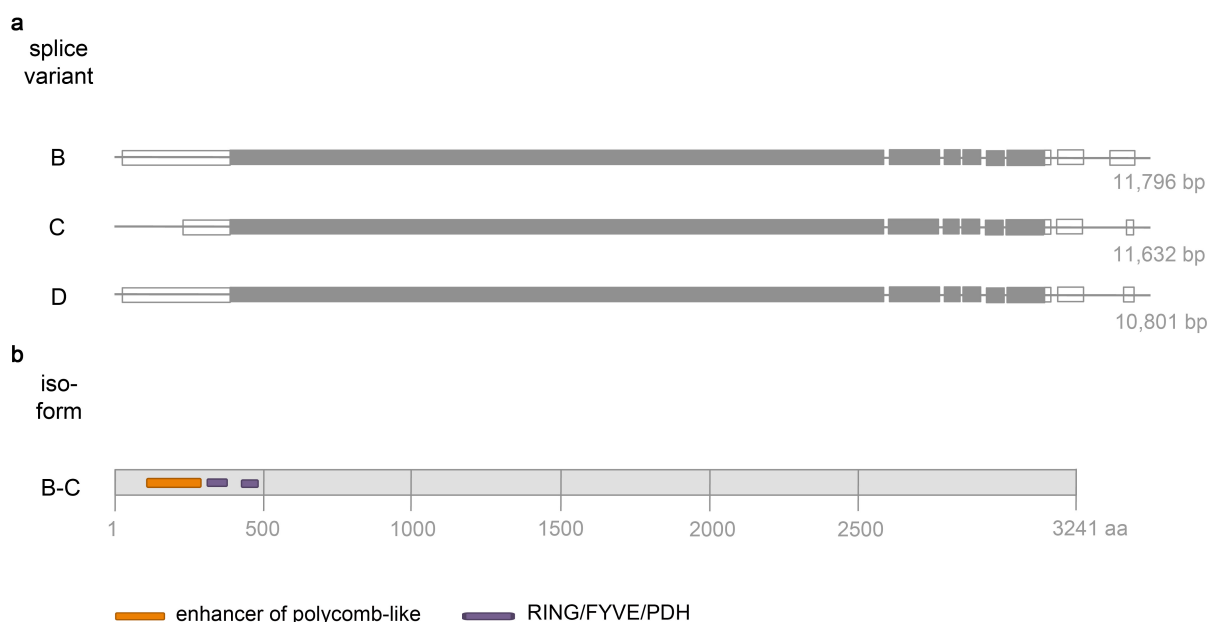


Figure 24: *rno* splice variants and Rno isoforms. (a) Three described splice variants of the *rno* gene. Empty boxes = 3' and 5' untranslated regions (UTR), filled boxes = exons, line = introns, numbers displayed on the right represent the size of the respective splice variant. (b) One Rno isoform with the following domains: enhancer of polycomb-like domain (orange) and a RING/FYVE/PHD domain (purple). Numbers displayed on the right represent the molecular weight of the respective isoform.

Table 9: Sequence analysis of *rno* gene and Rno protein

transcript variant/ isoform	accession pubmed	position start codon	length ORF	accession uniprot	amino acid number	calculated molecular weight
B	NM_206222.3	729-731 bp	9,723 bp	Q7YZH1	3,241 aa	356 kDa
C	NM_138163.2	513-515 bp	9,723 bp			
D	NM_001259599.2	565-567 bp	9,723 bp			
Isoform	domain	position	domain	position	domain	postion
	Enhancer polycomb-like, N-terminal		Zinc finger RING/FYVE/PHD-type		Zinc finger PHD-type	
B-D	+	aa 109-285	+	aa 306-375	+	aa 423-481

3.11 Radish antibody generation

My data analysis of 2D gel electrophoresis, sequence analysis and FlyNCAT experiments indicated that Rsh seems to influence the cellular protein expression pattern. Unfortunately,

no commercial antibody against Rsh is available to perform detailed analyses on the direct or indirect nature of protein-protein interaction, on protein-DNA interaction, or on subcellular localization of Rsh. Folkers *et al.* (2006) generated an antibody against Rsh using a synthetic peptide corresponding to amino acids 522-542 [123], a sequence existing only in the *wt* Rsh protein. Thus, the Rsh protein can only be investigated in the *wt* background but not in the mutant background with the help of this antibody.

Thus, an antibody against Rsh was generated using the initial nucleotide and amino acid sequences according to Folkers *et al.* (2006) covering amino acids 235-515 ([123], accession number: AAF48220.1, Figure 23b) of the Rsh protein recognizing both the *wt* and mutant Rsh isoforms (Figure 23b). The generated antisera (gp1-anti-Rsh, gp2-anti-Rsh, rb1-anti-Rsh and rb2-anti-Rsh) were tested for their specific binding to Rsh in GFP-Rsh²³⁴⁻⁵¹⁸ (aa 234 – 518 of Rsh protein) expressing Hek293T cells using immune fluorescence (IF) staining and western blot analysis.

The GFP-signal of transfected Hek293T cells revealed a reliable signal for GFP reflecting the correct expression of GFP-Rsh²³⁴⁻⁵¹⁸ or GFP (Figure 25a, 'GFP'). The immune fluorescence staining of the antibody in GFP-Rsh²³⁴⁻⁵¹⁸ expressing Hek293T cells was cluster-like in contrast to the homogeneous GFP signal in these cells (Figure 25a, arrow head). The signal intensity for Rsh was higher at the cell membrane compared to the rest of the cell. Unfortunately, a signal for Rsh was also observed in non-transfected Hek293T cells, indicating that the antibody binding is not exclusively restricted to Rsh (Figure 25a, circle). GFP expressing Hek293T cells or the incubation of Hek293T cells lysates with the preserum, served as controls and, showed no signal or only slight background staining for Rsh (Figure 25).

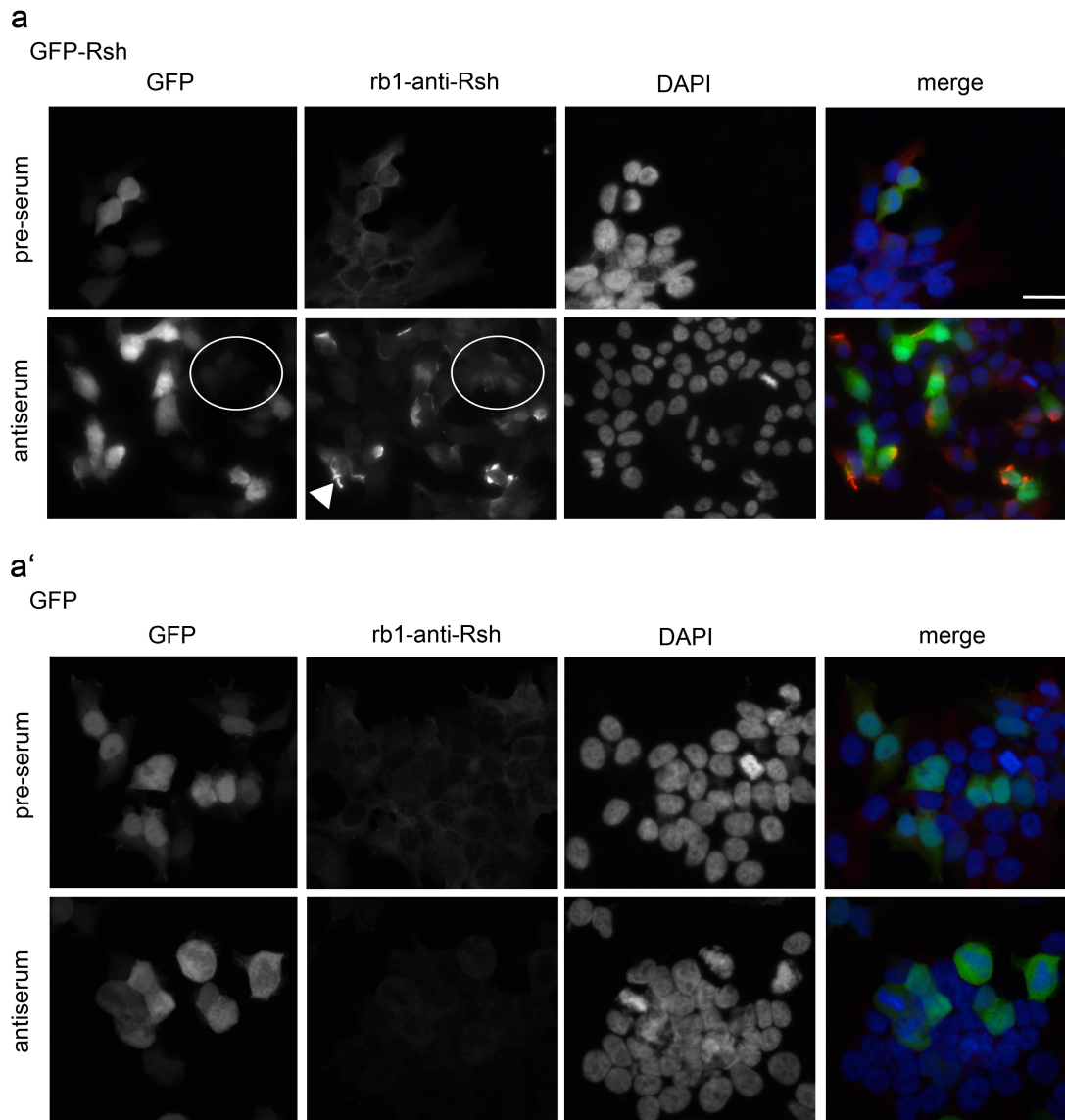


Figure 25: Antibody characterization of anti-Rsh antisera using IF staining. IF staining of transfected GFP-Rsh²³⁴⁻⁵¹⁸ Hek293T cells showed an inhomogenous staining pattern of the cells (a, arrow head). IF staining with rb1-anti-Rsh was not restricted to GFP-Rsh²³⁴⁻⁵¹⁸ transfected Hek293T cells but also stained non-transfected cells (a, circle). However, IF staining of controls showed no antibody binding to Rsh (a, a'). Scale bar = 25 μ m.

Western blot analysis of protein lysates from transfected Hek293T cells revealed correct GFP-Rsh²³⁴⁻⁵¹⁸ or GFP expression, respectively (Figure 26a, a', 'anti-GFP'). These protein lysates showed a specific signal for GFP-Rsh²³⁴⁻⁵¹⁸ at the expected molecular weight of 61 kDa on western blot after incubation with the generated antisera (Figure 26a, a'). In contrast, the control groups, GFP expressing Hek293T cells, showed no signal for Rsh (Figure 26a, a'). In total two out of four antisera revealed specific detection of GFP-Rsh²³⁴⁻⁵¹⁸ on western blot, whereas antisera derived from the immunization of the guinea pigs were excluded from subsequent analyses, as these antisera were unable to detect Rsh in GFP-Rsh²³⁴⁻⁵¹⁸ expressing Hek293T cells (data not shown). The two remaining antisera were tested for their specific binding to endogenous Rsh in head lysates of *wt* (*Canton-S*, *CS*) and *rsh*¹ mutant

flies using western blot. This analysis revealed that the two antisera detected several bands corresponding to different molecular weights, ranging from 50 to 300 kDa in the head lysates of *wt* and *rsh*¹ mutant flies (Figure 26b, b'). Rb2-anti-Rsh seemed to recognize fewer bands. Unfortunately, incubation of the western blot with pre-serum obtained from one rabbit showed the same staining pattern as the antisera (Figure 26b). Thus, this antibody will be excluded for further experiments, as this rabbit showed immune-reactivity before immunization. The pre-serum obtained from the second rabbit showed a band at 200 kDa (Figure 26b'). Among others, this band was also observed on western blot after antiserum treatment (Figure 26b'). According to the predicted molecular weight of Rsh (Table 8) this band could indeed represent Rsh but as this band was observed in the pre-serum as well, one can assume that the actual signal for Rsh might be masked by unspecific antibody binding to other proteins with an identical molecular weight. Thus, the specificity of the antibody binding needs to be determined for future applications of this antiserum. Furthermore, one would expect a difference in the band recognition pattern of the Rsh-antisera between *wt* and *rsh*¹ mutant flies, as the *rsh* mutation according to Folkers *et al.* (2006) would result in a truncated protein of around 57 kDa (Figure 23b, [123]). Thus, only one band at this molecular weight should be detected in head lysates of *rsh*¹ flies using the Rsh-antisera (Figure 23, Supplementary Figure 2). However, the band recognition pattern did not differ between *wt* and *rsh*¹ mutant flies (Figure 26b, b'), although *rsh*¹ flies were tested for the *rsh* mutation by DNA sequencing of single-fly PCR-products (data not shown). Note that the Rsh antibody is not able to recognize isoform N, as this isoform lacks the epitope of the antibody (Figure 23b, Supplementary Figure 2).

Summarizing, the specificity of the antibody binding to Rsh using IF staining and western blot analysis needs to be optimized in future experiments also taking into account that the here presented data are preliminary. These include affinity purification of the antibody, testing of different blocking conditions and different dilutions as well as a peptide competition assay. Last but not least this antibody needs to be tested for IF staining in brains of *Drosophila* larvae and flies to determine if there are suitable to detect endogenously expressed Rsh.

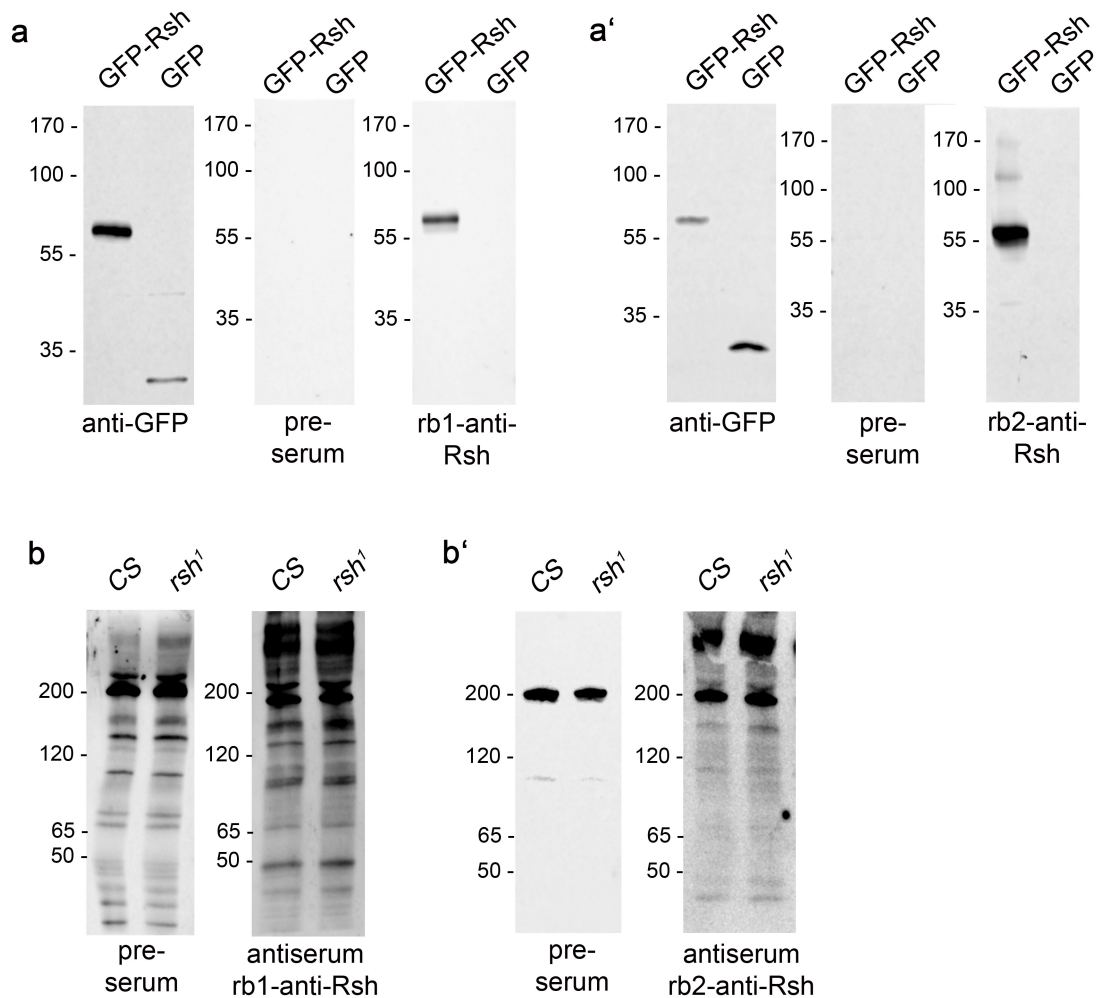


Figure 26: Antibody characterization of anti-Rsh antisera using western blot. (a, a') Western blot analysis of protein lysates of GFP-Rsh²³⁴⁻⁵¹⁸ or GFP expressing Hek293T cells showed that GFP-Rsh²³⁴⁻⁵¹⁸ and GFP were expressed in the expected molecular weight ('anti-GFP'). The same lysates were used for testing the specificity of anti-Rsh antibody binding on western blot. Here, a signal at 61 kDa was only detectable when Hek293T cells expressed the GFP-Rsh²³⁴⁻⁵¹⁸ fusion protein, whereas no signal for Rsh was detectable when Hek293T cells expressed GFP alone. Pre-serum showed no binding to GFP-Rsh²³⁴⁻⁵¹⁸ or GFP. (c) Testing of antibody binding in head lysates of *wt* and *rsh*¹ mutant flies showed that antiserum obtained from rabbit 1 binds not specifically to Rsh as the pre-serum control showed the same band recognition pattern as the antiserum (b). The pre-serum of rabbit two only showed binding to a protein band at 200 kDa (b'). The band recognition pattern of the antiserum was not distinguishable between *wt* and *rsh*¹ mutant flies. CS = *Canton-S*, *rsh*¹ = *radish*¹, rb = rabbit, gp = guinea pig, n=3 independent experiments

4 Discussion

4.1 MetRS^{L10G}-mediated ANL incorporation enables cell-type specific identification of newly synthesized protein *in vivo*

Deciphering the sophisticated network architecture of the brain and thereby unraveling the underlying mechanisms of synaptic plasticity is one of the major challenges in neuroscience. For this, it is important to investigate the different cell-type specific proteomes within the synaptic complex and to understand how proteome dynamics are altered in terms of posttranslational modifications, protein synthesis and protein degradation upon neuronal activation or in the course of neurodegenerative disease. However, the identification of the synaptic proteome is troublesome. On the one hand the different cell types (pre-synaptic neuron, post-synaptic neuron, adjacent glia cell) at a synapse are tightly connected and share a variety of identical proteins, including transmembrane receptors, neurotransmitters and cell adhesion molecules. On the other hand all proteins, old or new ones, share the same pool of amino acids. Hence, using the previously reported labeling and tracking methods deciphering the cellular origin of a certain protein was not possible. Recently, Müller *et al.* (2015) showed, that cell-type specific protein labeling using GINCAT and BONCAT could separate astrocytic 60S ribosomal protein L10a (Rpl10a) from neuronal Rpl10a in neuron-glia co-cultures. Rpl10a is a protein known to be expressed ubiquitously in neurons and glia cells [161]. Another publication used an *in vivo* labeling of proteins with azido-L-phenylalanine (Azf) in *Caenorhabditis elegans* (*C. elegans*) upon expression of the mutant phenylalanyl tRNA-synthetase (PheRS) alpha subunit to profile the muscle proteome of *C. elegans* in combination with SILAC. Thereby, a number of proteins were identified that were previously unknown to be expressed in this cell type [73]. These two publications already show that cell-type specific labeling of proteins could be used to uncover cell-type specific proteomes and thereby helping to understand proteome dynamics. The here introduced cell-type selective metabolic protein labeling technique FlyNCAT expands the toolbox to uncover protein dynamics *in vivo* using *Drosophila melanogaster* as a model organism.

The FlyNCAT technique uses the cell-type specific incorporation of the non-canonical amino acid ANL upon target expression of a mutant MetRS variant. ANL is, like other non-canonical amino acids e.g. AHA and HPG, a Met surrogate, but is excluded from the binding pocket of the endogenous MetRS due to its enlarged side chain. The mutant *E. coli* MetRS variants, EcMetRS^{L13G} and EcMetRS^{NLL}, have been already widely used in bacterial and mammalian cell culture systems and showed a cell-type specific incorporation of ANL into protein [66-69]. However, the authors showed that the EcMetRS^{NLL} mutant only charged ANL onto the initiator methionyl-tRNA [69] and, thus, ANL is only incorporated at the very N-terminal end of proteins [69]. This is a severe limitation as ≈80% of the proteins undergoes proteolytic cleavage [164-166]. Generating transgenic *Drosophila melanogaster* larvae and flies

expressing the mutant MetRS^{LtoG} variant cell-type specifically solved this problem. For this, the mutant *E. coli* MetRS variant, which exhibits a single amino acid substitution (leucine → glycine) at position 13 within the amino acid sequence of the well-conserved MetRS binding pocket [160], was used as a blueprint to generate corresponding murine and *Drosophila* MetRS with the single amino acid substitution (leucine → glycine) at position 262 in the *Drosophila* MetRS or at position 274 in the murine MetRS variant [11, 161]. Upon cell-type specific target expression of either murine or *Drosophila* MetRS^{LtoG} variant ANL is incorporated robustly into proteins of the selected cell type using the GAL4/UAS-system [8, 9] (Figure 8-10, 12-14). ANL-labeled proteins were visualized or biochemically analyzed using the previously reported FUNCAT [49-51] and BONCAT [52, 53] techniques, respectively. For this, the staining, lysis and purification conditions needed to be adapted carefully in the course of this thesis to the *Drosophila* system to establish and optimize the detection of ANL-labeled biotin-tagged proteins [135]. Both FUNCAT and BONCAT confirmed that ANL is incorporated only in proteins of those cell types that express one of the mutant MetRS^{LtoG} variants (Figure 8-10, 12-14). BONCAT facilitates for the detection of ANL-labeled proteins across the whole molecular range, including a number of cell-type specific candidate proteins, like the presynaptic protein Synapsin, the postsynaptic protein Dlg at larval NMJs and in glia cells and transmembrane proteins, e.g. Draper I and Basigin (Figure 9, 10, 12, 14). ANL-labeling of these transmembrane proteins (Figure 9, 10) already suggests that ANL is incorporated not only at the very N-terminus of proteins, as transmembrane proteins, among others, are known to undergo proteolytic cleavage [72, 164-166, 168]. Identification of ANL-containing peptides by tandem mass spectrometry analysis (Supplementary Figure 1) as well as the identification of the ANL-labeled intracellular Notch fragment confirmed that the here reported MetRS^{LtoG} variants incorporate ANL at internal residues of the entire protein (Figure 14, [11, 140]). Thus, the previous limitation of N-terminal ANL incorporation by the EcMetRS^{NLL} mutant reported by Ngo *et al.* (2009) and Ngo, Schuman & Tirrell (2013) [68, 69] were solved using the MetRS^{LtoG} variants, which means that these MetRS^{LtoG} variants could be used to identify proteins of different protein classes, including cytosolic and membranous proteins using BONCAT. Remarkably all proteins can be labeled under physiological conditions, as the usage of MetRS^{LtoG} variants does not require Met-depleted culture medium. Link *et al.* (2006) showed that the activation rate of Met by the EcMetRS^{L13G} is 300-fold smaller compared to the activation rate of ANL [66]. Although the activation kinetics have to be determined for the here reported murine and *Drosophila* MetRS^{LtoG} variants, one can assume that the incorporation efficiency of ANL by either MetRS^{LtoG} variant is higher compared to that of Met as solid ANL incorporation was observed despite the presence of Met (Figure 8-10, 12-14). In contrast, the incorporation efficiency of Met analogs, like AHA, correlates strongly with their rates of activation by the

endogenous MetRS [70, 71], leading to a competition of both AHA and Met at the MetRS binding pocket. Thus, labeling of proteins with AHA or HPG requires Met-free culture medium and high concentrations of either AHA or HPG to outcompete Met at the binding pocket of the endogenous MetRS.

Despite the possibility that ANL can be applied under physiological conditions *in vivo* and *in vitro* its enlarged side chain (Figure 1a) could lead to protein misfolding resulting in malfunctioning of proteins and subsequent abnormal behavior. Nevertheless, proper protein function and localization are important to understand protein dynamics under physiological and pathological conditions. ANL incorporation caused only limited side effects on larval body weight (Figure 15a, a'), on the hatching rate of adult flies (Figure 15b-c') and on behavioral performances [11]. Most of the behavioral effects were rescued when ANL was applied acutely to *Drosophila* larvae and flies for 24 h or 48 h [11], although ANL was efficiently incorporated mediated by both MetRS^{LtoG}-EGFP variants (Figure 12a-b'). Besides that, reducing the time period of ANL exposure to a defined window of development or to a certain phase of the adult fly stage acutely monitors the synthesis of proteins made during this time interval. FUNCAT and BONCAT experiments showed that the longer *Drosophila* larvae and flies were exposed to ANL the more ANL was incorporated into the proteins of the investigated cell types (Figure 12, [11]). Together with the fact that reduction of the ANL exposure time rescued most the behavioral deficits [11] and the fact that the ANL incorporation rate into different cellular proteomes mediated by the mMetRS^{L274G}-EGFP seem to be higher than by the dMetRS^{L262G}-EGFP variant under varying ANL concentrations (Figure 10), the usage of either MetRS^{LtoG} variant, the ANL exposure time and the applied ANL concentration need to be chosen carefully with regard to the experimental question. Otherwise, the vitality of the larvae and flies and, thereby, the labeling efficiency of more sensitive cell types, e.g. neurons could be affected (Figure 15, [11]).

Taken together, the FlyNCAT technique provides a suitable basis to unravel for instance specifically the synaptic proteome by overcoming the problem that the pre- and postsynapse as well as the adjacent glia cell share a variety of identical proteins, and most importantly, cannot be physically untangled without disturbing their cellular function. In the scope of this work, this issue was addressed exemplarily by our finding that the postsynaptic protein Dlg is expressed in glia cells (Figure 9), which was not known previously. However, using FlyNCAT we were able to verify that Dlg is indeed expressed in glia cells of *Drosophila* flies, confirming previous observations of the presence of a slight Dlg immunoreactivity in glial cells using conventional immunostainings of *Drosophila* larval body walls (personal communication with Dr. Ulrich Thomas). Thus, FlyNCAT is capable to unravel new expression sites of proteins and providing a better understanding of functions at synapses. Tracking proteomes through different developmental stages showed another application of the FlyNCAT technique. The

morphology of the nervous system of *Drosophila melanogaster* is drastically changed and reorganized during metamorphosis [163]. However, it is unknown which structures are eventually preserved. This was exemplarily addressed by preliminary pulse-chase experiments with ANL in conjunction with the FlyNCAT technique to investigate if proteins that are expressed during larval phase are transferred into the adult stage during metamorphosis. This analysis revealed a substantial amount of larval synthesized ANL-labeled proteins in adult flies (Figure 13). However, it remains unclear if the proteins, synthesized during larval stage, are carried out into adulthood or whether the ANL-labeled proteins in adult flies reflect incorporation of recycled ANL from apoptotic cell material. This has to be clarified in future experiments, e.g. by expressing a candidate protein only from adult stage onwards using the Gal80 system [10] and analyzing this protein in terms of ANL-labeling.

These two examples show that the highly specific FlyNCAT technique can be used in several manners to study e.g. the synaptic proteome and the associated underlying proteome dynamics during neuronal activation. The close association of perisynaptic glia cells to pre- and postsynaptic specializations of a neuron gave rise to the concept of the tripartite synapse [176]. Glia cells support and contribute to a variety of neuronal development and functions, including the formation, maintenance and elimination of synaptic contacts as well as homeostatic scaling. The existence of a mammalian tripartite synapse concept is proofed [176]. However, only a few studies are available that addresses the existence of a tripartite synapse model system in *Drosophila melanogaster*. Danjo *et al.* (2014) and Strauss, Kawasaki and Ordway (2015) provided a new insight in the synaptic organization at the adult glutamatergic neuromuscular synapse (NMS) in *Drosophila melanogaster* [177, 178]. They reported the existence of a tripartite synapse model in *Drosophila* [178] and showed that the adjacent glia cells is a peripheral perisynaptic glia cell [177], similar to the perisynaptic Swan cell at the NMS in frog and mouse [179, 180]. This model of a tripartite synapse in the *Drosophila* can be used to decipher the activity-dependent changes of the neuronal and glia proteome by combining FlyNCAT with SILAC [59-62, 73]. Several studies showed that combining both SILAC and BONCAT yield a quantitative approach to investigate alteration of protein contents upon stimulation [59-62, 73]. Upon targeted expression of one of the MetRS^{LtoG} variants, ANL will be incorporated cell-type specifically either in neurons or in glia cells. Mass spectrometric analysis will then reveal ANL-labeled proteins of the respective cell type, thereby uncovering the synaptic proteome under baseline conditions. Following, FlyNCAT in combination with SILAC [59-62, 73] can quantify activity-dependent protein changes of the synaptic proteome by comparing the different proteomes during resting and activation state, as activation of synapses lead to the synthesis of new proteins [181]. In other words, combining SILAC and BONCAT gives to the possibility to separate newly

synthesized proteins of the investigated cell type from identical proteins existing in another (adjacent) cell type in a quantitative manner. This data will provide conserved mechanisms of the tripartite synapse function of glutamateric synapses under physiological and pathological conditions in *Drosophila melanogaster*. As this approach was beyond of this thesis it should be also addressed in the future.

In conclusion, FlyNCAT is a valuable extension of the preexisting toolbox to resolve complete cell-type specific proteomes, for instance regarding glial contribution to the functionality of synapses and regarding plasticity induced changes of the fly proteome upon long-lasting learning and memory. Notably, the usage of proteome labeling using FlyNCAT is not restricted to the nervous system, it can also be used to identify proteomes of other tissues, e.g. to identify the muscle proteome (Figure 9, 10, 12). Thus, this method can be applied to very diverse scientific questions to uncover proteomic changes. For instance, transgenic animals can also be used to track proteome changes cell-type specifically to investigate pathological events and thereby unraveling the cell type which is affected by a certain disease or is the causes the disease. This in turn will help to generate cell-type specific therapeutic treatments to reduce adverse events of certain medications as by now many medications are known to act systemically and not only at the site of a disease's cause. The application of FlyNCAT to investigate cell-type specific proteomes is addressed in more detail within the next section (see 4.2).

4.2 First applications of FlyNCAT in the nervous system of *Drosophila melanogaster* to unravel proteome dynamics under pathological conditions

4.2.1 Reduced protein synthesis rate in motor and sensory neurons of a *Drosophila* model for Charcot-Marie-Tooth neuropathy

Niehues and colleagues generated a GARS-associated *Drosophila* Charcot-Marie-Tooth (CMT) model that exhibits various crucial characteristics of CMT neuropathy such as distal muscle weakness and wasting, decreased reflexes, sensory loss and foot deformities [23]. Mutations in tRNA synthetases could lead to defects in protein translation *per se* and, thus, are one of many possibilities to give rise to this disease. The FlyNCAT technique revealed that, despite correct subcellular localization of mutant hGARS [23], the relative protein translation rate was reduced in larval motor and sensory neurons in larvae of the CMT *Drosophila* model (Figure 17a, b, [23]). As all three hGARS mutants cause developmental lethality of late L3 instar larvae, the protein translation rates in adult *Drosophila* flies was evaluated by expressing either of the mutant hGARS variants from adult stage onwards using an inducible Gal80^{ts} driver line [10]. Here, metabolic protein labeling with AHA was used rather than ANL. In the mutant background AHA-labeling was not sufficient enough to detect AHA-labeled proteins. This is probably due to the competition situation between AHA

and Met at the binding pocket of the endogenous MetRS [70, 71] - highlighting the advantage of ANL-labeling compared to AHA-labeling [70, 71]. Using radioactive labeling of proteins with S^{35} -methionine in adult GARS mutant flies instead revealed a reduction of the protein translation rate [23]. Nevertheless, this required ubiquitous expression of mutant hGARS protein to avoid dilution of the effect by non-expressing cells and was therefore not restricted to a certain cell type in the brain. In future experiments recombinant flies expressing either of the mutant hGARS proteins together with one of the MetRS^{LtoG} variants under the control of the inducible Gal80^{ts} promoters could solve these problems. This method will provide data about the protein expression rate in adult CMT flies cell-type specifically to characterize this disease in more detail.

Reduced global protein translation rates imply that the translation of the dMetRS^{L262G}-EGFP variant itself could possibly be reduced. This can lead to the reduction of ANL incorporation into proteins reflecting false-positive results. Thus, the expression level of the dMetRS^{L262G}-EGFP variant was evaluated on western blot in hGARS mutant larvae. hGARS^{E71G} and hGARS^{G240R} mutants showed a reduced dMetRS^{L262G}-EGFP expression by $\approx 20\%$ and $\approx 50\%$ respectively [23]. In contrast, the dMetRS^{L262G}-EGFP expression was not altered in mutant hGARS^{G526R} animals, although they exhibit a diminished protein translation rate [23]. Together with the finding that the protein translation rate was reduced as well when determined independently from the dMetRS^{L262G}-EGFP expression by using S^{35} -methionine [23], one can assume that the defective protein translation rate observed here may not be a result of reduced dMetRS^{L262G}-EGFP expression levels. This was underlined by the investigation of another CMT-associated model showing a reduction of the protein translation rate as well using FlyNCAT. Thus, defective protein synthesis can be assumed as a common pathogenic mechanism that underlies CMT [23]. The here presented application of the FlyNCAT technique demonstrates clearly, that the obtained results need to be interpreted carefully using appropriate control experiments, e.g. validation of MetRS^{LtoG} expression in the particular genotypic background and/or alternative metabolic labeling strategies.

4.2.2 Reduced protein synthesis rate in neurons of dFmr1 knockdown larvae

The current literature on global and local protein synthesis rates in *Fmr1* mutant or KO model is rather contradictory. Many studies in *Fmr1* KO models showed that the dendritic protein synthesis rate is increased in the absence of FMRP [87, 99, 100, 103-107], whereas other studies showed a reduced protein synthesis rate in synaptoneurosomes of *Fmr1* KO mice [110, 111]. Here, FlyNCAT was used as a more direct approach to investigate the role of dFMR1 (*Drosophila* homolog of FMRP) during global protein synthesis in *Drosophila* larvae. For this, dFMR1 was either knocked down or overexpressed in neurons of *Drosophila* larvae

and protein translation rates were determined using FlyNCAT by co-expressing the dMetRS^{L262G}-EGFP variant in neurons as well.

BONCAT analysis revealed a reduction of the global protein translation rate in dFMR1 knockdown larvae, whereas overexpression of dFMR1 in neurons of *Drosophila* larvae resulted in an elevated global protein translation rate (Figure 19b). These findings might be able to put new light on the functional role of FMRP for protein synthesis events. Disregulation of primary mRNA targets of FMRP could have secondary consequences on the global protein translation rate as well. Thus, the local and the global role of FMRP in mRNA transcription and translation need to be investigated in more detail to unravel the function of FMRP within the brain. This can be achieved by determining e.g. the amount of translated mRNA using translating ribosome affinity purification (TRAP) [182] in animals with knocked down or overexpressed dFMR1. Using TRAP, the large ribosomal subunit L10a is fused to EGFP and expressed cell-type specifically under the control of a specific promoter. EGFP enables not only for the visualization but also for the affinity purification of translating ribosomes together with the translated mRNA bound to the ribosome. Using standard techniques like northern blotting, quantitative PCR, microarray or RNA sequencing will (i) identify the amount of mRNA translated and (ii) specify the nature of the translated mRNA [182].

Larvae with knocked down or overexpressed dFMR1 showed larval lethality in the late L3 stage (data not shown). This could be substantiated by two reasons; either the manipulation of dFMR1 in larval neurons or the chronic application of 4 mM ANL have led to this effect (see 3.7). Reports of adult *Fmr1*, *Fmr1*³ and *Fmr1*^{B55} mutants, showing no dFMR1 expression within the brain, were alive and vital [108], whereas overexpression of dFMR1 in several tissues of *Drosophila* results in apoptotic cell loss in the respective tissues [109]. However, as larval lethality was observed in dFMR1 knockdown as well as in overexpressing animals, the chronic exposure of ANL to the mutant larvae is likely to either cause or severely worsen an putative hidden lethality, given the already severely challenged situation of the animals due to increased or limited amounts of dFMR1. Prospectively, to investigate the protein synthesis rate in neurons of adult flies with a dFMR1 mutant background shorter labeling periods, lower ANL concentrations and the usage of null allele *Fmr1* mutant flies could overcome this problem. For this, recombinant flies expressing one of the MetRS^{LtoG} variants in the mutant *Fmr1* background in neurons of *Drosophila* flies will be generated. Labeling of proteins with ANL (2 mM or 4 mM) for 24 h (or 48 h respectively) will reflect global *de novo* protein synthesis in neurons of *Fmr1* mutant flies using BONCAT analysis. These findings might help to give rise to the cause of FXS, thereby giving indications to design therapeutic treatments for FXS.

4.2.3 FlyNCAT and sequence analysis suggest a putative role for Rsh for protein synthesis

The function of the Rsh protein can be hardly predicted as the protein lacks almost any homology to proteins with known functions [123]. Re-assessed database analysis revealed again no striking homology to other proteins with known functions. It is only known that the Rsh protein seem to contribute to the formation of olfactory memory [22, 122, 123, 129, 130, 132, 133], but how it contributes remains elusive. There is evidence that protein expression rates might be impaired in *rsh*¹ mutant flies as initial mass spectromic analysis of protein lysates of *rsh*¹ and *wt* flies showed that the transcription factor Rno might differently expressed between *rsh*¹ mutant and *wt* flies (Figure 5). As both Rno and Rsh show features of either direct or indirect transcriptional and/or translational regulators (Figure 23, 24), protein translation in neurons of heterozygous *rsh*¹ mutant flies was evaluated using FlyNCAT. This analysis revealed that the protein expression rate was significantly reduced in neurons of heterozygous *rsh*¹ mutant flies compared to the protein synthesis rate of *wt* flies (Figure 20). This lies in line with the findings of Guan *et al.* (2011). They showed that several transcript are altered in *rsh*¹ mutant flies and hypothesized that Rsh as PKA target *in vitro* might be translocated between cytoplasm and nucleus upon PKA phosphorylation [134]. Its translocation into the nucleus will then affect transcription and mRNA processing, resulting in a modification of (long-term) synaptic function. This in turn would perfectly explain the behavioral deficits observed in *rsh*¹ mutant flies. Interestingly, both the Zinc-finger LIM like type domain and the BTB/POZ domain were found in the Rsh protein. Proteins harboring these domains are found to act as transcriptional regulators but in opposite ways. Meaning, that the LIM domain is mostly found in protein acting as transcriptional activators [183], whereas the BTB/POZ domain is mainly found in proteins acting as transcriptional repressors [184]. This indicates that Rsh might function either as a transcriptional activator or repressor probably depending on (i) its subcellular localization, linked to a certain cellular event, and/or (ii) the Rsh isoform, i.e. the existence and position of the different domains could reflect different function of the Rsh protein (Figure 23b). The RapGap (Rap GTPase activating protein) domain found in the protein sequence of Rsh implies that Rsh might be a Rap controlling protein and thereby influencing cytoskeletal arrangements at synapses as the Rap protein and its activators (Gefs – guanine nucleotide exchange factor) and inactivators (Gaps – GTPase activating proteins) are located at synapses [185-189]. Thus, Rsh as a RapGap controlling protein must be localized to synapses as it was already indicated by Guan and colleagues (2001) [134]. Thus, defective local protein synthesis, e.g. at synapses, which could lead to neurodegeneration accompanied by behavioral deficits could explain the phenotype of *rsh*¹ mutant flies. To address this hypothesis in more detail FUNCAT, rather than BONCAT, experiments will be used in future experiments to gain insights into the

cellular resolution of where and how many proteins are newly synthesized in *rsh*¹ mutant flies. Furthermore, future experiments need to be performed to proof if an interaction between Rsh and Rap exists, e.g. by immune precipitate studies. Formstecher *et al.* (2005) already showed that Rsh has the ability to bind small GTPases and thereby influencing their activation states. They showed that Rsh binds Rac1, a small GTPase of the Rho family [173]. Rac1 functions in axon growth, guidance and branching in *Drosophila* [190]. It was also shown that Rac1 lies in the same signaling pathways like Pak1 and FMRP. Both are known to have effects on synaptic and behavioral plasticity [191, 192]. That Rsh might act on cytoskeletal arrangements is underlined again by Guan *et al.* (2011). They already showed an altered synaptic connectivity in *rsh*¹ mutants [134]. This indicates that Rsh might functioning in ARM by changing synaptic morphology through Rac1 interaction or through interaction with others GTPases by changing their activational state [123].

Nevertheless, the reason why the protein expression rate is impaired in neurons of heterozygous *rsh*¹ mutant flies requires additional experiments, as the amount of the dMetRS^{L262G}-EGFP itself was reduced too (Figure 20c). Thus, this defect could be a result of an impaired mRNA translation or could be found already at the level of transcription [134]. As impaired protein synthesis might also influence Elav expression of the *elav*^{C155}-*Gal4* driver line in *rsh*¹ mutant flies, BONCAT and FUNCAT experiments will be repeated using another panneuronal driver line (e.g. *nsyb-Gal4*). Moreover, the protein synthesis rate was solely investigated in neurons of heterozygous *rsh*¹ mutant flies. However, as the expression site of Rsh is not entirely clear yet and the fact that there is evidence that glia cells contribute to learning and memory formation [193], the protein synthesis rates will be investigated additionally in glia cells of *rsh*¹ mutant flies using FlyNCAT. Nevertheless, one has to consider that Rsh could have an influence on other cell types, like on glia cells, *per se* without being expressed in them. For this, it is absolutely necessary to know which cell types do express Rsh (see section 4.3).

Often, rescue experiments are performed to gain insights into a possible function of a certain protein. Van Swinderen and Brembs (2010) rescued the behavioral deficits in the *rsh*¹ mutant using methylphenidate (MPH) treatment [22]. Studies have shown, that MPH increases the hippocampal dopamine and norepinephrin levels *in vivo* [194, 195]. Methylphenidate blocks dopamine transporters, thereby inhibiting the reuptake of dopamine from the synaptic cleft. Thus, the excess of dopamine in the cleft results in a continuous stimulation of dopamine receptors in the postsynaptic membrane [196-199]. This in turn affects LTP and LTD, which are both protein synthesis-dependent [200]. It was shown, that activated D1 receptor stimulates protein synthesis locally in dendrites of hippocampal neurons [201]. Thus, treating *rsh*¹ mutant flies with MPH may rescue the impaired protein expression rate in neurons of

*rsh*¹ mutant flies. This should be also addressed in the future but was beyond the scope of this thesis.

4.3 Comparison of the protein expression pattern in *rsh*¹ flies using 2D gel electrophoresis underlines the findings of the FlyNCAT analysis

As there is evidence that protein synthesis is impaired in *rsh*¹ mutant flies a detailed analysis of the protein expression pattern was performed using 2D gel electrophoresis. This analysis revealed a number regulated spots between *rsh*¹ mutant and *wt* flies. Within these spots several proteins were identified using MS analysis. Among them, proteins known to be involved in processes of mRNA transcription, protein translation and chromatin assembly, like the eukaryotic initiation factor 3 (EIF3J), the elongation factor 1-beta (EEF1B2) or the nucleoplasmin-like protein were found. Also proteins known to play a role in processes like synaptic plasticity, e.g. Complexin, were revealed using 2D gel electrophoresis. Complexin was identified in the upregulated spot 2009 in both *rsh*¹ mutant and *wt* flies (Table 7). It is a SNARE-binding protein known to be an important co-regulator for vesicle fusion [202, 203]. In other words, as a PKA target it changes basic neurotransmission through activity-dependent phosphorylation and thereby influences functional and structural plasticity in *Drosophila* [204]. Again, the Rno protein was found in this 2D gel analysis in upregulated spots. Due to its molecular weight of 354 kDa the Rno protein would normally be excluded from further analysis, as proteins of this molecular weight can not be separated using this method. However, there are several points that strengthen the assumption that Rno is differently expressed or processed between *rsh*¹ mutant and *wt* flies. The 'score' value of the Rno peptides found ranged between 77.8 and 179.8 [135], thus it is very likely that the protein is indeed Rno. Of course, one has to consider that Rno might be processed like the Futsch protein (see below), resulting in smaller Rno fragments that can be separated using this type of analysis. This assumption is underlined by western blot analysis of head lysates from *rsh*¹ mutant and *wt* flies using an antibody against Rno, which revealed an additional band at 55 kDa in female *rsh*¹ mutant flies [172]. The sequence analysis of the Rno protein ([174] and Figure 24b) suggests that Rno might play a role during protein degradation. The *rsh*¹ mutation influences proper Rno expression and thereby may influences pivotal Rno functioning during processes of protein degradation. Incorrect protein degradation in turn can impair memory formation as already shown [205], explaining the defective memory formation in *rsh*¹ mutant flies. Furthermore, the enhancer polycomb-like domain of Rno and Rno's homology to the mammalian Jade-1 [136] suggest that Rno might act as a transcriptional activator as well, through histone acetyltransferase activity. Meaning, that the different Rno expression in *rsh*¹ mutant flies could influence the HAT of Rno leading to alterations in gene

expression. This is underlined by the presence of the PHD domain within Rno, mostly found in proteins of chromatin remodeling complexes [139].

The here presented proteomic analysis only provides a basis for further analysis to investigate the role of Rsh in *Drosophila melanogaster* larvae and flies. Several verification studies have to be performed to substantiate the findings of the 2D gel electrophoresis. For instance, the expression rate of the individual proteins found in each regulated spot needs to be verified on quantitative western blots as the down- or upregulation of a certain spot does not imply that the proteins found in this spot are regulated in the same manner. Furthermore, a high number of proteins were found at molecular weights that do not fit to the actual molecular weight (Table 7). These peptides could refer to cleavage products after protein processing as this might be the case for the micotuble-associated protein Futsch, which is required for neuronal growth and development [206, 207]. Futsch has a predicted molecular weight of 591 kDa (Table 7). Thus, according to its molecular weight, Futsch would normally be excluded from further analysis. However, Zou *et al.* (2008) could show that the *futsch* gene encodes a precursor that will be cleaved into a heavy chain of ≈ 565 kDa and a light chain of ≈ 10 -20 kDa [208]. Interestingly, the Futsch peptides of the 2D gel electrophoresis were found in two regulated spots of the *wt* group. In spot 7405 at a molecular weight of ≈ 27 kDa and in spot 6202 at a molecular weight of ≈ 20 kDa (Table 7). One peptide of spot 7405 was found in the MS analysis and refers to the sequence at the beginning of the light chain of the Futsch protein [208] between aa 5,203-5,209. This indicates that the existence of proteins with differing experimental and theoretical molecular weights need to be investigated carefully in terms of protein processing in future experiments, e.g. using western blot analysis. Moreover, as a number of proteins are exclusively found in only one of the genotypes, western blot analysis needs to be performed in order to investigate if this is indeed the case. After verifying the findings of the 2D gel electrophoresis, the identified proteins can be used for further experiments and analyses, including an Ingenuity pathway analysis to investigate if specific pathways are influenced upon Rsh function.

For following experiments, e.g. protein-protein interaction studies and such, antibodies against Rsh were generated allowing the analysis of *wt* and the truncated mutant version of Rsh to investigate its potential molecular functions within the *Drosophila* brain in more detail. Previously, Folkers *et al.* (2006) generated an antibody against Rsh using a synthetic peptide covering the amino acids 522-542 of the initial Rsh protein. However, this antibody was not able to detect Rsh in the *rsh*¹ mutant background [123]. Crucially, protein sequence analysis performed within the scope of this thesis revealed, that the Rsh protein seems to be larger than initially expected (Figure 23, [123]). Furthermore, it revealed the Rsh protein seems to be expressed in six different isoforms and not as previously assumed in only one (Figure 23b, [123]). Because of these facts, new antibodies were raised against an MBP-Rsh²³⁵⁻⁵¹⁵ fusion

protein representing the amino acids 235-515, upstream from the amino acid substitution in the mutant Rsh protein. Preliminary experiments of the antibody characterization revealed that the here generated antibodies need to be investigated in much more detail in future experiments in terms of their specific binding to Rsh. For instance, the pre- and the antiserum of rabbit 2 showed an immune reactivity towards a band at 200 kDa, likely due to unspecific antibody binding. However, this immune reactivity might mask the actual signal for Rsh as five out of the six described Rsh isoforms have a molecular weight of 179-198 kDa. To investigate this assumption the 'masking' proteins need to be separated from the Rsh proteins by using for example 1D or 2D gel electrophoresis with subsequent western blot analysis using the pre- and purified antiserum. As the expression pattern between *rsh*¹ and *wt* flies did not differ as expected, the antibody will be tested in a Rsh-deficient background using RNAi-based knockdown of Rsh in *Drosophila* flies. This will help to determine the specificity of the antibody towards Rsh. If these analyses reveal that the antibody binds specifically to Rsh, the conditions during antibody binding need to be optimized, e.g. testing other dilutions of the antibody, testing different blocking and permeabilization conditions/solutions as well as affinity purification of the Rsh antisera to reduce background binding. Otherwise another antibody against a different epitope should be generated. Another reason for the poor antibody binding could be low expression levels of Rsh in *Drosophila* larvae and flies. Entries from flybase.org indicate the Rsh is expressed only at very low rates in larvae and flies. There is also a severe difference in the expression level between female and male flies. In female flies Rsh seem to be expressed only in 1 day old flies, whereas expression levels in male flies last for 30d, though at very low levels. The head lysates used here were derived from female and male flies at the same ratio probably leading to dilutionary effects, decreasing the possibility to detect endogenous Rsh on western blot level using the here generated antisera. This finding will be taken into account for future experiments.

As Rno was found to be differently expressed between *rsh*¹ and *wt* flies and its molecular function within the fly brain is not fully understood yet, an antibody was generated and characterized against Rno. Julia Abele (Neural Plasticity and Communication at the Institute for Pharmacology and Toxicology, OvGU, Magdeburg) performed characterization of the antisera in the scope of her master thesis. Specific binding of Rno-antisera to Rno was shown in immunofluorescent (only transfected Hek203T cells) staining and on western blot level [172]. A competition assay showed that the binding of the antisera to Rno on western blot level were highly specific [172].

Once the antisera against Rsh are fully characterized, both Rsh and Rno antibodies can be used for a variety of experiments to investigate the function of Rsh and Rno in *Drosophila* larvae and flies in terms of biochemical characteristics, tissue- and cell-specific expression

and putative interaction partners, thereby unraveling their function in *Drosophila melanogaster*. For example, in future experiments, immune precipitation (IP) studies should be performed to investigate possible interaction partners of Rsh and Rno. These findings will extend and verify the results of the sequence analysis and the 2D gel electrophoresis and will address the character of the link between Rsh and Rno. This link is quite likely, as both proteins yield domains promoting protein-protein interaction and both seem to function as transcriptional/translational regulators. In this respect Guan *et al.* (2011) already performed cell-localization studies of Rsh expressing *UAS-rsh-GFP* in larval salivary glands. Here, the authors found that the GFP staining overlaps with the nuclear DAPI staining. Weaker staining was found throughout the cytoplasm of salivary glands. Similar findings were observed when *UAS-rsh-GFP* was expressed in muscle cells. When Rsh was expressed in the larval brain using the pan-neuronal driver *elav^{C155}-Gal4*, it was mainly localized in cytoplasm of neuronal cell bodies and larval axons. Thus, Rsh is localized within the cytoplasm and the nucleus, to which extent depends on the cell type. However, as Guan *et al.* (2011) used overexpression studies one cannot be sure about the endogenous expression level and the correct localization within a cell. Furthermore, they showed only the possible expression sites of Rsh in *Drosophila* larvae based on the old 'shorter' Rsh protein [123]. Thus, the here generated antibody against Rsh will be used (i) to confirm the localization studies of Guan *et al.* (2011) in *Drosophila* larvae on the endogenous Rsh expression level, (ii) to investigate the localization of Rsh in the brain of adult *Drosophila* flies and (iii) to investigate the appearance of Rsh in other cell types, e.g. glia cells in *Drosophila* larvae and flies. As there might be a link between Rsh and Rno expression in *rsh¹* mutant flies, the localization of Rno within the *Drosophila* brain will be investigated as well using the generated antibody against Rno [172]. Co-localization studies of both Rsh and Rno could provide first evidence about their interaction with each other. Another way, to investigate the putative expression sites of both Rsh and Rno is the here-established FlyNCAT technique. FlyNCAT experiments revealed that Dlg was not found exclusively in muscle cells, but also in glia cells (Figure 9). Thus, the same FlyNCAT approach will be used to identify possible cell types, which express Rsh and Rno by detecting ANL-labeled biotin-tagged Rsh and Rno in eluate fractions of protein lysates from different MetRS^{LtoG}-expressing cell types.

Hence, the here represent proteomic analysis of the *rsh¹* mutant provides a basis for future experiments to investigate and characterize the molecular function of the Rsh protein within *Drosophila melanogaster*, e.g. by using Ingenuity pathway analysis and such. In doing so, the generated antibodies against Rsh and Rno can serve as a tool for a variety of future experiments to investigate the putative function of Rsh and Rno in the *Drosophila* brain giving more insights into the processes underlying learning and memory formation.

4.4 RNAi-based knockdown of Rsh in neurons and glia cells

Another tool, to investigate the potential role of a protein is RNA interference (RNAi) using respective RNAi fly stocks. RNAi silences gene expression of certain genes and is therefore used to unravel putative functions of the knocked down protein.

As the function of Rsh within the fly brain is not known yet and not predictable according to homologies to other proteins, RNAi was used to silence *rsh* gene expression cell-type specifically in neurons, glia and muscle cells of *Drosophila melanogaster* using the following UAS-inducible lines from the Vienna *Drosophila* Resource Center (VDRC): *UAS-Rsh^{GD39931}*, *UAS-Rsh^{GD39932}*, *UAS-Rsh^{KK101811}*. However, during the course of these experiments Green and colleagues (2014) reported that the RNAi-based knockdown of specific genes using the “KK” library from VDRC resulted in non-generic phenotypes that were non-compatible with the knockdown of the gene that has been targeted. Genome sequencing revealed two copies of the pKC43 target, which could lead to the integration of pKC26 vector at two possible insertion sites. They developed a PCR-based diagnosis assay to identify if the insertion site for pKC26 is in the annotated pKC43 target or not. Insertions of the pKC26 vector at the annotated pKC43 insertion site resulted in non-generic phenotypes. Furthermore they provide a recombination scheme to “clean” the affected strains [209]. Single-fly PCR of flies from the *UAS-RNAirsh^{KK101811}* strain indeed showed that the pKC26 was integrated into the annotated pKC43 insertion site (data not shown). Thus, for future experiments a “cleaned” version of the *UAS-RNAirsh^{KK101811}* line will be used to repeat the experiment.

Another way to investigate the effects resulting from gene knockdown is the previously reported Minos-mediated integration cassette (MiMIC) [210, 211]. The gene trap cassette is flanked by two Φ C31 *attP* target site that can easily be replaced by any other cassette flanked by attB sites using recombinase mediated cassette exchange (RMCE), e.g. to label proteins with GFP or any other epitope tag [211]. A gene knockdown can be achieved by RNAi-mediated knockdown of GFP-tagged transcripts (iGFPI) [210]. This knockdown does not display any off-target effects nor gives rise to false negatives. Introducing genomic transgenes rather than cDNA, reflects the endogenous expression pattern and level of a certain protein [212, 213]. Genomic transgenes are integrated by site-specific integrases in defined docking sites, thus allowing for spatial and temporal protein expression without altering the expression of the endogenous copy. Generating MiMIC gene trap vectors enables not only for knockdown of target transcripts, but also enables the investigation of the protein expression pattern and subcellular localization using commercial antibodies against the used epitope tag. Furthermore, GFP- and other epitope tags allow for purification, immune precipitation followed by mass spectrometry, identification of RNA-binding proteins and in the case of transcription factors for chromatin immune precipitation (ChIP, cis-regulatory map) [214] to investigate protein-DNA interactions of target proteins. For Rsh two

insertions are reported for generating MiMIC (MI10840, MI12368). Thus, in future experiments a MiMIC vector will be generated for Rsh as another opportunity to investigate the Rsh function within *Drosophila melanogaster* using RNAi-based knockdown. Additionally, this provides another tool to investigate the Rsh protein and its putative function within *Drosophila* flies as epitope-tagged Rsh can be used for a variety of immune fluorescent and biochemical approaches.

5 Outlook

The here reported cell-type specific metabolic labeling approach FlyNCAT enables for the spatial and temporal resolution of proteome dynamics. It provides the means to investigate alterations on the protein entity under physiological and pathological conditions cell-type specifically *in vivo* and might, therefore, help to uncover new therapeutic treatments for neurological diseases. For instance, unraveling the synaptic proteome and its dynamics under physiological and pathological conditions would provide new starting points to develop cell-type specific therapeutic treatments in order to reduced putative side effects in non-affected cell types of common medications. As the applicability of the FlyNCAT method is not restricted to the brain of *Drosophila melanogaster*, it can be used in a wide range of tissue and organs to unravel certain biological questions.

First applications of this method show that the protein synthesis rate was impaired in neurons of *rsh*¹ mutant flies. Gel electrophoresis and sequence analysis of the *rsh* gene and protein revealed possible function of Rsh in protein homeostasis, cytoskeleton arrangement and developmental processes, extending the findings from several behavioral studies. Taken these findings together, they gave new insights in the function of Rsh and can now be used to address detailed questions about the function of Rsh in *Drosophila melanogaster* larvae and flies. It is still elusive (i) which cell types expresses Rsh, (ii) which proteins are up- or downregulated in *rsh*¹ mutant flies and how they contribute to learning and memory formation and (iii) how the interaction between Rsh and Rno influences memory formation and/or protein homeostasis. Unraveling the function of Rsh and Rno within the fly brain of *Drosophila melanogaster* would help to understand certain cross-links between the different stages of memory formation, thereby provide new insights into the basic underlying mechanisms of learning and memory formation.

6 References

1. Oswald, D., S. Lin, and S. Waddell, *Light, heat, action: neural control of fruit fly behaviour*. Philos Trans R Soc Lond B Biol Sci, 2015. **370**(1677): p. 20140211.
2. Ashburner, M., K.G. Golic, and R.S. Hawley, *Drosophila: A Laboratory Handbook*. 2nd ed. 2005: Cold Spring Harbor Laboratory Press.
3. Ashburner, M. and J.N. Thompson, *The laboratory culture of Drosophila*. In: *The genetics and biology of Drosophila*. Vol. 2A. 1978: Academic Press. 81.
4. Zhang, B., M.R. Freemann, and S. Waddell, *Drosophila Neurobiology - A laboratory manual*. 2010: Cold Spring Harbor Laboratory Press.
5. Hallermann, S. and R.A. Silver, *Sustaining rapid vesicular release at active zones: potential roles for vesicle tethering*. Trends Neurosci, 2013. **36**(3): p. 185-94.
6. Menon, K.P., R.A. Carrillo, and K. Zinn, *Development and plasticity of the Drosophila larval neuromuscular junction*. Wiley Interdiscip Rev Dev Biol, 2013. **2**(5): p. 647-70.
7. Bellen, H.J., C. Tong, and H. Tsuda, *100 years of Drosophila research and its impact on vertebrate neuroscience: a history lesson for the future*. Nat Rev Neurosci, 2010. **11**(7): p. 514-22.
8. Brand, A.H. and N. Perrimon, *Targeted gene expression as a means of altering cell fates and generating dominant phenotypes*. Development, 1993. **118**(2): p. 401-15.
9. Elliott, D.A. and A.H. Brand, *The GAL4 system : a versatile system for the expression of genes*. Methods Mol Biol, 2008. **420**: p. 79-95.
10. McGuire, S.E., et al., *Spatiotemporal rescue of memory dysfunction in Drosophila*. Science, 2003. **302**(5651): p. 1765-8.
11. Erdmann, I., et al., *Cell-selective labelling of proteomes in Drosophila melanogaster*. Nat Commun, 2015. **6**: p. 7521.
12. Shimosako, N., D. Hadjieconomou, and I. Salecker, *Flybow to dissect circuit assembly in the Drosophila brain*. Methods Mol Biol, 2014. **1082**: p. 57-69.
13. Adams, M.D., et al., *The genome sequence of Drosophila melanogaster*. Science, 2000. **287**(5461): p. 2185-95.
14. Reiter, L.T., et al., *A systematic analysis of human disease-associated gene sequences in Drosophila melanogaster*. Genome Res, 2001. **11**(6): p. 1114-25.
15. Ellisen, L.W., et al., *TAN-1, the human homolog of the Drosophila notch gene, is broken by chromosomal translocations in T lymphoblastic neoplasms*. Cell, 1991. **66**(4): p. 649-61.
16. Weinmaster, G., V.J. Roberts, and G. Lemke, *A homolog of Drosophila Notch expressed during mammalian development*. Development, 1991. **113**(1): p. 199-205.
17. Krauss, S., J.P. Concordet, and P.W. Ingham, *A functionally conserved homolog of the Drosophila segment polarity gene hh is expressed in tissues with polarizing activity in zebrafish embryos*. Cell, 1993. **75**(7): p. 1431-44.

18. Rijsewijk, F., et al., *The Drosophila homolog of the mouse mammary oncogene int-1 is identical to the segment polarity gene wingless*. Cell, 1987. **50**(4): p. 649-57.
19. O'Kane, C.J., *Drosophila as a model organism for the study of neuropsychiatric disorders*. Curr Top Behav Neurosci, 2011. **7**: p. 37-60.
20. Freeman, M.R. and J. Doherty, *Glial cell biology in Drosophila and vertebrates*. Trends Neurosci, 2006. **29**(2): p. 82-90.
21. Kettenmann, H. and B.R. Ransom, *Neuroglia*. 3rd ed. 2005: Oxford University Press.
22. van Swinderen, B. and B. Brembs, *Attention-like deficit and hyperactivity in a Drosophila memory mutant*. J Neurosci, 2010. **30**(3): p. 1003-14.
23. Niehues, S., et al., *Impaired protein translation in Drosophila models for Charcot-Marie-Tooth neuropathy caused by mutant tRNA synthetases*. Nat Commun, 2015. **6**: p. 7520.
24. Burkhart, J.M., et al., *The first comprehensive and quantitative analysis of human platelet protein composition allows the comparative analysis of structural and functional pathways*. Blood, 2012. **120**(15): p. e73-82.
25. Grant, M.M., D. Scheel-Toellner, and H.R. Griffiths, *Contributions to our understanding of T cell physiology through unveiling the T cell proteome*. Clin Exp Immunol, 2007. **149**(1): p. 9-15.
26. Lonngren, T., Z. Chen, and R. Lahesmaa, *From a gene-centric to whole-proteome view of differentiation of T helper cell subsets*. Brief Funct Genomics, 2013. **12**(6): p. 471-82.
27. Wasbrough, E.R., et al., *The Drosophila melanogaster sperm proteome-II (DmSP-II)*. J Proteomics, 2010. **73**(11): p. 2171-85.
28. Wilkins, M.R., et al., *High-throughput mass spectrometric discovery of protein post-translational modifications*. J Mol Biol, 1999. **289**(3): p. 645-57.
29. Panse, V.G., et al., *A proteome-wide approach identifies sumoylated substrate proteins in yeast*. J Biol Chem, 2004. **279**(40): p. 41346-51.
30. Peng, J., et al., *A proteomics approach to understanding protein ubiquitination*. Nat Biotechnol, 2003. **21**(8): p. 921-6.
31. Pielot, R., et al., *SynProt: A Database for Proteins of Detergent-Resistant Synaptic Protein Preparations*. Front Synaptic Neurosci, 2012. **4**: p. 1.
32. Ong, S.E., et al., *Stable isotope labeling by amino acids in cell culture, SILAC, as a simple and accurate approach to expression proteomics*. Mol Cell Proteomics, 2002. **1**(5): p. 376-86.
33. Dieterich, D.C., *Chemical reporters for the illumination of protein and cell dynamics*. Curr Opin Neurobiol, 2010. **20**(5): p. 623-30.
34. Link, A.J., M.L. Mock, and D.A. Tirrell, *Non-canonical amino acids in protein engineering*. Curr Opin Biotechnol, 2003. **14**(6): p. 603-9.
35. Liu, J., et al., *Imaging protein synthesis in cells and tissues with an alkyne analog of puromycin*. Proc Natl Acad Sci U S A, 2012. **109**(2): p. 413-8.

36. Prescher, J.A. and C.R. Bertozzi, *Chemistry in living systems*. Nat Chem Biol, 2005. **1**(1): p. 13-21.
37. Prescher, J.A. and C.R. Bertozzi, *Chemical technologies for probing glycans*. Cell, 2006. **126**(5): p. 851-4.
38. Chen, Z.Y. and M.J. Wu, *Reaction of (Z)-1-aryl-3-hexen-1,5-diyne with sodium azide: synthesis of 1-aryl-1H-benzotriazoles*. Org Lett, 2005. **7**(3): p. 475-7.
39. Griffin, B.A., S.R. Adams, and R.Y. Tsien, *Specific covalent labeling of recombinant protein molecules inside live cells*. Science, 1998. **281**(5374): p. 269-72.
40. Link, A.J., M.K. Vink, and D.A. Tirrell, *Presentation and detection of azide functionality in bacterial cell surface proteins*. J Am Chem Soc, 2004. **126**(34): p. 10598-602.
41. Zhang, X. and Y. Zhang, *Applications of azide-based bioorthogonal click chemistry in glycobiology*. Molecules, 2013. **18**(6): p. 7145-59.
42. Luchansky, S.J., S. Goon, and C.R. Bertozzi, *Expanding the diversity of unnatural cell-surface sialic acids*. Chembiochem, 2004. **5**(3): p. 371-4.
43. Luchansky, S.J., et al., *Constructing azide-labeled cell surfaces using polysaccharide biosynthetic pathways*. Methods Enzymol, 2003. **362**: p. 249-72.
44. Mahal, L.K., K.J. Yarema, and C.R. Bertozzi, *Engineering chemical reactivity on cell surfaces through oligosaccharide biosynthesis*. Science, 1997. **276**(5315): p. 1125-8.
45. Saxon, E., et al., *Investigating cellular metabolism of synthetic azidosugars with the Staudinger ligation*. J Am Chem Soc, 2002. **124**(50): p. 14893-902.
46. Kho, Y., et al., *A tagging-via-substrate technology for detection and proteomics of farnesylated proteins*. Proc Natl Acad Sci U S A, 2004. **101**(34): p. 12479-84.
47. Rostovtsev, V.V., et al., *A stepwise Huisgen cycloaddition process: copper(I)-catalyzed regioselective "ligation" of azides and terminal alkynes*. Angew Chem Int Ed Engl, 2002. **41**(14): p. 2596-9.
48. Baskin, J.M., et al., *Copper-free click chemistry for dynamic in vivo imaging*. Proc Natl Acad Sci U S A, 2007. **104**(43): p. 16793-7.
49. Beatty, K.E., et al., *Fluorescence visualization of newly synthesized proteins in mammalian cells*. Angew Chem Int Ed Engl, 2006. **45**(44): p. 7364-7.
50. Dieterich, D.C., et al., *In situ visualization and dynamics of newly synthesized proteins in rat hippocampal neurons*. Nat Neurosci, 2010. **13**(7): p. 897-905.
51. Tom Dieck, S., et al., *Metabolic labeling with noncanonical amino acids and visualization by chemoselective fluorescent tagging*. Curr Protoc Cell Biol, 2012. **Chapter 7**: p. Unit7 11.
52. Dieterich, D.C., et al., *Labeling, detection and identification of newly synthesized proteomes with bioorthogonal non-canonical amino-acid tagging*. Nat Protoc, 2007. **2**(3): p. 532-40.

53. Dieterich, D.C., et al., *Selective identification of newly synthesized proteins in mammalian cells using bioorthogonal noncanonical amino acid tagging (BONCAT)*. Proc Natl Acad Sci U S A, 2006. **103**(25): p. 9482-7.
54. Link, A.J. and D.A. Tirrell, *Cell surface labeling of Escherichia coli via copper(I)-catalyzed [3+2] cycloaddition*. J Am Chem Soc, 2003. **125**(37): p. 11164-5.
55. Hodas, J.J., et al., *Dopaminergic modulation of the hippocampal neuropil proteome identified by bioorthogonal noncanonical amino acid tagging (BONCAT)*. Proteomics, 2012. **12**(15-16): p. 2464-76.
56. Tcherkezian, J., et al., *Transmembrane receptor DCC associates with protein synthesis machinery and regulates translation*. Cell, 2010. **141**(4): p. 632-44.
57. Yoon, B.C., et al., *Local translation of extranuclear lamin B promotes axon maintenance*. Cell, 2012. **148**(4): p. 752-64.
58. Hinz, F.I., et al., *Non-canonical amino acid labeling in vivo to visualize and affinity purify newly synthesized proteins in larval zebrafish*. ACS Chem Neurosci, 2012. **3**(1): p. 40-49.
59. Howden, A.J., et al., *QuaNCAT: quantitating proteome dynamics in primary cells*. Nat Methods, 2013. **10**(4): p. 343-6.
60. Cohen, L.D., et al., *Metabolic turnover of synaptic proteins: kinetics, interdependencies and implications for synaptic maintenance*. PLoS One, 2013. **8**(5): p. e63191.
61. Eichelbaum, K. and J. Krijgsveld, *Combining pulsed SILAC labeling and click-chemistry for quantitative secretome analysis*. Methods Mol Biol, 2014. **1174**: p. 101-14.
62. Bowling, H., et al., *BONLAC: A combinatorial proteomic technique to measure stimulus-induced translational profiles in brain slices*. Neuropharmacology, 2016. **100**: p. 76-89.
63. Schwanhauser, B., et al., *Global analysis of cellular protein translation by pulsed SILAC*. Proteomics, 2009. **9**(1): p. 205-9.
64. van Kasteren, S.I., et al., *Site-selective glycosylation of proteins: creating synthetic glycoproteins*. Nat Protoc, 2007. **2**(12): p. 3185-94.
65. van Kasteren, S.I., et al., *Expanding the diversity of chemical protein modification allows post-translational mimicry*. Nature, 2007. **446**(7139): p. 1105-9.
66. Link, A.J., et al., *Discovery of aminoacyl-tRNA synthetase activity through cell-surface display of noncanonical amino acids*. Proc Natl Acad Sci U S A, 2006. **103**(27): p. 10180-5.
67. Tanrikulu, I.C., et al., *Discovery of Escherichia coli methionyl-tRNA synthetase mutants for efficient labeling of proteins with azidonorleucine in vivo*. Proc Natl Acad Sci U S A, 2009. **106**(36): p. 15285-90.
68. Ngo, J.T., et al., *Cell-selective metabolic labeling of proteins*. Nat Chem Biol, 2009. **5**(10): p. 715-7.

69. Ngo, J.T., E.M. Schuman, and D.A. Tirrell, *Mutant methionyl-tRNA synthetase from bacteria enables site-selective N-terminal labeling of proteins expressed in mammalian cells*. Proc Natl Acad Sci U S A, 2013. **110**(13): p. 4992-7.
70. Kiick, K.L., et al., *Incorporation of azides into recombinant proteins for chemoselective modification by the Staudinger ligation*. Proc Natl Acad Sci U S A, 2002. **99**(1): p. 19-24.
71. Kiick, K.L., J.C. van Hest, and D.A. Tirrell, *Expanding the Scope of Protein Biosynthesis by Altering the Methionyl-tRNA Synthetase Activity of a Bacterial Expression Host* Scott Ross was helpful in conducting the 1D TOCSY NMR experiments and Pratip Bhattachary is thanked for assistance in other NMR experiments. We are grateful to Yves Mechulam for a sample of plasmid pBSM547W305F and to Hieronim Jakubowski of UMDNJ-New Jersey Medical School, Newark, New Jersey, for plasmid pGG3. K.L.K. thanks the U.S. Department of Defense for a National Defense Science and Engineering Graduate Fellowship. This work was supported by grants from the Polymers and Genetics Programs of the National Science Foundation and from the U.S. Army Research Office. Angew Chem Int Ed Engl, 2000. **39**(12): p. 2148-2152.
72. Hu, Y., Y. Ye, and M.E. Fortini, *Nicastrin is required for gamma-secretase cleavage of the Drosophila Notch receptor*. Dev Cell, 2002. **2**(1): p. 69-78.
73. Yuet, K.P., et al., *Cell-specific proteomic analysis in Caenorhabditis elegans*. Proc Natl Acad Sci U S A, 2015. **112**(9): p. 2705-10.
74. Martyn, C.N. and R.A. Hughes, *Epidemiology of peripheral neuropathy*. J Neurol Neurosurg Psychiatry, 1997. **62**(4): p. 310-8.
75. Pareyson, D. and C. Marchesi, *Diagnosis, natural history, and management of Charcot-Marie-Tooth disease*. Lancet Neurol, 2009. **8**(7): p. 654-67.
76. Patzko, A. and M.E. Shy, *Update on Charcot-Marie-Tooth disease*. Curr Neurol Neurosci Rep, 2011. **11**(1): p. 78-88.
77. Steffes, G. and E. Storkebaum, *Drosophila as a model for CMT peripheral neuropathy: mutations in tRNA synthetases as an example*. Drosophila melanogaster Models of Motor Neuron Disease eds Cauchi R.J. Nova Biomedical, 2013.
78. Antonellis, A., et al., *Glycyl tRNA synthetase mutations in Charcot-Marie-Tooth disease type 2D and distal spinal muscular atrophy type V*. Am J Hum Genet, 2003. **72**(5): p. 1293-9.
79. Gonzalez, M., et al., *Exome sequencing identifies a significant variant in methionyl-tRNA synthetase (MARS) in a family with late-onset CMT2*. J Neurol Neurosurg Psychiatry, 2013. **84**(11): p. 1247-9.
80. Jordanova, A., et al., *Disrupted function and axonal distribution of mutant tyrosyl-tRNA synthetase in dominant intermediate Charcot-Marie-Tooth neuropathy*. Nat Genet, 2006. **38**(2): p. 197-202.
81. Latour, P., et al., *A major determinant for binding and aminoacylation of tRNA(Ala) in cytoplasmic Alanyl-tRNA synthetase is mutated in dominant axonal Charcot-Marie-Tooth disease*. Am J Hum Genet, 2010. **86**(1): p. 77-82.

82. McLaughlin, H.M., et al., *A recurrent loss-of-function alanyl-tRNA synthetase (AARS) mutation in patients with Charcot-Marie-Tooth disease type 2N (CMT2N)*. Hum Mutat, 2012. **33**(1): p. 244-53.
83. Vester, A., et al., *A loss-of-function variant in the human histidyl-tRNA synthetase (HARS) gene is neurotoxic in vivo*. Hum Mutat, 2013. **34**(1): p. 191-9.
84. Antonellis, A., et al., *Functional analyses of glycyl-tRNA synthetase mutations suggest a key role for tRNA-charging enzymes in peripheral axons*. J Neurosci, 2006. **26**(41): p. 10397-406.
85. Nangle, L.A., et al., *Charcot-Marie-Tooth disease-associated mutant tRNA synthetases linked to altered dimer interface and neurite distribution defect*. Proc Natl Acad Sci U S A, 2007. **104**(27): p. 11239-44.
86. Stum, M., et al., *An assessment of mechanisms underlying peripheral axonal degeneration caused by aminoacyl-tRNA synthetase mutations*. Mol Cell Neurosci, 2011. **46**(2): p. 432-43.
87. Bagni, C. and W.T. Greenough, *From mRNP trafficking to spine dysmorphogenesis: the roots of fragile X syndrome*. Nat Rev Neurosci, 2005. **6**(5): p. 376-87.
88. Hagerman, R.J., K. Amiri, and A. Cronister, *Fragile X checklist*. Am J Med Genet, 1991. **38**(2-3): p. 283-7.
89. Hernandez, R.N., et al., *Autism spectrum disorder in fragile X syndrome: a longitudinal evaluation*. Am J Med Genet A, 2009. **149A**(6): p. 1125-37.
90. Kaufmann, W.E., et al., *Autism spectrum disorder in fragile X syndrome: communication, social interaction, and specific behaviors*. Am J Med Genet A, 2004. **129A**(3): p. 225-34.
91. O'Donnell, W.T. and S.T. Warren, *A decade of molecular studies of fragile X syndrome*. Annu Rev Neurosci, 2002. **25**: p. 315-38.
92. Swanson, M.S. and H.T. Orr, *Fragile X tremor/ataxia syndrome: blame the messenger!* Neuron, 2007. **55**(4): p. 535-7.
93. Oberle, I., et al., *Instability of a 550-base pair DNA segment and abnormal methylation in fragile X syndrome*. Science, 1991. **252**(5009): p. 1097-102.
94. Verkerk, A.J., et al., *Identification of a gene (FMR-1) containing a CGG repeat coincident with a breakpoint cluster region exhibiting length variation in fragile X syndrome*. Cell, 1991. **65**(5): p. 905-14.
95. Warren, S.T. and D.L. Nelson, *Advances in molecular analysis of fragile X syndrome*. JAMA, 1994. **271**(7): p. 536-42.
96. Antar, L.N., et al., *Metabotropic glutamate receptor activation regulates fragile x mental retardation protein and FMR1 mRNA localization differentially in dendrites and at synapses*. J Neurosci, 2004. **24**(11): p. 2648-55.
97. Feng, Y., et al., *FMRP associates with polyribosomes as an mRNP, and the I304N mutation of severe fragile X syndrome abolishes this association*. Mol Cell, 1997. **1**(1): p. 109-18.

98. Miyashiro, K.Y., et al., *RNA cargoes associating with FMRP reveal deficits in cellular functioning in Fmr1 null mice*. Neuron, 2003. **37**(3): p. 417-31.
99. Weiler, I.J., et al., *Fragile X mental retardation protein is translated near synapses in response to neurotransmitter activation*. Proc Natl Acad Sci U S A, 1997. **94**(10): p. 5395-400.
100. Zalfa, F., et al., *The fragile X syndrome protein FMRP associates with BC1 RNA and regulates the translation of specific mRNAs at synapses*. Cell, 2003. **112**(3): p. 317-27.
101. Huber, K.M., et al., *Altered synaptic plasticity in a mouse model of fragile X mental retardation*. Proc Natl Acad Sci U S A, 2002. **99**(11): p. 7746-50.
102. Darnell, J.C., et al., *FMRP stalls ribosomal translocation on mRNAs linked to synaptic function and autism*. Cell, 2011. **146**(2): p. 247-61.
103. Lagerbauer, B., et al., *Evidence that fragile X mental retardation protein is a negative regulator of translation*. Hum Mol Genet, 2001. **10**(4): p. 329-38.
104. Li, Z., et al., *The fragile X mental retardation protein inhibits translation via interacting with mRNA*. Nucleic Acids Res, 2001. **29**(11): p. 2276-83.
105. Qin, M., et al., *Postadolescent changes in regional cerebral protein synthesis: an in vivo study in the FMR1 null mouse*. J Neurosci, 2005. **25**(20): p. 5087-95.
106. Bhakar, A.L., G. Dolen, and M.F. Bear, *The pathophysiology of fragile X (and what it teaches us about synapses)*. Annu Rev Neurosci, 2012. **35**: p. 417-43.
107. Santoro, M.R., S.M. Bray, and S.T. Warren, *Molecular mechanisms of fragile X syndrome: a twenty-year perspective*. Annu Rev Pathol, 2012. **7**: p. 219-45.
108. Bolduc, F.V., et al., *Excess protein synthesis in Drosophila fragile X mutants impairs long-term memory*. Nat Neurosci, 2008. **11**(10): p. 1143-5.
109. Wan, L., et al., *Characterization of dFMR1, a Drosophila melanogaster homolog of the fragile X mental retardation protein*. Mol Cell Biol, 2000. **20**(22): p. 8536-47.
110. Greenough, W.T., et al., *Synaptic regulation of protein synthesis and the fragile X protein*. Proc Natl Acad Sci U S A, 2001. **98**(13): p. 7101-6.
111. Weiler, I.J., et al., *Fragile X mental retardation protein is necessary for neurotransmitter-activated protein translation at synapses*. Proc Natl Acad Sci U S A, 2004. **101**(50): p. 17504-9.
112. Chen, C.N., S. Denome, and R.L. Davis, *Molecular analysis of cDNA clones and the corresponding genomic coding sequence of the Drosophila dunce gene, the structural gene for cAMP-dependent phosphodiesterase*. Proc. Natl. Acad. Sci. USA, 1986. **83**: p. 9313-9317.
113. Dudai, Y., et al., *dunce, a mutant of Drosophila deficient in learning*. Proc Natl Acad Sci U S A, 1976. **73**(5): p. 1684-8.
114. Krupinski, J., et al., *Adenylyl cyclase amino acid sequence: possible channel- or transporter-like structure*. Science, 1989. **244**(4912): p. 1558-64.

115. Levin, L.R., et al., *The Drosophila learning and memory gene rutabaga encodes a Ca²⁺/Calmodulin-responsive adenylyl cyclase*. Cell, 1992. **68**(3): p. 479-89.
116. Livingstone, M.S., P.P. Sziber, and W.G. Quinn, *Loss of calcium/calmodulin responsiveness in adenylyl cyclase of rutabaga, a Drosophila learning mutant*. Cell, 1984. **37**(1): p. 205-15.
117. Feany, M.B. and W.G. Quinn, *A neuropeptide gene defined by the Drosophila memory mutant amnesiac*. Science, 1995. **268**(5212): p. 869-73.
118. Moore, M.S., et al., *Ethanol intoxication in Drosophila: Genetic and pharmacological evidence for regulation by the cAMP signaling pathway*. Cell, 1998. **93**(6): p. 997-1007.
119. Quinn, W.G., P.P. Sziber, and R. Booker, *The Drosophila memory mutant amnesiac*. Nature, 1979. **277**(5693): p. 212-4.
120. Waddell, S., et al., *The amnesiac gene product is expressed in two neurons in the Drosophila brain that are critical for memory*. Cell, 2000. **103**(5): p. 805-13.
121. Yin, J.C., et al., *Induction of a dominant negative CREB transgene specifically blocks long-term memory in Drosophila*. Cell, 1994. **79**(1): p. 49-58.
122. Folkers, E., P. Drain, and W.G. Quinn, *Radish, a Drosophila mutant deficient in consolidated memory*. Proc Natl Acad Sci U S A, 1993. **90**(17): p. 8123-7.
123. Folkers, E., S. Waddell, and W.G. Quinn, *The Drosophila radish gene encodes a protein required for anesthesia-resistant memory*. Proc Natl Acad Sci U S A, 2006. **103**(46): p. 17496-500.
124. Keene, A.C., et al., *Drosophila dorsal paired medial neurons provide a general mechanism for memory consolidation*. Curr Biol, 2006. **16**(15): p. 1524-30.
125. Krashes, M.J., et al., *Sequential use of mushroom body neuron subsets during drosophila odor memory processing*. Neuron, 2007. **53**(1): p. 103-15.
126. Tully, T. and W.G. Quinn, *Classical conditioning and retention in normal and mutant Drosophila melanogaster*. J Comp Physiol A, 1985. **157**(2): p. 263-77.
127. Li, W., T. Tully, and D. Kalderon, *Effects of a conditional Drosophila PKA mutant on olfactory learning and memory*. Learn Mem, 1996. **2**(6): p. 320-33.
128. Dubnau, J. and T. Tully, *Gene discovery in Drosophila: new insights for learning and memory*. Annu Rev Neurosci, 1998. **21**: p. 407-44.
129. Tully, T., et al., *Genetic dissection of consolidated memory in Drosophila*. Cell, 1994. **79**(1): p. 35-47.
130. Krashes, M.J. and S. Waddell, *Rapid consolidation to a radish and protein synthesis-dependent long-term memory after single-session appetitive olfactory conditioning in Drosophila*. J Neurosci, 2008. **28**(12): p. 3103-13.
131. Isabel, G., A. Pascual, and T. Preat, *Exclusive consolidated memory phases in Drosophila*. Science, 2004. **304**(5673): p. 1024-7.
132. Drier, E.A., et al., *Memory enhancement and formation by atypical PKM activity in Drosophila melanogaster*. Nat Neurosci, 2002. **5**(4): p. 316-24.

133. Lee, P.T., et al., *Serotonin-mushroom body circuit modulating the formation of anesthesia-resistant memory in Drosophila*. Proc Natl Acad Sci U S A, 2011. **108**(33): p. 13794-9.
134. Guan, Z., et al., *Altered gene regulation and synaptic morphology in Drosophila learning and memory mutants*. Learn Mem, 2011. **18**(4): p. 191-206.
135. Erdmann, I., *Establishment and Implementation of Metabolic Labeling of Proteins in Drosophila Melanogaster*. 2011, Otto-von-Guercke Universität: Magdeburg. p. 54.
136. Voas, M.G. and I. Rebay, *The novel plant homeodomain protein rhinoceros antagonizes Ras signaling in the Drosophila eye*. Genetics, 2003. **165**(4): p. 1993-2006.
137. Panchenko, M.V., M.I. Zhou, and H.T. Cohen, *von Hippel-Lindau partner Jade-1 is a transcriptional co-activator associated with histone acetyltransferase activity*. J Biol Chem, 2004. **279**(53): p. 56032-41.
138. Zhou, M.I., et al., *The von Hippel-Lindau tumor suppressor stabilizes novel plant homeodomain protein Jade-1*. J Biol Chem, 2002. **277**(42): p. 39887-98.
139. Aasland, R., T.J. Gibson, and A.F. Stewart, *The PHD finger: implications for chromatin-mediated transcriptional regulation*. Trends Biochem Sci, 1995. **20**(2): p. 56-9.
140. Müller, A., *Zell-spezifische, metabolische Markierung von neu synthetisierten Proteinen in einem Neuron-Glia-Netzwerk*, in Faculty für Natural Science 2012, Otto-von-Guericke University: Magdeburg. p. 157.
141. Müller, A., et al., *Monitoring Astrocytic Proteome Dynamics by Cell-type Specific Protein Labeling*.
142. Link, A.J., M.K. Vink, and D.A. Tirrell, *Synthesis of the functionalizable methionine surrogate azidohomoalanine using Boc-homoserine as precursor*. Nat Protoc, 2007. **2**(8): p. 1884-7.
143. Link, A.J., M.K. Vink, and D.A. Tirrell, *Preparation of the functionalizable methionine surrogate azidohomoalanine via copper-catalyzed diazo transfer*. Nat Protoc, 2007. **2**(8): p. 1879-83.
144. Birnboim, H.C. and J. Doly, *A rapid alkaline extraction procedure for screening recombinant plasmid DNA*. Nucleic Acids Res, 1979. **7**(6): p. 1513-23.
145. Lin, D.M. and C.S. Goodman, *Ectopic and increased expression of Fasciclin II alters motoneuron growth cone guidance*. Neuron, 1994. **13**(3): p. 507-23.
146. Halter, D.A., et al., *The homeobox gene repo is required for the differentiation and maintenance of glia function in the embryonic nervous system of Drosophila melanogaster*. Development, 1995. **121**(2): p. 317-32.
147. Thomas, U. and S.J. Sigrist, *Glutamate receptors in synaptic assembly and plasticity: case studies on fly NMJs*. Adv Exp Med Biol, 2012. **970**: p. 3-28.
148. Chen, J.V. and T.L. Megraw, *Spermitin: a novel mitochondrial protein in Drosophila spermatids*. PLoS One, 2014. **9**(9): p. e108802.

149. Mahr, A. and H. Aberle, *The expression pattern of the Drosophila vesicular glutamate transporter: a marker protein for motoneurons and glutamatergic centers in the brain*. Gene Expr Patterns, 2006. **6**(3): p. 299-309.
150. Hinz, U., B. Giebel, and J.A. Campos-Ortega, *The basic-helix-loop-helix domain of Drosophila lethal of scute protein is sufficient for proneural function and activates neurogenic genes*. Cell, 1994. **76**(1): p. 77-87.
151. Ainsley, J.A., et al., *Enhanced locomotion caused by loss of the Drosophila DEG/ENaC protein Pickpocket1*. Curr Biol, 2003. **13**(17): p. 1557-63.
152. Becker, F., *In Die Anfärbemethode von papierelektrophoretisch aufgetrenntem Serumweiß mit Amidoschwarz 10 B Fresenius' Journal of Analytical Chemistry*, 1966. **220**(310).
153. Laemmli, U.K., *Cleavage of structural proteins during the assembly of the head of bacteriophage T4*. Nature, 1970. **227**(5259): p. 680-5.
154. Heukeshoven, J. and R. Dernick, *Simplified method for silver staining of proteins in polyacrylamide gels and the mechanism of silver staining*. Electrophoresis, 1985. **6**(3): p. 103.
155. Blum, H., H. Beier, and H.J. Gross, *Improved silver staining of plant proteins, RNA and DNA in polyacrylamide gels*. Electrophoresis, 1987. **8**(2).
156. Towbin, H., T. Staehelin, and J. Gordon, *Electrophoretic transfer of proteins from polyacrylamide gels to nitrocellulose sheets: procedure and some applications*. Proc Natl Acad Sci U S A, 1979. **76**(9): p. 4350-4.
157. O'Farrell, P.Z., H.M. Goodman, and P.H. O'Farrell, *High resolution two-dimensional electrophoresis of basic as well as acidic proteins*. Cell, 1977. **12**(4): p. 1133-41.
158. Franco, M., et al., *A novel strategy to isolate ubiquitin conjugates reveals wide role for ubiquitination during neural development*. Mol Cell Proteomics, 2011. **10**(5): p. M110 002188.
159. Mahdavi, A., et al., *Identification of secreted bacterial proteins by noncanonical amino acid tagging*. Proc Natl Acad Sci U S A, 2014. **111**(1): p. 433-8.
160. Serre, L., et al., *How methionyl-tRNA synthetase creates its amino acid recognition pocket upon L-methionine binding*. J Mol Biol, 2001. **306**(4): p. 863-76.
161. Muller, A., et al., *Monitoring Astrocytic Proteome Dynamics by Cell Type-Specific Protein Labeling*. PLoS One, 2015. **10**(12): p. e0145451.
162. Bachmann, A., et al., *A perisynaptic ménage à trois between Dlg, DLin-7, and Metro controls proper organization of Drosophila synaptic junctions*. J Neurosci, 2010. **30**(17): p. 5811-24.
163. Tissot, M. and R.F. Stocker, *Metamorphosis in drosophila and other insects: the fate of neurons throughout the stages*. Prog Neurobiol, 2000. **62**(1): p. 89-111.
164. Brown, J.L., *The N-terminal region of soluble proteins from procaryotes and eucaryotes*. Biochim Biophys Acta, 1970. **221**(3): p. 480-8.
165. Matheson, A.T., M. Yaguchi, and L.P. Visentin, *The conservation of amino acids in the n-terminal position of ribosomal and cytosol proteins from Escherichia coli*,

- Bacillus stearothermophilus*, and *Halobacterium cutirubrum*. *Can J Biochem*, 1975. **53**(12): p. 1323-7.
166. Waller, J.P., *The N_h2-Terminal Residues of the Proteins from Cell-Free Extracts of E. Coli*. *J Mol Biol*, 1963. **7**: p. 483-96.
167. Kopan, R. and A. Goate, *A common enzyme connects notch signaling and Alzheimer's disease*. *Genes Dev*, 2000. **14**(22): p. 2799-806.
168. Fortini, M.E., *Notch and presenilin: a proteolytic mechanism emerges*. *Curr Opin Cell Biol*, 2001. **13**(5): p. 627-34.
169. Nichols, C.D., J. Becnel, and U.B. Pandey, *Methods to assay Drosophila behavior*. *J Vis Exp*, 2012(61).
170. Schmidt, I., et al., *Kinesin heavy chain function in Drosophila glial cells controls neuronal activity*. *J Neurosci*, 2012. **32**(22): p. 7466-76.
171. Maples, T. and A. Rothenfluh, *A simple way to measure ethanol sensitivity in flies*. *J Vis Exp*, 2011(48).
172. Abele, J., *A big protein in a small organism - Illuminating the role of rhinoceros in Drosophila and memory formation*. 2013.
173. Formstecher, E., et al., *Protein interaction mapping: a Drosophila case study*. *Genome Res*, 2005. **15**(3): p. 376-84.
174. Bateman, A., et al., *The Pfam protein families database*. *Nucleic Acids Res*, 2002. **30**(1): p. 276-80.
175. Selleck, W., et al., *The Saccharomyces cerevisiae Piccolo NuA4 histone acetyltransferase complex requires the Enhancer of Polycomb A domain and chromodomain to acetylate nucleosomes*. *Mol Cell Biol*, 2005. **25**(13): p. 5535-42.
176. Araque, A., et al., *Tripartite synapses: glia, the unacknowledged partner*. *Trends Neurosci*, 1999. **22**(5): p. 208-15.
177. Strauss, A.L., F. Kawasaki, and R.W. Ordway, *A Distinct Perisynaptic Glial Cell Type Forms Tripartite Neuromuscular Synapses in the Drosophila Adult*. *PLoS One*, 2015. **10**(6): p. e0129957.
178. Danjo, R., F. Kawasaki, and R.W. Ordway, *A tripartite synapse model in Drosophila*. *PLoS One*, 2011. **6**(2): p. e17131.
179. Sugiura, Y. and W. Lin, *Neuron-glia interactions: the roles of Schwann cells in neuromuscular synapse formation and function*. *Biosci Rep*, 2011. **31**(5): p. 295-302.
180. Feng, Z. and C.P. Ko, *Neuronal glia interactions at the vertebrate neuromuscular junction*. *Curr Opin Pharmacol*, 2007. **7**(3): p. 316-24.
181. Malenka, R.C. and M.F. Bear, *LTP and LTD: an embarrassment of riches*. *Neuron*, 2004. **44**(1): p. 5-21.
182. Heiman, M., et al., *Cell type-specific mRNA purification by translating ribosome affinity purification (TRAP)*. *Nat Protoc*, 2014. **9**(6): p. 1282-91.

183. German, M.S., et al., *Synergistic activation of the insulin gene by a LIM-homeo domain protein and a basic helix-loop-helix protein: building a functional insulin minienhancer complex*. *Genes Dev*, 1992. **6**(11): p. 2165-76.
184. Deweindt, C., et al., *The LAZ3/BCL6 oncogene encodes a sequence-specific transcriptional inhibitor: a novel function for the BTB/POZ domain as an autonomous repressing domain*. *Cell Growth Differ*, 1995. **6**(12): p. 1495-503.
185. Chen, H.J., et al., *A synaptic Ras-GTPase activating protein (p135 SynGAP) inhibited by CaM kinase II*. *Neuron*, 1998. **20**(5): p. 895-904.
186. Husi, H., et al., *Proteomic analysis of NMDA receptor-adhesion protein signaling complexes*. *Nat Neurosci*, 2000. **3**(7): p. 661-9.
187. Kim, J.H., et al., *SynGAP: a synaptic RasGAP that associates with the PSD-95/SAP90 protein family*. *Neuron*, 1998. **20**(4): p. 683-91.
188. Pak, D.T., et al., *Regulation of dendritic spine morphology by SPAR, a PSD-95-associated RapGAP*. *Neuron*, 2001. **31**(2): p. 289-303.
189. Ye, B., et al., *GRASP-1: a neuronal RasGEF associated with the AMPA receptor/GRIP complex*. *Neuron*, 2000. **26**(3): p. 603-17.
190. Ng, J., et al., *Rac GTPases control axon growth, guidance and branching*. *Nature*, 2002. **416**(6879): p. 442-7.
191. Hayashi, M.L., et al., *Altered cortical synaptic morphology and impaired memory consolidation in forebrain-specific dominant-negative PAK transgenic mice*. *Neuron*, 2004. **42**(5): p. 773-87.
192. Schenck, A., et al., *CYFIP/Sra-1 controls neuronal connectivity in Drosophila and links the Rac1 GTPase pathway to the fragile X protein*. *Neuron*, 2003. **38**(6): p. 887-98.
193. Matsuno, M., et al., *Long-term memory formation in Drosophila requires training-dependent glial transcription*. *J Neurosci*, 2015. **35**(14): p. 5557-65.
194. Weikop, P., T. Yoshitake, and J. Kehr, *Differential effects of adjunctive methylphenidate and citalopram on extracellular levels of serotonin, noradrenaline and dopamine in the rat brain*. *Eur Neuropsychopharmacol*, 2007. **17**(10): p. 658-71.
195. Kuczenski, R. and D.S. Segal, *Exposure of adolescent rats to oral methylphenidate: preferential effects on extracellular norepinephrine and absence of sensitization and cross-sensitization to methamphetamine*. *J Neurosci*, 2002. **22**(16): p. 7264-71.
196. Ritz, M.C., et al., *Cocaine receptors on dopamine transporters are related to self-administration of cocaine*. *Science*, 1987. **237**(4819): p. 1219-23.
197. Volkow, N.D., et al., *Cardiovascular effects of methylphenidate in humans are associated with increases of dopamine in brain and of epinephrine in plasma*. *Psychopharmacology (Berl)*, 2003. **166**(3): p. 264-70.
198. Volkow, N.D., et al., *Long-lasting inhibition of in vivo cocaine binding to dopamine transporters by 3 beta-(4-iodophenyl)tropane-2-carboxylic acid methyl ester: RTI-55 or beta CIT*. *Synapse*, 1995. **19**(3): p. 206-11.

199. Stoops, W.W., P.E. Glaser, and C.R. Rush, *Reinforcing, subject-rated, and physiological effects of intranasal methylphenidate in humans: a dose-response analysis*. *Drug Alcohol Depend*, 2003. **71**(2): p. 179-86.
200. Kettenmann, H. and B.R. Ransom, *Neuroglia*. 2 ed. 2005: Oxford University Press. 601.
201. Smith, W.B., et al., *Dopaminergic stimulation of local protein synthesis enhances surface expression of GluR1 and synaptic transmission in hippocampal neurons*. *Neuron*, 2005. **45**(5): p. 765-79.
202. McMahon, H.T., et al., *Complexins: cytosolic proteins that regulate SNAP receptor function*. *Cell*, 1995. **83**(1): p. 111-9.
203. Cao, P., X. Yang, and T.C. Sudhof, *Complexin activates exocytosis of distinct secretory vesicles controlled by different synaptotagmins*. *J Neurosci*, 2013. **33**(4): p. 1714-27.
204. Cho, R.W., et al., *Phosphorylation of Complexin by PKA Regulates Activity-Dependent Spontaneous Neurotransmitter Release and Structural Synaptic Plasticity*. *Neuron*, 2015. **88**(4): p. 749-61.
205. Kaang, B.K. and J.H. Choi, *Synaptic protein degradation in memory reorganization*. *Adv Exp Med Biol*, 2012. **970**: p. 221-40.
206. Roos, J., et al., *Drosophila Futsch regulates synaptic microtubule organization and is necessary for synaptic growth*. *Neuron*, 2000. **26**(2): p. 371-82.
207. Hummel, T., et al., *Drosophila Futsch/22C10 is a MAP1B-like protein required for dendritic and axonal development*. *Neuron*, 2000. **26**(2): p. 357-70.
208. Zou, B., et al., *MAP1 structural organization in Drosophila: in vivo analysis of FUTSCH reveals heavy- and light-chain subunits generated by proteolytic processing at a conserved cleavage site*. *Biochem J*, 2008. **414**(1): p. 63-71.
209. Green, E.W., et al., *A Drosophila RNAi collection is subject to dominant phenotypic effects*. *Nat Methods*, 2014. **11**(3): p. 222-3.
210. Nagarkar-Jaiswal, S., et al., *A library of MiMICs allows tagging of genes and reversible, spatial and temporal knockdown of proteins in Drosophila*. *Elife*, 2015. **4**.
211. Venken, K.J., et al., *MiMIC: a highly versatile transposon insertion resource for engineering Drosophila melanogaster genes*. *Nat Methods*, 2011. **8**(9): p. 737-43.
212. Ejsmont, R.K., et al., *A toolkit for high-throughput, cross-species gene engineering in Drosophila*. *Nat Methods*, 2009. **6**(6): p. 435-7.
213. Venken, K.J., et al., *Recombineering-mediated tagging of Drosophila genomic constructs for in vivo localization and acute protein inactivation*. *Nucleic Acids Res*, 2008. **36**(18): p. e114.
214. Negre, N., et al., *A cis-regulatory map of the Drosophila genome*. *Nature*, 2011. **471**(7339): p. 527-31.

7 Appendix

7.1 Used primers for cloning

Supplementary Table 1: Primers used for vector cloning

Nr.	Name	primer sequence (5'→3')	DNA-template/position	application/vector
1	pMalc2xradishfw	TCA GTC TAG AGC ATC CCG GCG CGG ATC C	genomic DNA 703-720 bp	vector cloning pMal-c2x
2	pMalc2xradishrv	CTA GCT GCA GCT ATC CCC TGG CGA TCA G	genomic DNA 1,531-1,545 bp + TAG	vector cloning pMal-c2x
3	Rsh_BglII_5	GAA GAT CTG CAT CCC GGC GCG GAT CCG GT	genomic DNA 703-720 bp	vector cloning pEGFP- C1 for genotyping
4	Rsh_PstI_neu_3	AAC TGC AGC TAC CGG CGG AAT CCC CTG GC	genomic DNA 1,537-1,554 bp + TAG	vector cloning pEGFP- C1 for genotyping
7	C_Genomic_F	GCC CAC TGT CAG CTC TCA AC	genomic DNA[209]	single-fly PCR
8	pKC26_R	TGT AAA ACG ACG GCC AGT	genomic DNA[209]	single-fly PCR

7.2 Used vectors for cloning

Supplementary Table 2: Cloning vectors

vector	system	company
pMal-c2x	MBP-fusion protein, expression in <i>E. coli</i>	NEB
pEGFP-C1	Living Colors™ Fluorescent Proteins, expression in Hek293T cells	Clontech

7.3 Expression vectors

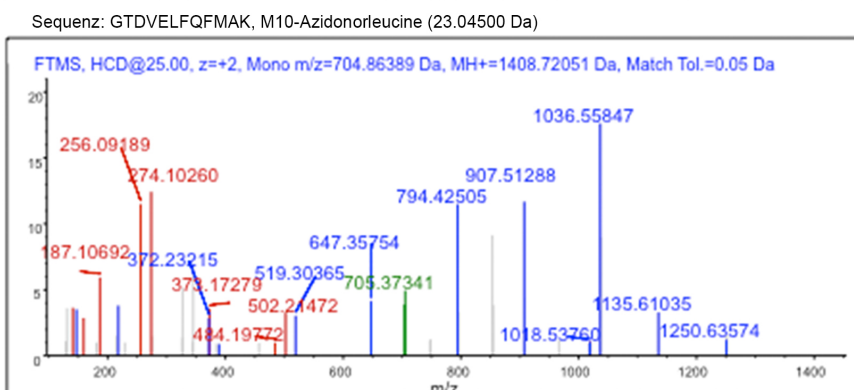
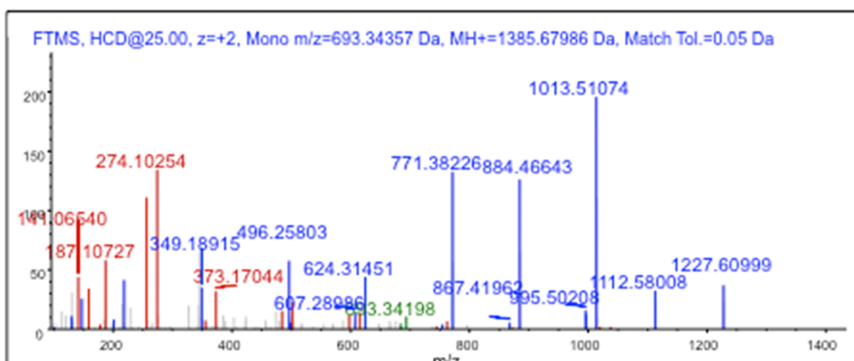
Supplementary Table 3: Expression vectors

Nr.	Name	Insert	vector	restriction interferences	application
1	pMal-c2x-Rsh	Rsh bp: 703-1,545	pMal-c2x	XbaI/PstI	expression
2	pEGFP-C1-Rsh	Rsh bp: 703-1,554	pEGFP-C1	BglII/PstI	expression

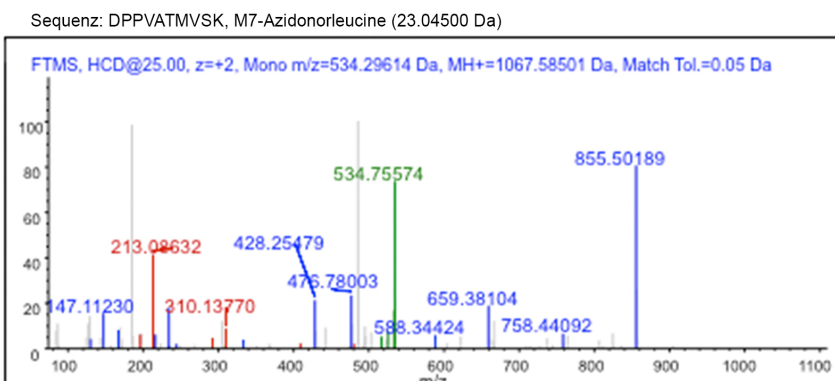
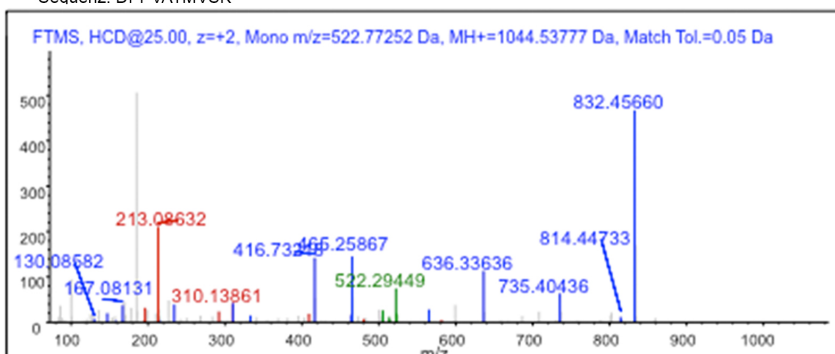
7.4 Supplementary figures

Supplementary Figure 1:

a dMetRS^{L262G}-EGFP (aa 535-546; M544ANL)
Sequenz: GTDVLFQFMAK



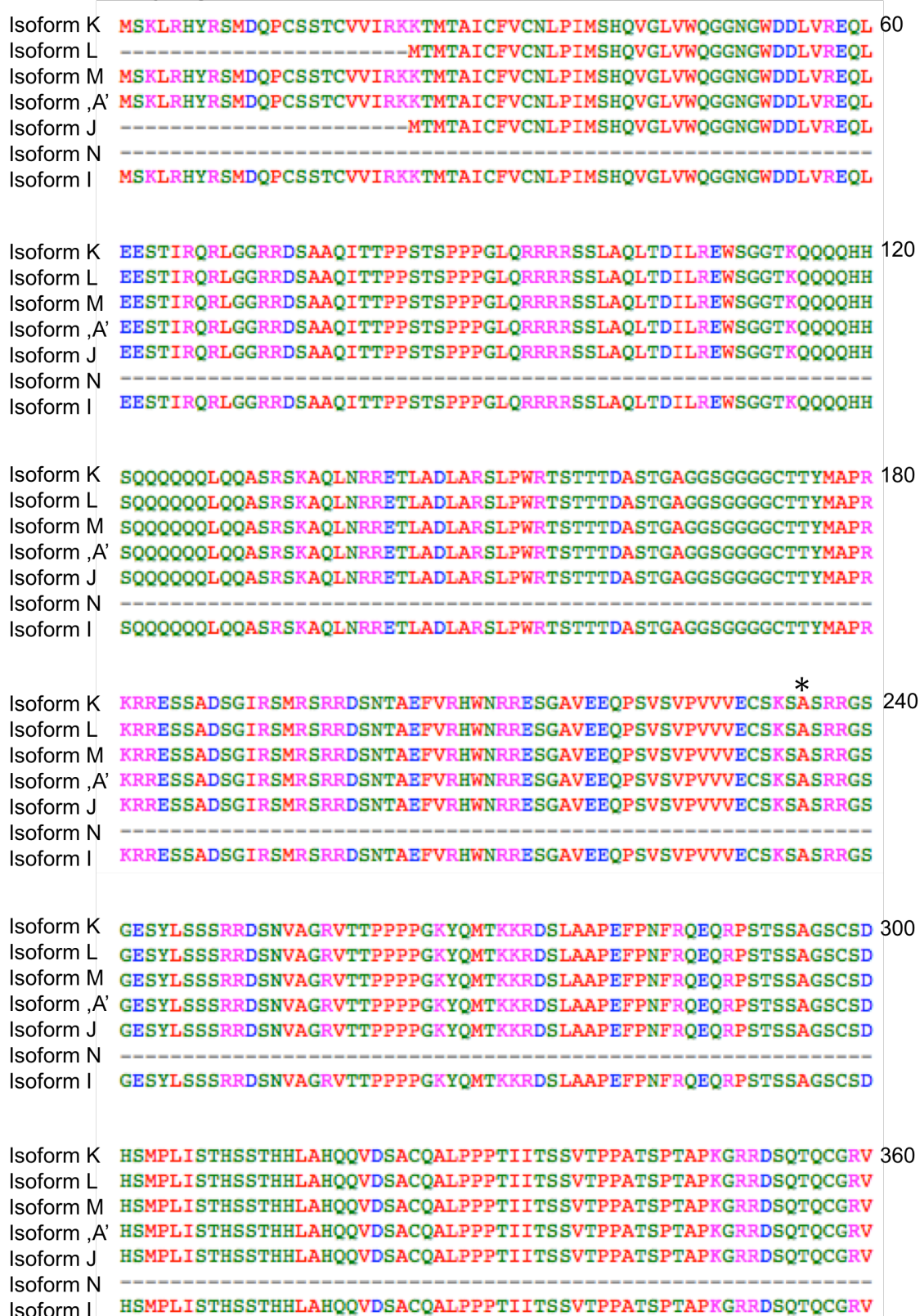
b dMetRS^{L262G}-EGFP (aa 1030-1039; M1036ANL)
Sequenz: DPPVATMVSK



Supplementary Figure 1: MetRS^{LtoG} results in incorporation of ANL into internal methionine residues. MS/MS spectra of two internal dMetRS^{L262G}-EGFP peptides (*a*, aa 535-546; *b*, aa 1030-1039) identified from ANL-labeled dMetRS^{L262G}-EGFP purified from larval body walls after chronic treatment with 4 mM ANL. *b* ions are marked in red and *y* ions in blue. Shown are in the upper panels the unmodified peptides and in the lower panels the two ANL-modified ones. All identified peptides

were filtered with 1% FDR (false discovery rate), top rank, mass accuracy, and a minimum of 3 identified peptides. Note, that the ratio of ANL-labeled to unlabeled peptide is 1:10.

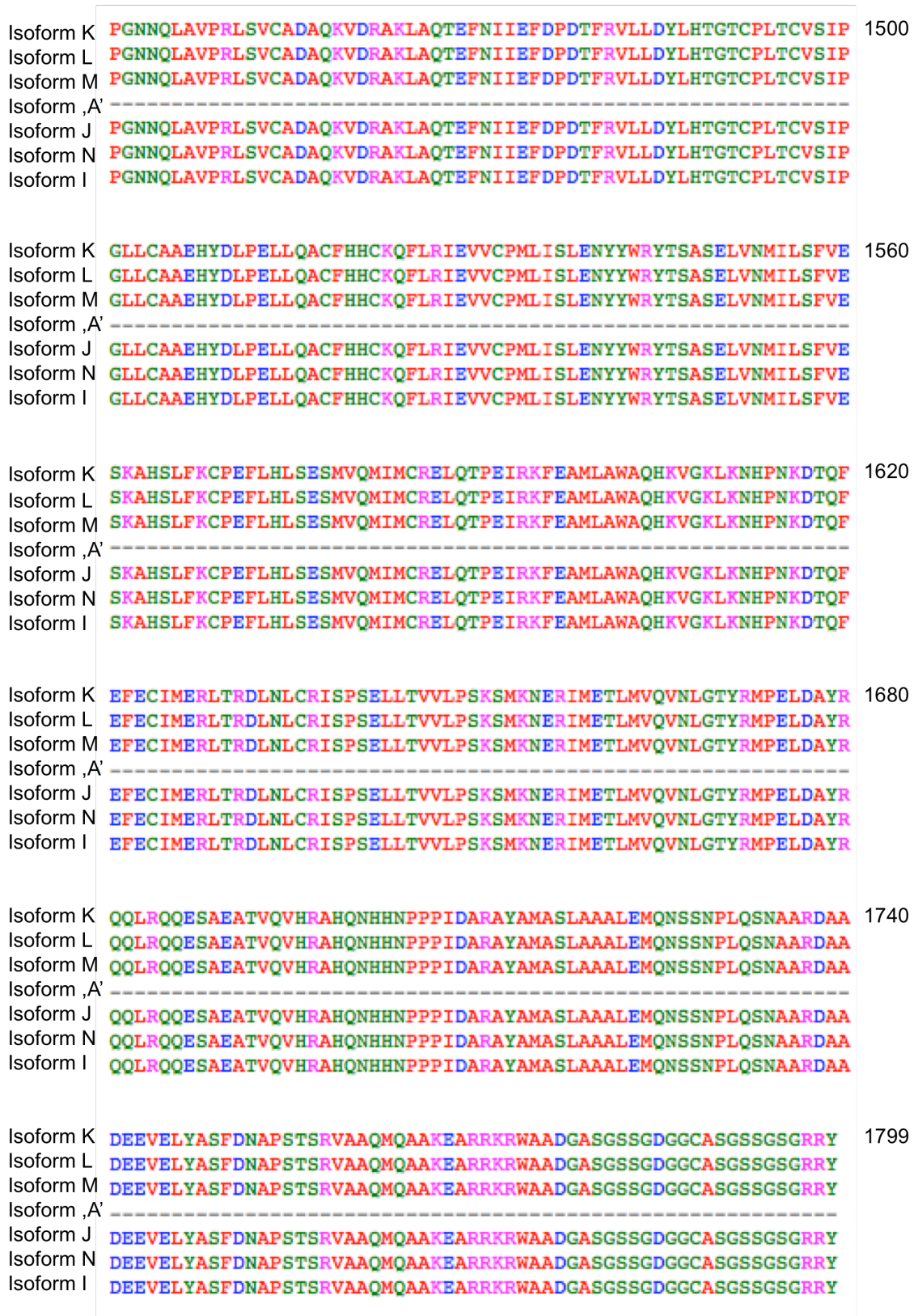
Supplementary Figure 2:



Isoform K	NRRDSKAGVSPERAPRLQRLQIQATAFDEGCLPGGSRGSPALSPDPPDDCERRTSRRD	420
Isoform L	NRRDSKAGVSPERAPRLQRLQIQATAFDEGCLPGGSRGSPALSPDPPDDCERRTSRRD	
Isoform M	NRRDSKAGVSPERAPRLQRLQIQATAFDEGCLPGGSRGSPALSPDPPDDCERRTSRRD	
Isoform ,A'	NRRDSKAGVSPERAPRLQRLQIQATAFDEGCLPGGSRGSPALSPDPPDDCERRTSRRD	
Isoform J	NRRDSKAGVSPERAPRLQRLQIQATAFDEGCLPGGSRGSPALSPDPPDDCERRTSRRD	
Isoform N	-----	
Isoform I	NRRDSKAGVSPERAPRLQRLQIQATAFDEGCLPGGSRGSPALSPDPPDDCERRTSRRD	
Isoform K	SLSPDSASRGGRRDSRTHLSPDRSHERDGSPPRRHTLRRQSSSAARSPRSPDNSNCCSSRD	480
Isoform L	SLSPDSASRGGRRDSRTHLSPDRSHERDGSPPRRHTLRRQSSSAARSPRSPDNSNCCSSRD	
Isoform M	SLSPDSASRGGRRDSRTHLSPDRSHERDGSPPRRHTLRRQSSSAARSPRSPDNSNCCSSRD	
Isoform ,A'	SLSPDSASRGGRRDSRTHLSPDRSHERDGSPPRRHTLRRQSSSAARSPRSPDNSNCCSSRD	
Isoform J	SLSPDSASRGGRRDSRTHLSPDRSHERDGSPPRRHTLRRQSSSAARSPRSPDNSNCCSSRD	
Isoform N	-----	
Isoform I	SLSPDSASRGGRRDSRTHLSPDRSHERDGSPPRRHTLRRQSSSAARSPRSPDNSNCCSSRD	
Isoform K	PSPCSRPTQTQTVEQNQRPAIRRQSTTEEILIIARGFRRQSTTEEMIRCNFRFRQSSQSDD	540
Isoform L	PSPCSRPTQTQTVEQNQRPAIRRQSTTEEILIIARGFRRQSTTEEMIRCNFRFRQSSQSDD	
Isoform M	PSPCSRPTQTQTVEQNQRPAIRRQSTTEEILIIARGFRRQSTTEEMIRCNFRFRQSSQSDD	
Isoform ,A'	PSPCSRPTQTQTVEQNQRPAIRRQSTTEEILIIARGFRRQSTTEEMIRCNFRFRQSSQSDD	
Isoform J	PSPCSRPTQTQTVEQNQRPAIRRQSTTEEILIIARGFRRQSTTEEMIRCNFRFRQSSQSDD	
Isoform N	-----	
Isoform I	PSPCSRPTQTQTVEQNQRPAIRRQSTTEEILIIARGFRRQSTTEEMIRCNFRFRQSSQSDD	
Isoform K	VCRYRGRDSSAQIIDGTIGTMTVETTSTFFDSSTQTEPSPLYDNNHYHEECLRCNSCGL	600
Isoform L	VCRYRGRDSSAQIIDGTIGTMTVETTSTFFDSSTQTEPSPLYDNNHYHEECLRCNSCGL	
Isoform M	VCRYRGRDSSAQIIDGTIGTMTVETTSTFFDSSTQTEPSPLYDNNHYHEECLRCNSCGL	
Isoform ,A'	VCRYRGRDSSAQIIDGTIGTMTVETTSTFFDSSTQTEPSPLYDNNHYHEECLRCNSCGL	
Isoform J	VCRYRGRDSSAQIIDGTIGTMTVETTSTFFDSSTQTEPSPLYDNNHYHEECLRCNSCGL	
Isoform N	-----	
Isoform I	VCRYRGRDSSAQIIDGTIGTMTVETTSTFFDSSTQTEPSPLYDNNHYHEECLRCNSCGL	
Isoform K	NLTGPNQKRARRFKNQILCDLHFADVALMECSDFMQQLRSFKPQSLGCAVARRKSSTTLI	660
Isoform L	NLTGPNQKRARRFKNQILCDLHFADVALMECSDFMQQLRSFKPQSLGCAVARRKSSTTLI	
Isoform M	NLTGPNQKRARRFKNQILCDLHFADVALMECSDFMQQLRSFKPQSLGCAVARRKSSTTLI	
Isoform ,A'	-----	
Isoform J	NLTGPNQKRARRFKNQILCDLHFADVALMECSDFMQQLRSFKPQSLGCAVARRKSSTTLI	
Isoform N	-----MECSDFMQQLRSFKPQSLGCAVARRKSSTTLI	
Isoform I	NLTGPNQKRARRFKNQILCDLHFADVALMECSDFMQQLRSFKPQSLGCAVARRKSSTTLI	
Isoform K	FPLPPQACSDDEFCEEYPHNLMPTPGYWIECSRQKITMPTPHTIWDESSEHEDIRAGSAS	720
Isoform L	FPLPPQACSDDEFCEEYPHNLMPTPGYWIECSRQKITMPTPHTIWDESSEHEDIRAGSAS	
Isoform M	FPLPPQACSDDEFCEEYPHNLMPTPGYWIECSRQKITMPTPHTIWDESSEHEDIRAGSAS	
Isoform ,A'	-----	
Isoform J	FPLPPQACSDDEFCEEYPHNLMPTPGYWIECSRQKITMPTPHTIWDESSEHEDIRAGSAS	
Isoform N	FPLPPQACSDDEFCEEYPHNLMPTPGYWIECSRQKITMPTPHTIWDESSEHEDIRAGSAS	
Isoform I	FPLPPQACSDDEFCEEYPHNLMPTPGYWIECSRQKITMPTPHTIWDESSEHEDIRAGSAS	

Isoform K	DAYLERECSDLYEDDEDSEATPSPRKKTTEEQWDQQGAFELISVEQETYEKYFYGTEHW	780
Isoform L	DAYLERECSDLYEDDEDSEATPSPRKKTTEEQWDQQGAFELISVEQETYEKYFYGTEHW	
Isoform M	DAYLERECSDLYEDDEDSEATPSPRKKTTEEQWDQQGAFELISVEQETYEKYFYGTEHW	
Isoform ,A'	-----	
Isoform J	DAYLERECSDLYEDDEDSEATPSPRKKTTEEQWDQQGAFELISVEQETYEKYFYGTEHW	
Isoform N	DAYLERECSDLYEDDEDSEATPSPRKKTTEEQWDQQGAFELISVEQETYEKYFYGTEHW	
Isoform I	DAYLERECSDLYEDDEDSEATPSPRKKTTEEQWDQQGAFELISVEQETYEKYFYGTEHW	
Isoform K	NYFTSDEDLGPVILSIKQETLNGRDQFRILVRAGSYTVHGLIPASCVFADRYNREEVRS	840
Isoform L	NYFTSDEDLGPVILSIKQETLNGRDQFRILVRAGSYTVHGLIPASCVFADRYNREEVRS	
Isoform M	NYFTSDEDLGPVILSIKQETLNGRDQFRILVRAGSYTVHGLIPASCVFADRYNREEVRS	
Isoform ,A'	-----	
Isoform J	NYFTSDEDLGPVILSIKQETLNGRDQFRILVRAGSYTVHGLIPASCVFADRYNREEVRS	
Isoform N	NYFTSDEDLGPVILSIKQETLNGRDQFRILVRAGSYTVHGLIPASCVFADRYNREEVRS	
Isoform I	NYFTSDEDLGPVILSIKQETLNGRDQFRILVRAGSYTVHGLIPASCVFADRYNREEVRS	
Isoform K	LGKEVNLPPLTLGQLPDTPEELLKLDQVFIKSELKVGVIKEDQYTEEQILDNNNSP	900
Isoform L	LGKEVNLPPLTLGQLPDTPEELLKLDQVFIKSELKVGVIKEDQYTEEQILDNNNSP	
Isoform M	LGKEVNLPPLTLGQLPDTPEELLKLDQVFIKSELKVGVIKEDQYTEEQILDNNNSP	
Isoform ,A'	-----	
Isoform J	LGKEVNLPPLTLGQLPDTPEELLKLDQVFIKSELKVGVIKEDQYTEEQILDNNNSP	
Isoform N	LGKEVNLPPLTLGQLPDTPEELLKLDQVFIKSELKVGVIKEDQYTEEQILDNNNSP	
Isoform I	LGKEVNLPPLTLGQLPDTPEELLKLDQVFIKSELKVGVIKEDQYTEEQILDNNNSP	
Isoform K	LFDEFLTLLGDRVRLRGFDKYKGLDVTVDLDTGLFSVYTNWRNIEIMFHVSTLLPYEKHD	960
Isoform L	LFDEFLTLLGDRVRLRGFDKYKGLDVTVDLDTGLFSVYTNWRNIEIMFHVSTLLPYEKHD	
Isoform M	LFDEFLTLLGDRVRLRGFDKYKGLDVTVDLDTGLFSVYTNWRNIEIMFHVSTLLPYEKHD	
Isoform ,A'	-----	
Isoform J	LFDEFLTLLGDRVRLRGFDKYKGLDVTVDLDTGLFSVYTNWRNIEIMFHVSTLLPYEKHD	
Isoform N	LFDEFLTLLGDRVRLRGFDKYKGLDVTVDLDTGLFSVYTNWRNIEIMFHVSTLLPYEKHD	
Isoform I	LFDEFLTLLGDRVRLRGFDKYKGLDVTVDLDTGLFSVYTNWRNIEIMFHVSTLLPYEKHD	
Isoform K	PQKLQRKRHIGNDIVCVVFLADNTRFSPACIKSHFLHTFILVRVSARIKHKPTRYEVSV	1020
Isoform L	PQKLQRKRHIGNDIVCVVFLADNTRFSPACIKSHFLHTFILVRVSARIKHKPTRYEVSV	
Isoform M	PQKLQRKRHIGNDIVCVVFLADNTRFSPACIKSHFLHTFILVRVSARIKHKPTRYEVSV	
Isoform ,A'	-----	
Isoform J	PQKLQRKRHIGNDIVCVVFLADNTRFSPACIKSHFLHTFILVRVSARIKHKPTRYEVSV	
Isoform N	PQKLQRKRHIGNDIVCVVFLADNTRFSPACIKSHFLHTFILVRVSARIKHKPTRYEVSV	
Isoform I	PQKLQRKRHIGNDIVCVVFLADNTRFSPACIKSHFLHTFILVRVSARIKHKPTRYEVSV	
Isoform K	VTRDEVGAYKPYLWEQSVFEKGPWFREWLLTKIVNGERASYSAPKFARMQERTRSQMLD	1080
Isoform L	VTRDEVGAYKPYLWEQSVFEKGPWFREWLLTKIVNGERASYSAPKFARMQERTRSQMLD	
Isoform M	VTRDEVGAYKPYLWEQSVFEKGPWFREWLLTKIVNGERASYSAPKFARMQERTRSQMLD	
Isoform ,A'	-----	
Isoform J	VTRDEVGAYKPYLWEQSVFEKGPWFREWLLTKIVNGERASYSAPKFARMQERTRSQMLD	
Isoform N	VTRDEVGAYKPYLWEQSVFEKGPWFREWLLTKIVNGERASYSAPKFARMQERTRSQMLD	
Isoform I	VTRDEVGAYKPYLWEQSVFEKGPWFREWLLTKIVNGERASYSAPKFARMQERTRSQMLD	

Isoform K	LVMNLSNHAETGQIPKPYRRGSRPIG-----+-----	1140
Isoform L	LVMNLSNHAETGQIPKPYRRGSRPIG-----	
Isoform M	LVMNLSNHAETGQIPKPYRRGSRPIG-----	
Isoform ,A'	-----	
Isoform J	LVMNLSNHAETGQIPKPYRRGSRPIGEDEYIKMLHARVLDNNTTHHEQQQQLLLQQQHMQ	
Isoform N	LVMNLSNHAETGQIPKPYRRGSRPIGEDEYIKMLHARVLDNNTTHHEQQQQLLLQQQHMQ	
Isoform I	LVMNLSNHAETGQIPKPYRRGSRPIGEDEYIKMLHARVLDNNTTHHEQQQQLLLQQQHMQ	
Isoform K	-----	1200
Isoform L	-----	
Isoform M	-----	
Isoform ,A'	-----	
Isoform J	HTQHMQHLP SHNICCYCNNA TELHTAGAIHNNNDNNNTTTTTT FTHRHNNNNNNNYSEQQ	
Isoform N	HTQHMQHLP SHNICCYCNNA TELHTAGAIHNNNDNNNTTTTTT FTHRHNNNNNNNYSEQQ	
Isoform I	HTQHMQHLP SHNICCYCNNA TELHTAGAIHNNNDNNNTTTTTT FTHRHNNNNNNNYSEQQ	
Isoform K	-----+-----	1260
Isoform L	-----HMRPSSP	
Isoform M	-----HMRPSSP	
Isoform ,A'	-----	
Isoform J	QQQLPQQQQHDSQQQQQLLPQQHQLLHQLQLSTSSLTHTSCCAMLHLCARHSHMRPSSP	
Isoform N	QQQLPQQQQHDSQQQQQLLPQQHQLLHQLQLSTSSLTHTSCCAMLHLCARHSHMRPSSP	
Isoform I	QQQLPQQQQHDSQQQQQLLPQQHQLLHQLQLSTSSLTHTSCCAMLHLCARHSHMRPSSP	
Isoform K	LLDSVRDQFEDYDQLAKDFTRVFLNEEPSCLTNAHLFDVVFLVGQSKQKARFIGVRAILG	1320
Isoform L	LLDSVRDQFEDYDQLAKDFTRVFLNEEPSCLTNAHLFDVVFLVGQSKQKARFIGVRAILG	
Isoform M	LLDSVRDQFEDYDQLAKDFTRVFLNEEPSCLTNAHLFDVVFLVGQSKQKARFIGVRAILG	
Isoform ,A'	-----	
Isoform J	LLDSVRDQFEDYDQLAKDFTRVFLNEEPSCLTNAHLFDVVFLVGQSKQKARFIGVRAILG	
Isoform N	LLDSVRDQFEDYDQLAKDFTRVFLNEEPSCLTNAHLFDVVFLVGQSKQKARFIGVRAILG	
Isoform I	LLDSVRDQFEDYDQLAKDFTRVFLNEEPSCLTNAHLFDVVFLVGQSKQKARFIGVRAILG	
Isoform K	VRSRVFQEMLYGIQTGF GSPQIPVAEIFARPAPSLVSPQNQKPKSNNYLTVPDSDSIRPK	1380
Isoform L	VRSRVFQEMLYGIQTGF GSPQIPVAEIFARPAPSLVSPQNQKPKSNNYLTVPDSDSIRPK	
Isoform M	VRSRVFQEMLYGIQTGF GSPQIPVAEIFARPAPSLVSPQNQKPKSNNYLTVPDSDSIRPK	
Isoform ,A'	-----	
Isoform J	VRSRVFQEMLYGIQTGF GSPQIPVAEIFARPAPSLVSPQNQKPKSNNYLTVPDSDSIRPK	
Isoform N	VRSRVFQEMLYGIQTGF GSPQIPVAEIFARPAPSLVSPQNQKPKSNNYLTVPDSDSIRPK	
Isoform I	VRSRVFQEMLYGIQTGF GSPQIPVAEIFARPAPSLVSPQNQKPKSNNYLTVPDSDSIRPK	
Isoform K	SVPSSPMVKRAF SRLGTITAGWGRSIRNKNTNQLNPDDKKKWI SSTDY--RDSKDKDKDK	1440
Isoform L	SVPSSPMVKRAF SRLGTITAGWGRSIRNKNTNQLNPDDKKKWI SSTDCSNRDSKDKDKDK	
Isoform M	SVPSSPMVKRAF SRLGTITAGWGRSIRNKNTNQLNPDDKKKWI SSTDCSNRDSKDKDKDK	
Isoform ,A'	-----	
Isoform J	SVPSSPMVKRAF SRLGTITAGWGRSIRNKNTNQLNPDDKKKWI SSTDY--RDSKDKDKDK	
Isoform N	SVPSSPMVKRAF SRLGTITAGWGRSIRNKNTNQLNPDDKKKWI SSTDCSNRDSKDKDKDK	
Isoform I	SVPSSPMVKRAF SRLGTITAGWGRSIRNKNTNQLNPDDKKKWI SSTDCSNRDSKDKDKDK	



Supplementary Figure 2: Multiple sequence alignment of Rsh isoforms. Clustal Omega 1.2.1 sequence alignment of all six different Rsh isoforms and the former isoform ,A' revealed that the position of the initial Met differs between isoforms. Isoform I, K, M and ,A' start at position 1, isoform J and L start at position 24, whereas isoform N starts at position 629. Furthermore isoforms K, L and M lack 145 aa at position 1,108-1,253 aa ('+') and isoforms K and J lack two aa at position 1,429-1,430 aa ('+'). The remaining protein sequence is identical between isoforms. The arrow points towards the glutamine (Q) which is transformed into a 'stop' in the mutated Rsh protein. The two asterisks indicate

the amino acid sequence that should be recognized by the Rsh antibody. The amino acid positions within the respective sequence are indicated at the right.

Curriculum vitae

PERSONAL INFORMATION

Name	Ines Erdmann
Nationality	German
Date of birth	30.03.1988

ACADEMIC QUALIFICATIONS

- 12/2011 – until now** **PhD thesis** in the laboratory of Prof. Dr. Daniela C. Dieterich at the Institute for Pharmacology and Toxicology, Otto-von-Guericke University (OvGU) of Magdeburg (Germany) and at Leibniz Institute for Neurobiology, Magdeburg (Germany)
- 12/2011 – 02/2016:
“Deciphering proteome dynamics using cell-type selective metabolic protein labeling in the fruit fly *Drosophila melanogaster*“
 - 10/2012 – 02/2013:
Course of “Einführung in tierexperimentelle Methoden für Doktoranden, wissenschaftliches und nichtwissenschaftliches Personal der Hochschule“, OvGU Magdeburg (Germany)
 - 08/2012:
3rd LIN-Symposium “Translating synaptic activity into neuronal plasticity“ (attendee), Tangermünde (Germany)
 - 04/2013 – 12/2013:
Experimental supervision of a master thesis
- 10/2009 – 11/2011** **Master of Science** in Integrative Neuroscience, OvGU Magdeburg (Germany)
- 04/2011 – 11/2011:
Master thesis (“Establishment and Implementation of Metabolic Labeling of Proteins in *Drosophila melanogaster*“) in the laboratory of Prof. Dr. Daniela C. Dieterich at the Leibniz Institute for Neurobiology, Magdeburg (Germany)
 - 04/2010 – 03/2011:
Research assistant in the laboratory of Prof. Daniela C. Dieterich at the Leibniz Institute for Neurobiology, Magdeburg (Germany)
- 10/2006 – 09/2009** **Bachelor of Science** in Biology, University Hamburg
- 04/2010 – 03/2011:
Bachelor thesis (“Comparison of the cone and Müller cell rateration in the retina of a diurnal and a nocturnal animal“) in the laboratory of Prof. Dr. Andreas Reichenbach at Paul-Flechsig-Institute for Brain Research, Leipzig (Germany)
- 09/1998 – 07/2006** **Abitur** at Friedrich-Arnold-Brockhaus-Gymnasium, Leipzig (Germany)
- 10/2004 – 07/2006:
Thesis (“The Müller cell - the dominant glia cell of the retina“) in the lab of Prof. Dr. Andreas Reichenbach at Paul-Flechsig-Institut for brain research, Leipzig (Germany)

MEETINGS, CONFERENCES AND PRESENTATIONS

02/2015 13th Learning and Memory Meeting, Magdeburg, Germany (poster presentation)

10/2014	Neurofly Meeting, Hersonissos, Crete, Greece (poster presentation)
07/2014	9 th FENS Conference, Milan, Italy (poster presentation)
02/2014	2 nd Retreat of the Leibniz Graduate School SynaptoGenetics, Weimar, Germany (oral presentation)
01/2013	1 st Retreat of the Leibniz Graduate School SynaptoGenetics, Wernigerode, Germany (oral presentation)
09/2012	Neurofly Meeting, Padua, Italy (poster presentation)
07/2012	8 th FENS conference, Barcelona, Spain (poster presentation)

AWARDS

12/2015	2. Award of the Hugo-Junkers-Preis for Research and Innovation of Saxony-Anhalt in the category „Most innovative purposes in basic research“ with the project “ <i>In vivo</i> cell-selective protein labeling using click chemistry“
03/2006	Special award „Jugend forscht“ for the “Best media and print technique“ with the thesis “The Müller cell - the dominant glia cell of the retina“

SKILLS AND INTERESTS

Relevant Scientific Interests	<p><i>Flies</i>: rearing and crossing of <i>Drosophila melanogaster</i></p> <p><i>Biochemical methods</i>: cell lysis, click chemistry (BONCAT), protein quantification, gel electrophoresis and western/dot blot, protein purification, antibody characterization, production of fusion proteins, PCR, bacterial transformation, DNA purification</p> <p><i>Immunofluorescence</i>: click chemistry (FUNCAT), immunocytochemistry of cell lines, retina slices and larval body walls</p>
Languages	German (native speaker), English (fluent in speech and writing), Russian (basics)
Computer Skills	<p><i>Professional level</i>: Microsoft Office, PhotoShop und GraphPadPris</p> <p><i>Good knowledge</i>: ImageJ</p> <p><i>basic knowledge</i>: Matlab</p>
Interest	Baking, Pilates, Travelling

Magdeburg, 03.03.2016

Ines Erdmann

List of Publications

Wurm A, Erdmann I, Bringmann A, Reichenbach A, Pannicke T (2009) "Expression and function of P2Y receptors on Müller cells of the postnatal rat retina." *Glia* 57(15)

Agte S, Junek S, Matthias S, Ulbricht E, Erdmann I, Wurm A, Schild D, Käs JA, Reichenbach A (2011) "Müller glial cell-provided cellular light guidance through the vital guinea-pig retina." *Biophys J* 101(11)

Erdmann I, Marter K, Kobler O, Niehues S, Abele J, Müller A, Busmann J, Storkebaum E, Tamar Z, Thomas U, Dieterich DC "Cell-selective labeling of proteomes in *Drosophila melanogaster*" *Nat Commun.* 6:7521 doi: 10.1038/ncomms8521 (2015)

Niehues S, Busmann J, Steffes G, Erdmann I, Köhrer C, Sun L, Wagner M, Schäfer K, Wang G, Koerdt SN, Stum M, RajBhandary UL, Thomas U, Aberle H, Burgess RW, Yang XL, Dieterich DC, Storkebaum E "Impaired protein translation in *Drosophila* models for Charcot-Marie-Tooth neuropathy caused by mutant tRNA synthetases" *Nat Commun.* 6:7520 doi: 10.1038/ncomms8520 (2015)

Statutory declaration

Hiermit erkläre ich, dass ich die von mir eingereichte Dissertation zu dem Thema

**Deciphering proteome dynamics using cell-type selective metabolic protein
labeling in the fruit fly *Drosophila melanogaster***

selbstständig verfasst, nicht schon als Dissertation verwendet habe und die benutzten Hilfsmittel und Quellen vollständig angegeben wurden.

Weiterhin erkläre ich, dass ich weder diese noch andere Arbeiten zur Erlangung des akademischen Grades doctor rerum naturalium (Dr. rer. nat.) an anderen Einrichtungen eingereicht habe.

Magdeburg, den